AFWAL-TR-80-3141
Part III

AD A101648

LEVEL I

A101647

INVESTIGATION OF HIGH-ANGLE-OF-ATTACK MANEUVER-LIMITING FACTORS
Part III: Appendices — Aerodynamic Models

DAVID G. MITCHELL
THOMAS T. MYERS
GARY L. TEPER
DONALD E. JOHNSTON

SYSTEMS TECHNOLOGY, INC.
13766 SOUTH HAWTHORNE BOULEVARD
HAWTHORNE, CALIFORNIA 90250

DTIC
JUL

DECEMBER 1980

TECHNICAL REPORT AFWAL-TR-80-3141, PART III
Final Report for Period May 1976 — July 1980

Approved for public release; distribution unlimited.

DTIC FILE COPY

FLIGHT DYNAMICS LABORATORY
AIR FORCE WRIGHT AERONAUTICAL LABORATORIES
WRIGHT-PATTERSON AIR FORCE BASE, OHIO 45433

81 7 21 016

NOTICE

When Government drawings, specifications, or other data are used for any purpose other than in connection with a definitely related Government procurement operation, the United States Government thereby incurs no responsibility nor any obligation whatsoever; and the fact that the government may have formulated, furnished, or in any way supplied the said drawings, specifications, or other data, is not to be regarded by implication or otherwise as in any manner licensing the holder or any other person or corporation, or conveying any rights or permission to manufacture, use, or sell any patented invention that may in any way be related thereto.

This report has been reviewed by the Office of Public Affairs (ASD/PA) and is releasable to the National Technical Information Service (NTIS). At NTIS, it will be available to the general public, including foreign nations.

This technical report has been reviewed and is approved for publication.

Michael E. Bise

MICHAEL E. BISE, Project Engineer
Control Dynamics Branch
Flight Control Division

R.O. Anderson

R. O. ANDERSON, Chief
Control Dynamics Branch
Flight Control Division

FOR THE COMMANDER

Robert C. Ettinger

ROBERT C. ETTINGER, Colonel, USAF
Chief, Flight Control Division

"If your address has changed, if you wish to be removed from our mailing list, or if the addressee is no longer employed by your organization please notify AFWAL/FIGC, W-PAFB, OH 45433 to help us maintain a current mailing list."

Copies of this report should not be returned unless return is required by security considerations, contractual obligations, or notice on a specific document.

AIR FORCE/56780/8 July 1981 — 440

Unclassified

SECURITY CLASSIFICATION OF THIS PAGE (When Data Entered)

REPORT DOCUMENTATION PAGE		READ INSTRUCTIONS BEFORE COMPLETING FORM
1. REPORT NUMBER AFWAL-TR-80-3141, Part III	2. GOVT ACCESSION NO. AD-A101 648	3. RECIPIENT'S CATALOG NUMBER
4. TITLE (and Subtitle) INVESTIGATION OF HIGH-ANGLE-OF-ATTACK MANEUVER-LIMITING FACTORS, Part III. Appendices - Aerodynamic Models		5. TYPE OF REPORT & PERIOD COVERED Final Report, 13 May 1976 - 30 July 1980
		6. PERFORMING ORG. REPORT NUMBER STI-TR-1081-1
7. AUTHOR(s) David G. Mitchell, Thomas T. Myers, Gary L. Teper, and Donald E. Johnston		8. CONTRACT OR GRANT NUMBER(s) F33615-76-C-3072
9. PERFORMING ORGANIZATION NAME AND ADDRESS Systems Technology, Inc. 13766 S. Hawthorne Blvd. Hawthorne, CA 90250		10. PROGRAM ELEMENT, PROJECT, TASK AREA & WORK UNIT NUMBERS PE 62201F 2403 05
11. CONTROLLING OFFICE NAME AND ADDRESS AFWAL/FIGC Air Force Wright Aeronautical Laboratories Air Force Systems Command Wright-Patterson AFB, OH 45433		12. REPORT DATE December 1980
		13. NUMBER OF PAGES 113
14. MONITORING AGENCY NAME & ADDRESS (if different from Controlling Office)		15. SECURITY CLASS. (of this report) Unclassified
		15a. DECLASSIFICATION/DOWNGRADING SCHEDULE

16. DISTRIBUTION STATEMENT (of this Report)

Approved for public release; distribution unlimited

17. DISTRIBUTION STATEMENT (of the abstract entered in Block 20, if different from Report)

18. SUPPLEMENTARY NOTES

19. KEY WORDS (Continue on reverse side if necessary and identify by block number)

High AOA
Flying Qualities
Stall/Departure
Simulation

20. ABSTRACT (Continue on reverse side if necessary and identify by block number)

The high-angle-of-attack, low-speed stall/departure characteristics of the F-4J and F-14A are analyzed, using a six-degree-of-freedom mathematical model with nonlinear aerodynamics. Cause-effect relationships are investigated for maneuver limiting factors including wing rock, nose slice, and rolling departures. Cross-derivatives of $\mathcal{L}_{\dot{\alpha}}$, $N_{\dot{\alpha}}$, and M_{β} alter key transfer function
(continued)

DD FORM 1473 1 JAN 73 EDITION OF 1 NOV 65 IS OBSOLETE

Unclassified 340425

SECURITY CLASSIFICATION OF THIS PAGE (When Data Entered) parameters. A piloted simulation validates analytic predictions and demonstrates that departure warning, susceptibility, and severity are strongly influenced by the static cross-derivatives. A connection between roll numerator parameter values and pilot perception of departure susceptibility and severity is identified. Potential modifications for the high AOA sections of the MIL-F-8785B Flying Qualities Specification are proposed: a criterion for the real part of the roll numerator root, further recommendations for minimizing departure susceptibility and certain sideslip influences, and a flying quality rating form for assessing departure and recovery characteristics.

Part I, Analysis and Simulation, presents a summary of the complete investigation and results. Part II, Piloted Simulation Assessment of Bihrle Departure Criteria, presents a detailed comparison of analytical prediction and piloted simulation results for a specific set of programmed control deflections. Part III, Appendices — Aerodynamic Models, contains the detailed aerodynamic models employed in the F-4J and F-14A high-angle-of-attack analysis and validation and the equations of motion, aerodynamic models, control system configurations, etc., employed in the piloted simulation.

FOREWORD

This research was sponsored by the Air Force Wright Aeronautical Laboratories, Air Force Systems Command, under Contract F33615-76-C-3072, Work Unit 24030514. Mr. Gary K. Hellmann was the initial project monitor. This responsibility was later transferred to Mr. Michael E. Bise (AFWAL/FIGC). Support of the piloted simulation was also provided by the Naval Air Development Center where Mr. Mark Stifel served as project monitor. The analytic work was performed at Systems Technology, Inc., Hawthorne, California. The work was performed during the period 13 May 1976 through 30 July 1980. The STI Technical Director was Mr. I. L. Ashkenas. Mr. D. E. Johnston was Principal Investigator and STI Project Engineer. The piloted simulation was accomplished at the McDonnell Aircraft Co., St. Louis, Missouri. The report manuscript was submitted in September 1980.

The authors wish to express acknowledgment and thanks to their many coworkers for contributions, both general and detailed, in the program: at STI, Mr. G. L. Teper for invaluable aid in accomplishing the digital simulation, Mr. T. T. Myers for development and validation of the F-4 and F-14 aerodynamic models and for most of the initial analytic support, and Mr. R. H. Hoh for checkout and accomplishment of the piloted simulation. Mr. Hoh also served as one of the subject pilots. At MCAIR, Mr. H. Passmore directed setup and operation of the piloted simulation. Special thanks are due to Lt. Col. R. M. Cooper, Maj. J. A. Fain, Jr., and Maj. J. Jannarone of the 6510th Test Wing and Maj. P. Tackabury of the Test Pilot School, Edwards Air Force Base, for their contribution in refining the high angle of attack flying quality rating scale and their professional approach in accomplishing the sometimes tedious simulation experiments.

Finally, appreciation is extended to Mr. P. Kelly of Grumman Aircraft Co. and Mr. M. Humphreys of the Naval Air Test Center for support in obtaining much of the F-14 data and information, to Mr. R. Wood of the Air Force Flight Test Center for invaluable comments and suggestions concerning the flying quality rating scale, and to Mr. R. Woodcock (AFWAL/FIGC) for his careful critique and editorial refinement of this final report.

TABLE OF CONTENTS

LIST OF ILLUSTRATIONS

LIST OF ILLUSTRATIONS (Cont'd.)

LIST OF ILLUSTRATIONS (Cont'd.)

LIST OF ILLUSTRATIONS (Cont'd.)

LIST OF TABLES

NOMENCLATURE

AOA	Angle of attack
$a_{x_{cg}}, a_{y_{cg}}, a_{z_{cg}}$	Body-mounted accelerometer signals at center of gravity for linear longitudinal, lateral, and normal acceleration, respectively, ft/sec^2
$a_{x'}, a_{y'}, a_{z'}$	Body-mounted accelerometer signals at any arbitrary point for linear longitudinal, lateral, and normal acceleration, respectively, ft/sec^2
b	Wing Reference span, ft
$\bar{c}$	Wing mean aerodynamic chord, ft
c.g.	Center of gravity
C_D	Dimensionless drag coefficient
$C_{D(\ )}$	Change in C_D with change in state variable quantity, ( ): $\frac{\partial C_D}{\partial(\ )}$
C_L	Dimensionless stability-axis lift coefficient
$C_{L(\ )}$	Change in C_L with change in state variable quantity, ( ): $\frac{\partial C_L}{\partial(\ )}$
C_ℓ	Dimensionless body-axis rolling moment coefficient
$C_{\ell(\ )}$	Change in C_ℓ with change in state variable quantity, ( ): $\frac{\partial C_\ell}{\partial(\ )}$
C_m	Dimensionless body-axis pitching moment coefficient
$C_{m(\ )}$	Change in C_m with change in state variable quantity, ( ): $\frac{\partial C_m}{\partial(\ )}$
C_n	Dimensionless body-axis yawing moment coefficient
$C_{n(\ )}$	Change in C_n with change in state variable quantity, ( ): $\frac{\partial C_n}{\partial(\ )}$

C_x	Dimensionless body-axis longitudinal force coefficient
C_y	Dimensionless body-or stability-axis side force coefficient
$C_{y_{(\ )}}$	Change in C_y with change in state variable quantity, ( ): $\frac{\partial C_y}{\partial (\ )}$
C_z	Dimensionless body-axis normal force coefficient
D	Total drag, $\bar{q}\ S\ C_D$, lbs
F_{LS}	Lateral stick force, Appendix I, lbs
F_p	Rudder pedal force, Appendix I, lbs
g	Gravitational acceleration, 32.2 ft/sec^2
H (or h)	Reference altitude, ft
I_x	Moment of inertia about x-body axis, slug-ft^2
I_y	Moment of inertia about y-body axis, slug-ft^2
I_z	Moment of inertia about z-body axis, slug-ft^2
I_{xz}	Product of inertia about x-z body axes, slug-ft^2
K_{xf}	Crossfeed gain for $\delta_{stk} \rightarrow \delta_r$ crossfeed, Appendix I, deg/in
K_{δ_a}	Gain for $\delta_{stk} \rightarrow \delta_a$ Control, Appendix I, deg/in
$K_{\beta}^{C_{m_{\delta_{stab}}}}$	Correction factor to account for effect of δ_{stab} on C_m with sideslip, $\frac{\partial C_{m_{\delta_{stab}}}}{\partial \beta}$, Appendix I, 1/deg^2

L	Total lift, $\bar{q}SC_L$, lbs
L_1	Aileron command travel limit for roll-rate-command augmentation, Appendix I, deg
L_2	Command travel limit for δ_r with $\delta_{stk} \rightarrow \delta_r$ crossfeed, Appendix I, deg
$\ell x, \ell y, \ell z$	Coordinates of an arbitrary point, relative to center of gravity, for accelerometer signal, body axes, ft
$\mathcal{L}$, M, N	Total body-axis rolling, pitching, and yawing moment, respectively, due to aerodynamics and thrust, ft/lbs
M	Mach Number
m	Aircraft mass, slugs
P, Q, R, (or p, q, r)	Total inertial angular body-axis roll, pitch, and yaw velocity, respectively, rad/sec
$\bar{q}$	Dynamic pressure, $1/2\ \rho V_T^2$, lbs/ft^2
S	Reference wing area, ft^2
T	Aircraft thrust, lbs
U, V, W	Components of total velocity along X–, Y–, and Z– body axes, respectively, ft/sec
V_T	Total aircraft inertial translational velocity, ft/sec
W	Aircraft weight, lbs
X, Y, Z	Reference longitudinal, lateral, and vertical axes, respectively
X_{cg}	Aircraft longitudinal center of gravity, % $\bar{c}$
X_{ref}	Reference longitudinal center of gravity, % $\bar{c}$
Y_A	Total side force, $\bar{q}SC_y$, lbs
z_j	Offset of thrustline from X-body axis, ft

NOMENCLATURE (cont'd)

α	Aircraft angle of attack, deg
β	Sideslip angle, deg
γ	Longitudinal flight path angle, deg
δ_a	Aileron surface position, deg
δ_{stk}	Lateral stick position, Appendix I, $\delta_{stk} = K_{\delta_a}\,\delta_a + 11.58\,\delta_{sp}$, in.
δ_r	Rudder surface position, deg
δ_{sp}	Spoiler position, deg
δ_{stab} (or δ_s)	Horizontal stabilizer position, deg
$\Delta C_{D_{STORES}}$	Incremental drag coefficient due to external stores, Appendix I
$\Delta C_{D(\ )}$	Incremental drag coefficient due to state variable
$\Delta C_{L_{\beta=0}}$	Incremental lift coefficient at zero sideslip, Appendix II
ΔC_m	Incremental pitching moment coefficient
$\Delta C_{m_{\beta=0}}$	Incremental pitching moment coefficient at zero sideslip
$\Delta C_{n_{\delta_s}}$	Incremental yawing moment coefficient due to stabilator position, Appendix II
λ	Lateral flight path angle, deg
ξ	Thrust inclination angle, deg
ψ, θ, φ	Directional, longitudinal, and lateral Euler angles, respectively, deg

NOMENCLATURE (concluded)

Subscripts

B	Body-axis
BASIC	Basic controls-fixed aerodynamic force or moment coefficient
cg	Center of gravity
i,j,k,ℓ	Parameters to identify various sets of derivative values, Appendix I
ref	Reference
s	Stability-axis
T	Trim
W	Wind-axis
( )	State variable, e.g., $\alpha, \beta, p, q, r, \delta_a$

Math Symbols

$(\dot{\ })$	Derivative, time rate of change
∂	Partial derivative

APPENDIX I

F-4J EXTENDED ANGLE-OF-ATTACK SIMULATION MODEL

A. INTRODUCTION

This appendix documents the mathematical model used in the unpiloted (digital) and piloted high AOA simulations of a generic high-speed, twin-jet, fighter-type airplane. The model represents a relatively "clean" aircraft (no flap, slat, or gear deflection) based upon an F-4J, with external stores consisting of one centerline fuel tank and one air-to-air missile. Four different generic configurations are generated by changing a limited number of aerodynamic coefficients.

The appendix is organized as follows: Section B presents the equations of motion including a discussion of assumptions, axis systems and transformations. The equations for the aerodynamic force and moment coefficients are presented in Section C. The airplane physical characteristics and control system are described in Section D. Section E summarized the data sources. The aerodynamic coefficient data are presented in Section F. The coefficient "lookup" tables are listed subsequentially in Table 9 and plotted in Figs. 5 to 28. Validation of the model with flight test data is given in Section G.

B. EQUATIONS OF MOTION

The nonlinear six-degree-of-freedom aircraft equations of motion used in the simulation programs are consistent with the following assumptions.

1. Assumptions

a. The airframe is assumed to be a rigid body.

b. The earth is assumed to be fixed in inertial space.

c. The mass and mass distribution of the vehicle are assumed to be constant.

d. The aircraft has a plane of symmetry.

e. Effects associated with rotation of the vertical relative to inertial space are assumed negligible; the magnitude of the gravity vector is assumed constant.

2. Axis Systems

All the axis systems (see Fig. 1) have their origin at the aircraft center of gravity (c.g.). The Earth Axis system is oriented with the Z_E axis along the local gravity vector and the X_E, Y_E axes in a horizontal plane with arbitrary, but fixed, direction.

The Body Axes are fixed in the aircraft with the X_B axis positive forward along the fuselage reference line. The Z_B axis is in the plane of symmetry, positive down, and the Y_B axis is perpendicular to the plane of symmetry, positive out the right wing. The Body Axes are located relative to the Earth Axes by conventional Euler Angles Ψ, Θ, and Φ. Ψ is a rotation of the Body Axes from the Earth Axes about the Z_E axis; Θ is a rotation about the intermediate Y_B axis; and, finally, Φ is about the X_B axis. All angles and angular rates are positive in a righthanded sense.

The final axis system is called Flight Path Axes. They are aligned with the aircraft inertial velocity. For the still-air case considered here they are identical to Wind Axes (usually aligned with the aircraft velocity relative to the air mass). Herein we use the more conventional W subscript and Flight Path, Flight, and Wind interchangeably. The X_W axis lies along the aircraft total velocity vector, V_T; the Z_W axis is in the aircraft plane of symmetry; and the Y_W axis completes the right-handed orthogonal set. The Wind or Flight Axes are located relative to the body by the angles of attack, α, and sideslip, β; α is a rotation about the Y_B axis and β a rotation about the Z_W axis (if $\alpha = 0$).

The transformation from Flight Path Axes to Body Axes is given by:

$$\begin{bmatrix} X_B \\ Y_B \\ Z_B \end{bmatrix} = \begin{bmatrix} \cos\alpha\cos\beta & -\cos\alpha\sin\beta & -\sin\alpha \\ \sin\beta & \cos\beta & 0 \\ \sin\alpha\cos\beta & -\sin\alpha\sin\beta & \cos\alpha \end{bmatrix} \begin{bmatrix} X_W \\ Y_W \\ Z_W \end{bmatrix} \qquad (1)$$

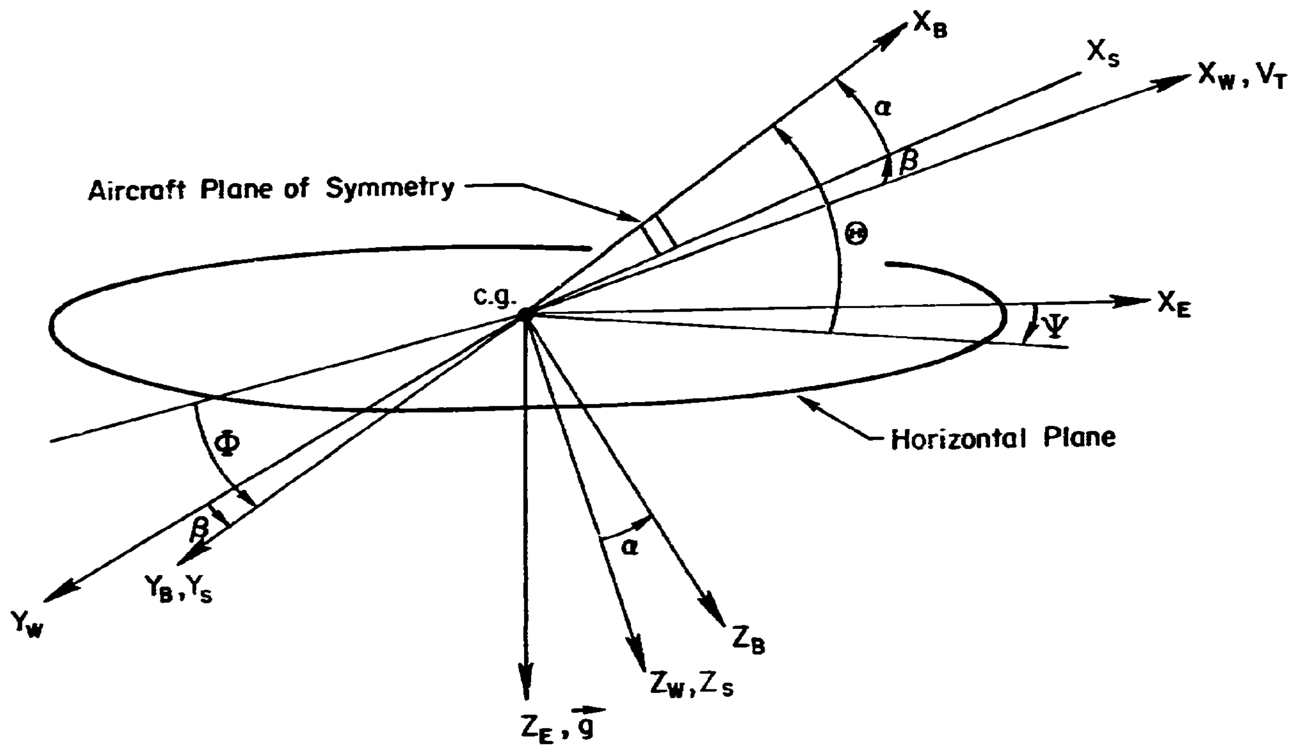

Figure 1. Axis Systems

3. Moment Equations

P, Q, and R are the instantaneous components of the aircraft total inertial angular velocity vector in the X_B, Y_B, Z_B Body Axes. The derivatives of these components with respect to time are related to the applied moments about the center of mass by:

$$\dot{P} = (c_1R + c_2P)Q + c_3\mathcal{L} + c_4\mathcal{N}$$

$$\dot{Q} = c_5RP + c_6(R^2 - P^2) + c_7\mathcal{M} \qquad (2)$$

$$\dot{R} = (c_8P + c_9R)Q + c_4\mathcal{L} + c_{10}\mathcal{N}$$

where

$$c_1 = G\left\{(I_y - I_z)I_z - I_{xz}^2\right\} \qquad c_6 = I_{xz}/I_y$$

$$c_2 = G\left\{I_x - I_y + I_z\right\}I_{xz} \qquad c_7 = 1./I_y \qquad (3)$$

$$c_3 = G\,I_z \qquad c_8 = G\left\{(I_x - I_y)I_x + I_{xz}^2\right\}$$

$$c_4 = G\,I_{xz} \qquad c_9 = G\left\{I_y - I_z - I_x\right\}I_{xz}$$

$$c_5 = (I_z - I_x)/I_y \qquad c_{10} = GI_x$$

$$G = 1/(I_xI_z - I_{xz}^2)$$

I_x, I_y, I_z, and I_{xz} are the moments and product of inertia with respect to the Body Axes. $\mathcal{L}$, $\mathcal{M}$, and $\mathcal{N}$ are moments about the Body Axes due to aerodynamics and aircraft thrust.

4. Force Equations

Flight Path Axes force equations are used for computational efficiency. The derivatives of α, β, and the aircraft total inertial translational velocity, V_T, are related to the external forces by:

$$\dot{\alpha} = Q - \tan \beta(P \cos \alpha + R \sin \alpha) + Z_W/(mV_T \cos \beta)$$

$$\dot{\beta} = P \sin \alpha - R \cos \alpha + Y_W/(mV_T) \qquad (4)$$

$$\dot{V}_T = X_W/m$$

X_W, Y_W, and Z_W are the components of the total external forces (aerodynamic, thrust, and gravity) along the Flight Path Axes. m is the aircraft mass.

The $\dot{\alpha}$ equation is limited in accuracy to small sideslip angles. The large excursions in angles of attack and sideslip encountered in the piloted simulation necessitated a change in definition of $\dot{\alpha}$. The Body-Axis equation for vertical acceleration, $\dot{w}$, was substituted:

$$\dot{w} = QV_T \cos \beta - V_T \sin \beta\ (P \cos \alpha + R \sin \alpha) + Z_W/m$$

and the definitions for α and β were $\alpha = \sin^{-1} w/V_T$, $\beta = \sin^{-1} v/V_T$. These excursions were not experienced in the preliminary analytical work performed in preparation for the piloted simulation.

5. Thrust Geometry

The thrust is assumed to lie in the aircraft plane of symmetry and is oriented with respect to the Body Axes by the thrust inclination, ξ, and offset, z_j, as indicated in the sketch below.

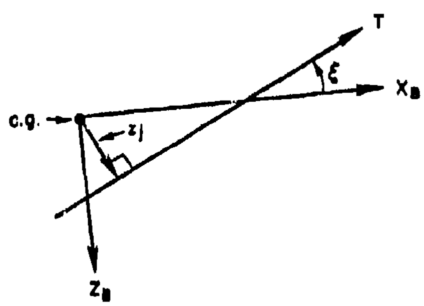

6. Body Axis Moments

The roll, $\mathcal{L}$, and yaw, $\mathcal{N}$, moments are due to aerodynamics only, while the pitching moment, $\mathcal{M}$, includes a thrust term. These are given by:

$$\mathcal{L} = \bar{q}SbC_\ell \quad ; \quad \mathcal{M} = \bar{q}S\bar{c}C_m + z_jT \quad ; \quad \mathcal{N} = \bar{q}SbC_n \qquad (5)$$

$\bar{q}$ is the dynamic pressure; b, $\bar{c}$, and S are the reference span, chord, and wing area, respectively. C_ℓ, C_m, and C_n are the total body-axis non-dimensional aerodynamic moment coefficients (referenced to the c.m.).

7. Flight Path Axis Forces

The forces along the Flight Path Axes have components due to thrust (T), weight (mg), and aerodynamics. They are given by:

$$\begin{aligned}
X_W &= T \cos\beta \cos(\alpha + \xi_o) \\
&\quad + mg\left\{\cos\Theta \cos\Phi \sin\alpha \cos\beta - \sin\Theta \cos\alpha \cos\beta + \cos\Theta \sin\Phi \sin\beta\right\} \\
&\quad + Y_A \sin\beta - D\cos\beta \\
Y_W &= -T \sin\beta \cos(\alpha + \xi_o) \\
&\quad + mg\left\{\cos\Theta \sin\Phi \cos\beta + \sin\Theta \cos\alpha \sin\beta - \cos\Theta \cos\Phi \sin\alpha \sin\beta\right\} \\
&\quad + Y_A \cos\beta + D \sin\beta \\
Z_W &= -T \sin(\alpha + \xi_o) + mg\left\{\sin\Theta \sin\alpha + \cos\Theta \cos\Phi \cos\alpha\right\} - L
\end{aligned} \tag{6}$$

L, D, and Y_A are the aerodynamic forces and are given by:

$$\begin{aligned}
L &= \bar{q}SC_L \\
D &= \bar{q}SC_D \\
Y_A &= \bar{q}SC_y
\end{aligned} \tag{7}$$

C_L, C_D, and C_y are the lift, drag, and side force coefficients. Lift, L, and drag, D, are assumed in the plane of symmetry; lift positive up and perpendicular to the velocity vector, drag positive aft and along the projection of the total velocity in the plane of symmetry. The side force Y_A is that component of the total aerodynamic force which is perpendicular to the plane of symmetry; it lies along the Y_B axis and is positive out the right wing.

It should be noted that the drag and side force are not the same as the X and Y Flight Path Axes forces for non-zero sideslip, see Fig. 2. The aerodynamic forces instead have been defined in terms of the axes in which aerodynamic data are most frequently available.

8. Body Axis Euler Angle Rates

The Body Axis Euler angle rates are related to the angular velocity components by:

$$\begin{aligned} \dot{\Psi} &= (R \cos \Phi + Q \sin \Phi)/\cos \Theta \\ \dot{\Theta} &= Q \cos \Phi - R \sin \Phi \\ \dot{\Phi} &= P + \dot{\Psi} \sin \Theta \end{aligned} \tag{8}$$

9. Body Axis Velocities

The components of the total velocity along the Body Axes are:

$$\begin{aligned} U &= V_T \cos \alpha \cos \beta \\ V &= V_T \sin \beta \\ W &= V_T \sin \alpha \cos \beta \end{aligned} \tag{9}$$

10. Earth Axis Velocities

The Body Axis velocities are transformed through the Euler angles to yield the Earth Axis velocities.

$$\begin{aligned} \dot{X}_E &= U \cos \Theta \cos \Psi + W(\cos \Phi \sin \Theta \cos \Psi + \sin \Phi \sin \Psi) \\ &\quad + V(\sin \Phi \sin \Theta \cos \Psi - \cos \Phi \sin \Psi) \\ \dot{Y}_E &= U \cos \Theta \sin \Psi + V(\sin \Phi \sin \Theta \sin \Psi + \cos \Phi \cos \Psi) \\ &\quad + W(\cos \Phi \sin \Theta \sin \Psi - \sin \Phi \cos \Psi) \\ \dot{Z}_E &= -U \sin \Theta + V \sin \Phi \cos \Theta + W \cos \Phi \cos \Theta \end{aligned} \tag{10}$$

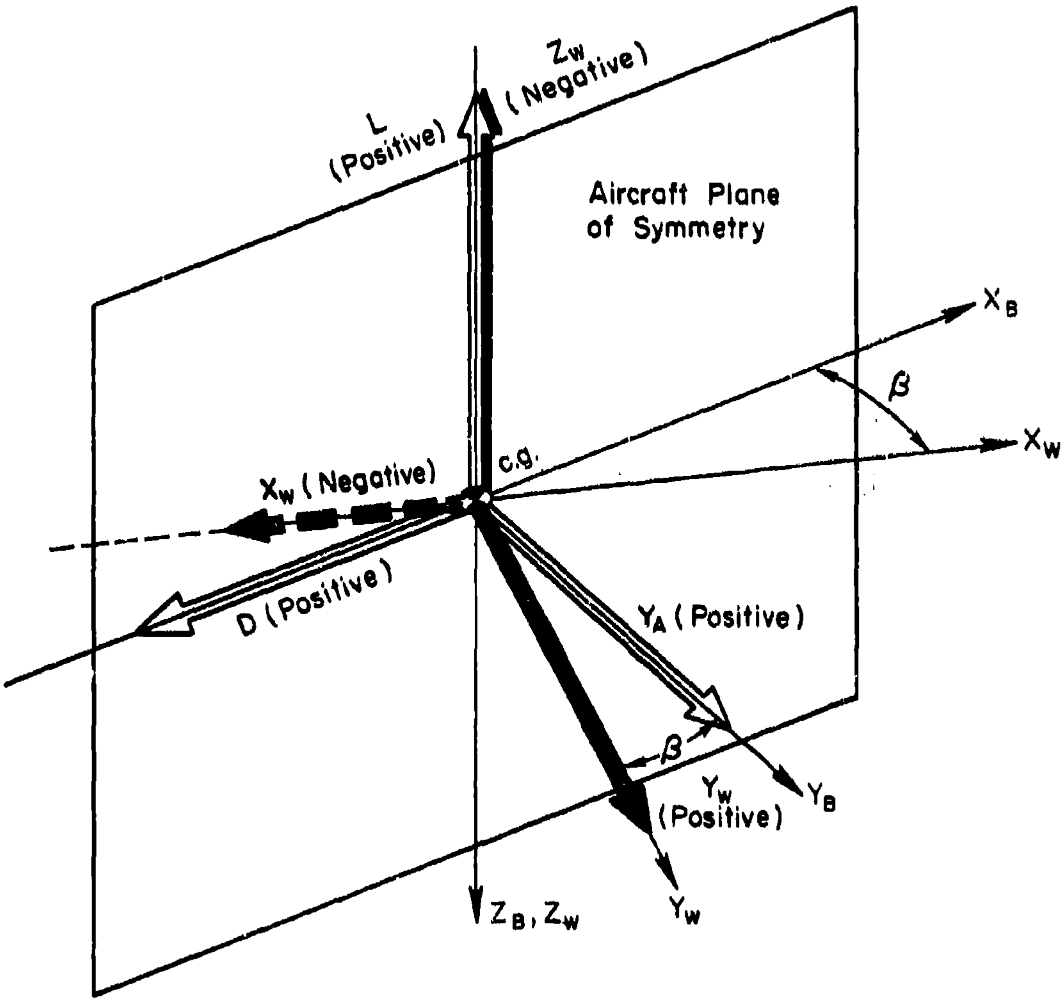

Figure 2. Relation of Aerodynamic Force Axis System to Wind Axes

11. **Aircraft Controls**

The aircraft is assumed to have pitch, roll, and yaw controls, i.e., δ_{stab}, δ_a, δ_{sp}, and δ_r. Positive deflections and travel limits for these controls are given in Section D of this appendix.

12. **Auxiliary Variables**

Additional variables which are useful in aircraft dynamics studies are given below.

a. Flight Path Inclination Angle, γ

$$\tan \gamma = -\dot{Z}/\sqrt{\dot{X}^2 + \dot{Y}^2}$$

or

$$\sin \gamma = -\dot{Z}/V_T \tag{11}$$

or

$$\sin \gamma = \sin \Theta \cos \alpha \cos \beta - \cos \Theta \sin \Phi \sin \beta - \cos \Theta \cos \Phi \sin \alpha \cos \beta$$

b. **Altitude Rate, $\dot{H}$**

$$\dot{H} = -\dot{Z} \tag{12}$$

c. Body-Mounted Accelerometer Signals, at Center of Gravity $a_{x_{cg}}$, $a_{y_{cg}}$, $a_{z_{cg}}$

$$\begin{bmatrix} a_{x_{cg}} \\ a_{y_{cg}} \\ a_{z_{cg}} \end{bmatrix} = \begin{bmatrix} \cos \alpha \cos \beta & -\cos \alpha \sin \beta & -\sin \alpha \\ \sin \beta & \cos \beta & 0 \\ \sin \alpha \cos \beta & -\sin \alpha \sin \beta & \cos \alpha \end{bmatrix} \times \begin{bmatrix} \dot{V}_T \\ V_T(\dot{\beta} - P \sin \alpha + R \cos \alpha) \\ V_T \cos \beta[\dot{\alpha} - Q + \tan \beta(P \cos \alpha + R \sin \alpha)] \end{bmatrix} - g \begin{bmatrix} -\sin \Theta \\ \cos \Theta \sin \Phi \\ \cos \Theta \cos \Phi \end{bmatrix} \tag{13}$$

or

$$\begin{bmatrix} a_{x_{cg}} \\ a_{y_{cg}} \\ a_{z_{cg}} \end{bmatrix} = \frac{1}{m} \begin{bmatrix} T \cos \xi_o - D \cos \alpha + L \sin \alpha \\ Y_A \\ -T \sin \xi_o - D \sin \alpha - L \cos \alpha \end{bmatrix}$$

d. Body-Mounted Accelerometer Signals at Arbitrary Point (ℓ_x, ℓ_y, ℓ_z) in Body, a_x', a_y', a_z'

$$\begin{bmatrix} a_x' \\ a_y' \\ a_z' \end{bmatrix} = \begin{bmatrix} a_{x_{cg}} \\ a_{y_{cg}} \\ a_{z_{cg}} \end{bmatrix} + \begin{bmatrix} 0 & \ell_z & -\ell_y \\ -\ell_z & 0 & \ell_x \\ \ell_y & -\ell_x & 0 \end{bmatrix} \begin{bmatrix} \dot{P} \\ \dot{Q} \\ \dot{R} \end{bmatrix}$$

$$+ \begin{bmatrix} 0 & -R & Q \\ R & 0 & -P \\ -Q & P & 0 \end{bmatrix} \begin{bmatrix} 0 & \ell_z & -\ell_y \\ -\ell_z & 0 & \ell_x \\ \ell_y & -\ell_x & 0 \end{bmatrix} \begin{bmatrix} P \\ Q \\ R \end{bmatrix} \quad (14)$$

ℓ_x, ℓ_y, and ℓ_z are the coordinates of the arbitrary point in Body Axes.

e. Stability-Axis Angular Velocities, P_s, Q_s, R_s

A body-fixed Stability Axes system (Ref. 1) may be defined which is located with respect to Body Axes by the trim angle of attack, α_o. The components of the aircraft's total inertial angular velocity in body-fixed Stability Axes are given by:

$$\begin{aligned} P_s &= P \cos \alpha_o + R \sin \alpha_o \\ Q_s &= Q \\ R_s &= -P \sin \alpha_o + R \cos \alpha_o \end{aligned} \quad (15)$$

f. Stability-Axis Euler Angles, Ψ_s, Θ_s, Φ_s

The body-fixed Stability Axes system defined above can be located relative to Earth Axes by a conventional Euler Angle set, Ψ_s, Θ_s, Φ_s. The Stability Axis Euler Angles are related to the Body Axes Euler Angles and the trim angle of attack by:

$$\tan \Psi_s = \frac{\cos \alpha_o \sin \Psi \cos \Theta + \sin \alpha_o(\sin \Psi \sin \Theta \cos \Phi - \cos \Psi \sin \Phi)}{\cos \alpha_o \cos \Psi \cos \Theta + \sin \alpha_o(\cos \Psi \sin \Theta \cos \Phi + \sin \Psi \sin \Phi)}$$

$$\sin \Theta_s = \cos \alpha_o \sin \Theta - \sin \alpha_o \cos \Theta \cos \Phi \tag{16}$$

or

$$\tan \Theta_s = \cos \Phi_s \left\{ \frac{\cos \alpha_o \sin \Theta - \sin \alpha_o \cos \Theta \cos \Phi}{\cos \alpha_o \cos \Theta \cos \Phi + \sin \alpha_o \sin \Theta} \right\}$$

and

$$\tan \Phi_s = \frac{\cos \Theta \sin \Phi}{\cos \alpha_o \cos \Theta \cos \Phi + \sin \alpha_o \sin \Theta}$$

g. Stability-Axis Euler Angle Rates, $\dot{\Psi}_s$, $\dot{\Theta}_s$, $\dot{\Phi}_s$

$$\dot{\Psi}_s = (R_s \cos \Phi_s + Q_s \sin \Phi_s)/\cos \Theta_s$$

$$\dot{\Theta}_s = Q_s \cos \Phi_s - R_s \sin \Phi_s \tag{17}$$

$$\dot{\Phi}_s = P_s + \dot{\Psi}_s \sin \Theta_s$$

h. Flight Path Azimuth Angle, λ

$$\tan \lambda = \dot{Y}/\dot{X} \tag{18}$$

C. AERODYNAMIC FORCE AND MOMENT COEFFICIENT EQUATIONS

Aerodynamic forces and moments have been defined in terms of the total non-dimensional aerodynamic coefficients, i.e., the stability-axis force coefficients C_L, C_D, C_y and the body-axis moment coefficients C_ℓ, C_m, C_n. As shown in Fig. 3, these are functions of the aircraft state, the control surfaces, tabular coefficient and derivative data, and constant parameters.

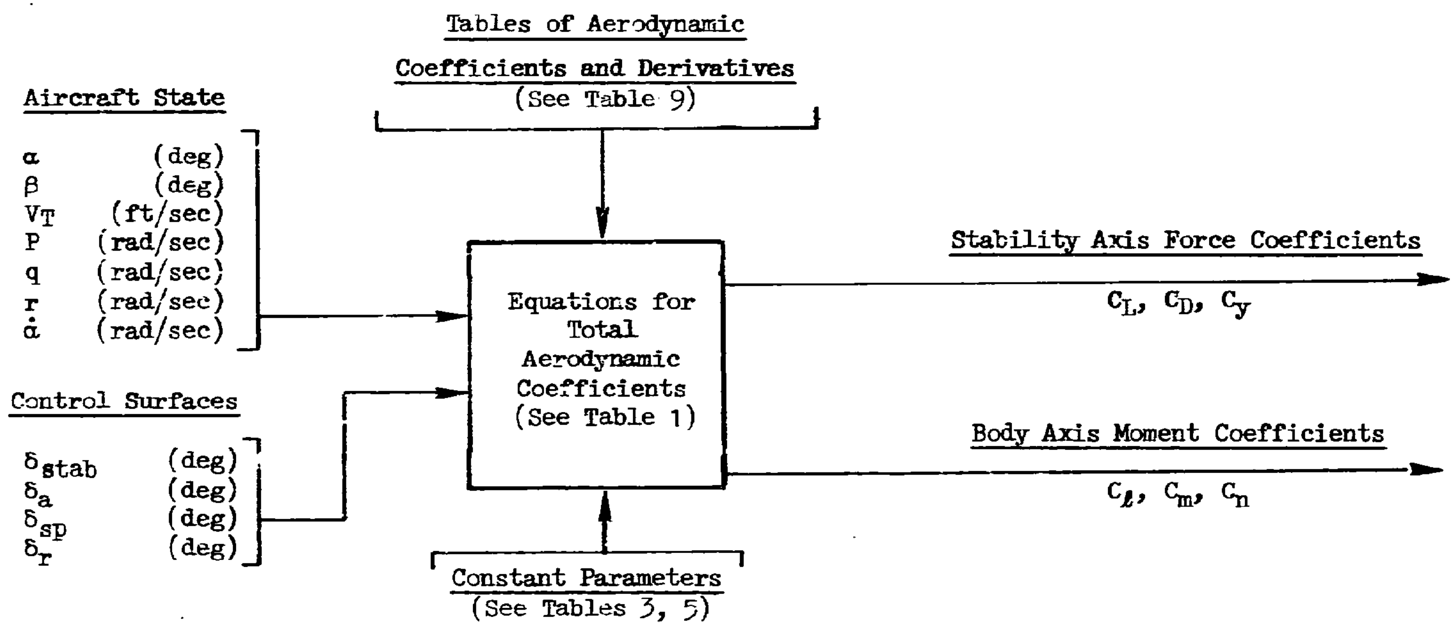

Figure 3. Schematic for Computation of Total Aerodynamic Force and Moment Coefficients

The coefficient equations are given in Table 1. A summary of the tabular functions is given in Table 2 (the data is given in Section F) and the constant parameters are presented in Tables 3 and 5. As indicated in Table 2, all tabular data are given for 5-deg increments in α for either 0 deg $\leq \alpha \leq$ 110 deg or 0 deg $\leq \alpha \leq$ 45 deg. Linear interpolation between adjacent data points was used to obtain derivative values for intermediate values of α. All coefficients and derivatives except $C_{L_{BASIC}}$ and $C_{m_{BASIC}}$ are symmetric functions of α and the absolute value of α was used to obtain the derivative value. $C_{m_{BASIC}}$ is an anti-symmetric function of α; as indicated in Table 1, $|\alpha|$ is used to obtain the table value and the sign of the appropriate term is changed for negative α's. In general for $|\alpha|$'s which exceed the range of the tables, the derivative value for the maximum $|\alpha|$ given in the table is used. This is shown explicitly in Table 1, where the complete equations have been given for each α range. It should be noted that, except for C_L, the equations themselves are not dependent on the α range. $C_{L_{BASIC}}$ is not quite anti-symmetric; the explicit equations for lift coefficient at negative angles of attack are given in Table 1.

ΔC_{m_k} is the only two-dimensional function used; the table contains values for $|\beta|$ from 0 deg to 30 deg in 5 deg increments. For $|\beta|$ > 30 deg, the table values for β = 30 deg were used. The organization of the data is discussed further in Section F.

As Table 2 indicates, there are two sets of data for each of the derivatives $C_{\ell_{\beta i}}$, $C_{\ell_{pj}}$, ΔC_{m_k}, and $C_{n_{\beta_\ell}}$. Selecting the proper combinations of these derivatives results in the desired four basic aircraft configurations as indicated in Table 4.

TABLE 1. AERODYNAMIC COEFFICIENT EQUATIONS

a) Stability Axis Force Coefficients

Coef.	α Range	Equation
Lift	$-180^\circ \le \alpha < -110^\circ$	$C_L = 2\,C_{L_{BASIC}}(0^\circ) - C_{L_{BASIC}}(110^\circ) + C_{L_{\delta_{stab}}}(110^\circ)\,\delta_{stab}$
	$-110^\circ \le \alpha < 0^\circ$	$C_L = 2\,C_{L_{BASIC}}(0^\circ) - C_{L_{BASIC}}(\lvert\alpha\rvert) + C_{L_{\delta_{stab}}}(\lvert\alpha\rvert)\,\delta_{stab}$
	$0^\circ \le \alpha < 110^\circ$	$C_L = C_{L_{BASIC}}(\alpha) + C_{L_{\delta_{stab}}}(\alpha)\,\delta_{stab}$
	$110^\circ \le \alpha < 180^\circ$	$C_L = C_{L_{BASIC}}(110^\circ) + C_{L_{\delta_{stab}}}(110^\circ)\,\delta_{stab}$
Drag	$\lvert\alpha\rvert < 110^\circ$	$C_D = C_{D_{BASIC}}(\lvert\alpha\rvert) + \Delta C_{D_{STORES}}$
	$110^\circ \le \lvert\alpha\rvert \le 180^\circ$	$C_D = C_{D_{BASIC}}(110^\circ) + \Delta C_{D_{STORES}}$
Sideforce	$\lvert\alpha\rvert < 45^\circ$	$C_y = C_{y_\beta}(\lvert\alpha\rvert)\,\beta + C_{y_{\delta a}}\,\delta a + C_{y_{\delta sp}}\,\delta sp + C_{y_{\delta r}}(\lvert\alpha\rvert)\,\delta r$
	$45^\circ \le \lvert\alpha\rvert < 110^\circ$	$C_y = C_{y_\beta}(\lvert\alpha\rvert)\,\beta + C_{y_{\delta a}}\,\delta a + C_{y_{\delta sp}}\,\delta sp + C_{y_{\delta r}}(45^\circ)\,\delta r$
	$110^\circ \le \lvert\alpha\rvert \le 180^\circ$	$C_y = C_{y_\beta}(110^\circ)\,\beta + C_{y_{\delta a}}\,\delta a + C_{y_{\delta sp}}\,\delta sp + C_{y_{\delta r}}(45^\circ)\,\delta r$

TABLE 1. AERODYNAMIC COEFFICIENT EQUATIONS (Concluded)

b) Body Axis Moment Coefficients

Coef.	α Range	Equation
Rolling Moment $\mathcal{L}$	$\lvert\alpha\rvert < 45°$	$C_\ell = C_{\ell_{\beta_i}}(\lvert\alpha\rvert)\beta + \frac{b}{2V_T}\{C_{\ell_p}(\lvert\alpha\rvert)p + C_{\ell_r}(\lvert\alpha\rvert)r\}$ $+ C_{\ell_{\delta_a}}(\lvert\alpha\rvert)\delta_a + C_{\ell_{\delta_{sp}}}(\lvert\alpha\rvert)\delta_{sp} + C_{\ell_{\delta_r}}(\lvert\alpha\rvert)\delta_r$
	$45° \le \lvert\alpha\rvert < 110°$	$C_\ell = C_{\ell_{\beta_i}}(\lvert\alpha\rvert)\beta + \frac{b}{2V_T}\{C_{\ell_{p_j}}(45°)p + C_{\ell_r}(45°)r\}$ $+ C_{\ell_{\delta_a}}(45°)\delta_a + C_{\ell_{\delta_{sp}}}(45°)\delta_{sp} + C_{\ell_{\delta_r}}(45°)\delta_r$
	$110° \le \lvert\alpha\rvert \le 180°$	$C_\ell = C_{\ell_{\beta_i}}(110°)\beta + \frac{b}{2V_T}\{C_{\ell_{p_j}}(45°)p + C_{\ell_r}(45°)r\}$ $+ C_{\ell_{\delta_a}}(45°)\delta_a + C_{\ell_{\delta_{sp}}}(45°)\delta_{sp} + C_{\ell_{\delta_r}}(45°)\delta_r$
Pitching Moment $\mathcal{M}$	$\lvert\alpha\rvert < 45°$	$C_{m_{REF}} = \{C_{m_{BASIC}}(\lvert\alpha\rvert)\} SGA + \Delta C_{m_K}(\lvert\alpha\rvert, \beta^*)$ $+ \frac{\bar{c}}{2V_T}\{C_{m_q}(\lvert\alpha\rvert)q + C_{m_{\dot\alpha}}(\lvert\alpha\rvert)\dot\alpha\}$ $+ \{C_{m_{\delta_{stab}}}(\lvert\alpha\rvert) + K_\beta^{C_{m_{\delta stab}}}\lvert\beta\rvert\}\delta_{stab}$ $+ C_{m_{\delta_a}}(\lvert\alpha\rvert)\lvert\delta_a\rvert + C_{m_{\delta_{sp}}}(\lvert\alpha\rvert)\lvert\delta_{sp}\rvert$
	$45° \le \lvert\alpha\rvert < 110°$	$C_{m_{REF}} = \{C_{m_{BASIC}}(\lvert\alpha\rvert)\} SGA + \Delta C_{m_K}(45°, \beta^*)$ $+ \frac{\bar{c}}{2V_T}\{C_{m_q}(45°)q + C_{m_{\dot\alpha}}(45°)\dot\alpha\}$ $+ \{C_{m_{\delta_{stab}}}(\lvert\alpha\rvert) + K_\beta^{C_{m_{\delta stab}}}\lvert\beta\rvert\}\delta_{stab}$ $+ C_{m_{\delta_a}}(45°)\lvert\delta_a\rvert + C_{m_{\delta_{sp}}}(45°)\lvert\delta_{sp}\rvert$
	$110° \le \lvert\alpha\rvert \le 180°$	$C_{m_{REF}} = \{C_{m_{BASIC}}(110°)\} SGA + \Delta C_{m_K}(45°, \beta^*)$ $+ \frac{\bar{c}}{2V_T}\{C_{m_q}(45°)q + C_{m_{\dot\alpha}}(45°)\dot\alpha\}$ $+ \{C_{m_{\delta_{stab}}}(110°) + K_\beta^{C_{m_{\delta stab}}}\lvert\beta\rvert\}\delta_{stab}$ $+ C_{m_{\delta_a}}(45°)\lvert\delta_a\rvert + C_{m_{\delta_{sp}}}(45°)\lvert\delta_{sp}\rvert$
	ALL α	NOTE: for $\lvert\beta\rvert \le 30°$; $\beta^* = \lvert\beta\rvert$ $\lvert\beta\rvert > 30°$; $\beta^* = 30°$ for $\alpha \ge 0$, $SGA = 1$ for $\alpha < 0$, $SGA = -1$ $C_m = C_{m_{REF}} + \left\{\frac{X_{cg} - X_{REF}}{100}\right\}\{C_L \cos(\alpha) + C_D \sin(\alpha)\}$
Yawing Moment $\mathcal{N}$	$\lvert\alpha\rvert < 45°$	$C_{n_{REF}} = C_{n_{\beta_\ell}}(\lvert\alpha\rvert)\beta + \frac{b}{2V_T}\{C_{n_p}(\lvert\alpha\rvert)p + C_{n_r}(\lvert\alpha\rvert)r\}$ $+ C_{n_{\delta_a}}(\lvert\alpha\rvert)\delta_a + C_{n_{\delta_{sp}}}(\lvert\alpha\rvert)\delta_{sp} + C_{n_{\delta_r}}(\lvert\alpha\rvert)\delta_r$
	$45° \le \lvert\alpha\rvert \le 180°$	$C_{n_{REF}} = C_{n_{\beta_\ell}}(45°)\beta + \frac{b}{2V_T}\{C_{n_p}(45°)p + C_{n_r}(45°)r\}$ $+ C_{n_{\delta_a}}(45°)\delta_a + C_{n_{\delta_{sp}}}(45°)\delta_{sp} + C_{n_{\delta_r}}(45°)\delta_r$
	ALL α	$C_n = C_{n_{REF}} + \left\{\frac{X_{cg} - X_{REF}}{100}\right\}\left\{\frac{\bar{c}}{b}\right\} C_y$

TABLE 2. ORGANIZATION OF
TABULAR AERODYNAMIC DATA

PARAMETERS	FUNCTION OF	UNITS	MNEMONIC AND ARRAY DIMENSIONS	LINE NUMBERS	α GRID*
$C_{L_{BASIC}}$	α	–	CLBAS(23)	2-8	0.(5.)110.
$C_{L_{\delta_{STAB}}}$	α	1/deg	CLSTAB(23)	9-15	0.(5.)110.
$C_{D_{BASIC}}$	α	–	CDBAS(23)	16-22	0.(5.)110.
C_{y_β}	α	1/deg	CYB(23)	23-29	0.(5.)110.
$C_{y_{\delta_r}}$	α	1/deg	CYDR(10)	30-33	0.(5.)45.
$C_{\ell_{\beta_1}}$	α	1/deg	CRB1(23)	34-40	0.(5.)110.
$C_{\ell_{\beta_2}}$	α	1/deg	CRB2(23)	41-47	0.(5.)110.
$C_{\ell_{p_1}}$	α	1/rad	CRP1(10)	48-51	0.(5.)45.
$C_{\ell_{p_2}}$	α	1/rad	CRP2(10)	52-55	0.(5.)45.
C_{ℓ_r}	α	1/rad	CRR(10)	56-59	0.(5.)45.
$C_{\ell_{\delta_a}}$	α	1/deg	CRDA(10)	60-63	0.(5.)45.
$C_{\ell_{\delta_{sp}}}$	α	1/deg	CRDSP(10)	64-67	0.(5.)45.
$C_{\ell_{\delta_r}}$	α	1/deg	CRDR(10)	68-71	0.(5.)45.
$C_{m_{BASIC}}$	α	–	CMBAS(23)	72-78	0.(5.)110.
ΔC_{m_1}	α, β	–	DCM1(10,7)	79-95	0.(5.)45.
ΔC_{m_2}	α, β	–	DCM2(10,7)	96-112	0.(5.)45.
C_{m_q}	α	1/rad	CMQ(10)	113-116	0.(5.)45.
$C_{m_{\dot{\alpha}}}$	α	1/rad	CMAD(10)	117-120	0.(5.)45.
$C_{m_{\delta_{STAB}}}$	α	1/deg	CMSTAB(23)	121-127	0.(5.)110.
$C_{m_{\delta_a}}$	α	1/deg	CMDA(10)	128-131	0.(5.)45.
$C_{m_{\delta_{sp}}}$	α	1/deg	CMDSP(10)	132-135	0.(5.)45.
$C_{n_{\beta_1}}$	α	1/deg	CNB1(10)	136-139	0.(5.)45.
$C_{n_{\beta_2}}$	α	1/deg	CNB2(10)	140-143	0.(5.)45.
C_{n_p}	α	1/rad	CNP(10)	144-147	0.(5.)45.
C_{n_r}	α	1/rad	CNR(10)	148-151	0.(5.)45.
$C_{n_{\delta_a}}$	α	1/deg	CNDA(10)	152-155	0.(5.)45.
$C_{n_{\delta_{sp}}}$	α	1/deg	CNDSP(10)	156-159	0.(5.)45.
$C_{n_{\delta_r}}$	α	1/deg	CNDR(10)	160-163	0.(5.)45.

* 0.(5.)110. indicates values are given for α from 0 deg to 110 deg in 5 deg increments, i.e., 0°., 5°., 10°., ... 100°., 105°., 110°.

TABLE 3. CONSTANT AERODYNAMIC COEFFICIENTS

$\Delta C_{D_{STORES}}(-)$	.0037
$C_{y_{\delta_a}}(1/\text{deg})$	-.000167
$C_{y_{\delta_{sp}}}(1/\text{deg})$	-.00006
$K_{\beta}^{C_{m_{\delta stab}}}(1/\text{deg}^2)$	.00011

TABLE 4. AIRCRAFT CONFIGURATION/DERIVATIVE COMBINATIONS

AIRCRAFT CONFIGURATION	DERIVATIVE INDEX			
	$C_{\ell_{\beta_i}}$ i	$C_{\ell_{p_j}}$ j	ΔC_{m_k} k	$C_{n_{\beta_\ell}}$ ℓ
A	1	1	1	1
B	1	2	1	1
C	2	1	1	1
D	1	1	2	2

D. AIRPLANE PHYSICAL CHARACTERISTICS AND CONTROL SYSTEM

1. Physical Characteristics

This section describes the pertinent dimensions of the airplane (weight, wing area, inertias, etc.) and defines the control surfaces. The model is based upon the F-4J, but is considered to be representative of a generic fighter-type airplane.

The major dimensional parameters for this model are listed in Table 5, the control surfaces are outlined below and control surface limits are given in Table 6.

2. Control System

Longitudinal control is provided by an all-moving horizontal tail. Lateral control is provided by a combination of spoilers and ailerons. The ailerons deflect downward only; the spoilers deflect upward only. The left aileron and right spoiler operate simultaneously, as do the right aileron and left spoiler. Spoiler and aileron deflection are combined by a simple relation:

$$\delta_{sp} = 1.433\delta_a$$

Directional control is provided by a conventional rudder.

The longitudinal control system is outlined in Table 7, and the lateral/directional control system is shown in Fig. 4.

TABLE 5. AIRPLANE DIMENSIONAL PARAMETERS

SYMBOL	DEFINITION	VALUE
b	Wing span, ft	38.67
$\bar{c}$	Wing mean aerodynamic chord, ft	16.04
S	Wing area, ft^2	530
W	Airplane weight, lb	37,000
X_{ref}	Reference center of gravity, $\%\bar{c}$	31
X_{cg}	Actual center of gravity, $\%\bar{c}$	29.3
I_x	Moment of inertia about X-body axis, slug-ft^2	23,850.
I_y	Moment of inertia about Y-body axis, slug-ft^2	127,400.
I_z	Moment of inertia about Z-body axis, slug-ft^2	146,000.
I_{xz}	Product of inertia about X-Z axes, slug-ft^2	2210.
ξ_o	Thrust inclination, deg	5.25
z_j	Thrust offset, ft	-0.336
H	Reference altitude, ft	15,000

TABLE 6.

CONTROL SURFACE DEFINITIONS

SURFACE	DEFLECTION LIMITS, DEG
δ_{stab}, Positive TED	21 up, 9 down
δ_a, Positive Left TED	0 up, 30 down
δ_{sp}, Positive Right TEU	43 up, 0 down
δ_r, Positive TEL	±30

TABLE 7.

LONGITUDINAL CONTROL SYSTEM

- No SAS or CAS
- Basic F-4 manual control system gain, $\delta_{stab} \rightarrow \delta_{long} = 4.16$ deg/in.
- Feel system — simple spring/damper (gradient ~ 3.5 lb/in)
- Breakout — 1.5 to 2 lb

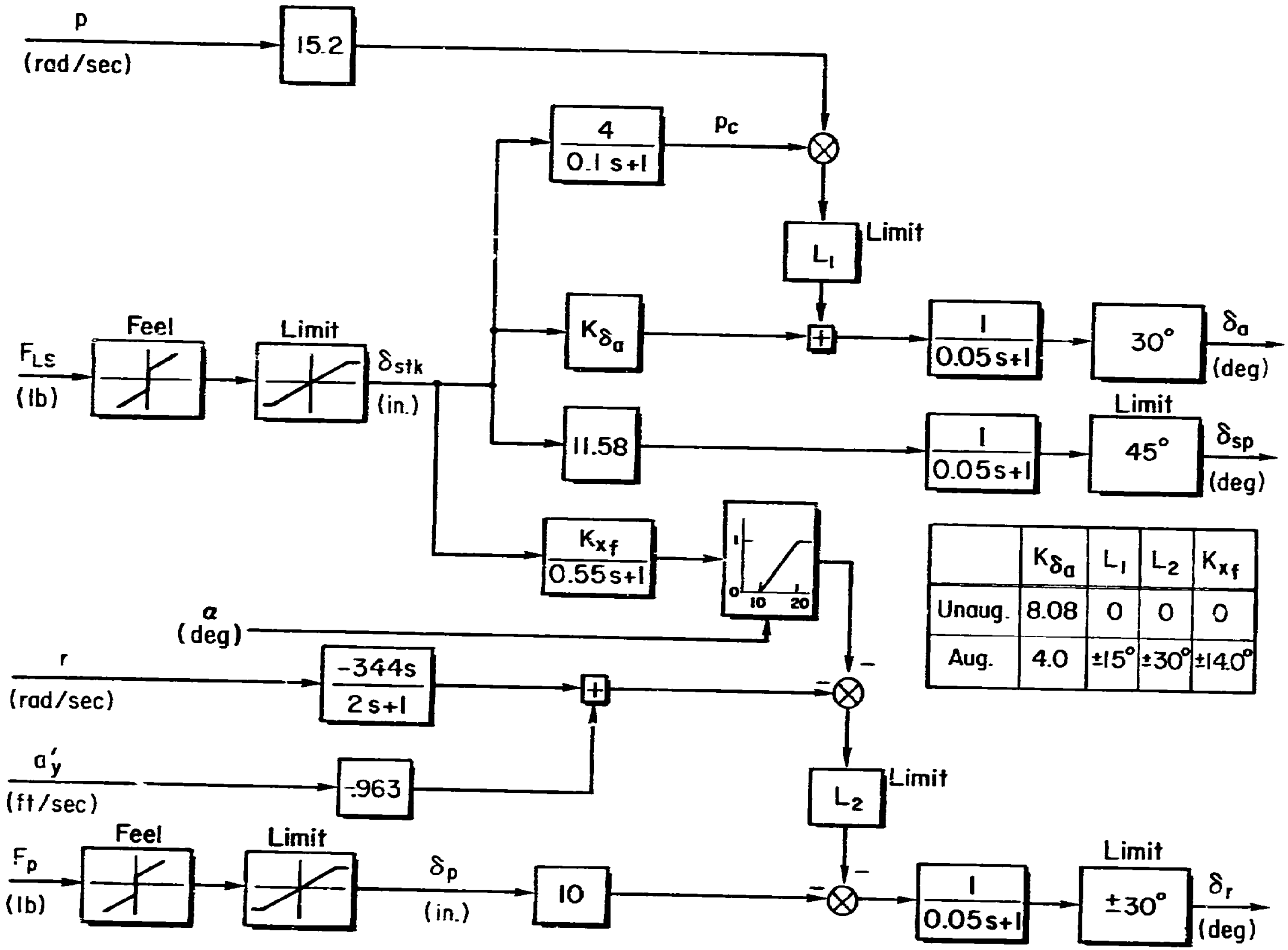

	K_{δ_a}	L_1	L_2	K_{x_f}
Unaug.	8.08	0	0	0
Aug.	4.0	±15°	±30°	±14.0°

Figure -. Lateral/Directional Control System

E. DATA SOURCES

This section outlines the sources for the aerodynamic data presented in this appendix. Reference 16 was used as the initial data base for this simulation model. The Ref. 16 data covers an α range of −5 deg to 31 deg and a β range of −10 deg to 10 deg. Wind tunnel tests of an F-4 model (Ref. 2), covering an α range of −10 deg to 110 deg and a β range of −40 deg to 40 deg, were the primary sources for the extension of static coefficients. Dynamic coefficients were extrapolated based on trends of data available from other sources to 60 deg angle-of-attack, with the intent of making such coefficients simple to mechanize.

Because of the nature of the reference (an STI working paper), some discussion is in order on the data which was used to develop the initial data set. Three separate sources were utilized in Ref. 16.

The first two sets of data were supplied to STI for a previous study. One, Ref. 3, was based on the spin study data (Ref. 4). The second was supplied by NASA Langley and was based on several NASA tunnel investigations (e.g., Refs. 5 and 6). The Ref. 3 tabulation was a function of α, β, and δ_{stab} for the range:

$$0 < \alpha < 90 \text{ deg} \quad ; \quad 0 < \beta < 40 \text{ deg} \quad ; \quad -21 < \delta_{stab} < 0 \text{ deg}$$

The NASA tabulation was a function of α and β for the range:

$$-10 < \alpha < 120 \text{ deg} \; ; \quad -40 < \beta < +40 \text{ deg}$$

Both sets are limited to the very low speed regime (M = 0.2). As a result of comparison, several erroneous data points were discovered in the Ref. 3 data and were reported to the AFFDL.

The third set of data (Ref. 7) was obtained from the NASA Langley Differential Maneuvering Simulation (DMS) investigation of the F-4J and slatted F-4E aircraft. Several key damping derivatives were updated from Ref. 7 based upon NASA correlation between several sets of tunnel data and evaluation of aircraft response obtained in the simulation. These data also are in look-up table format with coefficients as functions of α, M, and H over the range:

$$-5 < \alpha < 30 \text{ deg} \; ; \quad .2 < M < 2.4 \; ; \quad 15{,}000 < H < 45{,}000 \text{ ft}$$

The sideslip coefficients are valid over the range $\beta = \pm 40$ deg. Thrust and drag effects are also modeled in detail.

As originally received, the data did not coalesce at 0.2 M. The data of Ref. 4 were therefore given the most weight at this low Mach and were smoothed into the DMS data by about 0.4 M. The resulting data provide an excellent model of the aircraft over the range:

$$-4 < \alpha < 30 \text{ deg} \; ; \quad -10 < \beta < 10 \text{ deg} \; ; \quad 0.2 < M < 1.0 \; ; \quad 0 < H < 25{,}000 \text{ ft}$$

Besides extension of coefficients for high angles of attack and sideslip, several changes were made to the Ref. 16 data to simplify use of the data. These included normalizing the data for trim Mach Number (determined from previous digital simulations using the Ref. 16 data set), using a single altitude (15,000 ft), and defining values for the second set of the parameters C_{ℓ_β}, C_{n_β}, C_{ℓ_p}, and ΔC_m.

F. AERODYNAMIC COEFFICIENT DATA

The aerodynamic coefficients are tabulated in Table 9 on pages 25 to 27 and plotted in Figs. 5 to 28. All coefficients are functions either of α or of α and β. The aerodynamic data file in Table 9 includes a one-line identifier for each coefficient, plus one or two lines describing the independent variable(s). The formats of these identifying lines are given in Table 8. All coefficients are presented, five to a line, in 5-degree angle-of-attack increments.

For those coefficients which are functions of $0 \leq \alpha \leq 110^\circ$, the values given correspond to α as follows:

```
(0) . . . . . . . . . . . . . . . . . (20)
 .       .       .                  .
 .       .       .                  .
 .       .       .                  .
 .       .       .                  .
(100)  (105)   (110)
```

For $0 \leq \alpha \leq 45^\circ$ the values are as follows:

(0) . . . . (20)

(25) . . . . (45)

TABLE 8.

DATA FILE IDENTIFICATION LINES

Coefficient identifier:	VARIABLE NAME	VARIABLE UNITS	NUMBER OF INDEPENDENT VARIABLES	DATA POINTS PER LINE	NUMBER OF LINES	TOTAL NO. OF POINTS
(1 line)	(A8)	(A8)	(I2)	(I2)	(I2)	(I3)

Independent variable identifier(s):	INDEPENDENT VARIABLE NAME	INDEPENDENT VARIABLE UNITS	MINIMUM VALUE	INCREMENT	MAXIMUM VALUE	NO. OF VALUES
(1-2 lines)	(A8)	(A8)	(E14.6)	(E14.6)	(E14.6)	(I2)

The coefficients DCM1 and DCM2 are functions of both α and β. In this case, α is incremented first, then β:

(0,0) . . . . (20,0)
(25,0) . . . . (45,0)
(0,5) . . . . (20,5)
: :
(25,30). . . . . (α,β)

As an example in interpreting the data file, the file for Cy_β is given below:

```
CYB      PER DEG  1 5 5 23
ALPHA    DEGREES  Ø.,5.,11Ø.,23
-.Ø11    -.Ø11    -.Ø11    -.Ø11    -.Ø11
-.Ø11    -.Ø11    -.ØØ92   -.ØØ79   -.ØØ65
-.ØØ5Ø   -.ØØ36   -.ØØ23   -.ØØØ8   .ØØØ6
.ØØ2Ø    .ØØ3Ø    .ØØ3Ø    .ØØ3Ø    .ØØ3Ø
.ØØ3Ø    .ØØ3Ø    .ØØ3Ø
```

The first line identifies the coefficient; gives the units; indicates that it is a function of one variable, and that it is listed five points per line in five lines, with a total of 23 data points given. The second line identifies α as the independent variable; gives its units; gives the minimum value as 0 deg, the $\Delta\alpha$ increment as 5 deg, and the maximum value as 110 deg, for a total of 23 separate $\Delta\alpha$ points.

TABLE 9. AERODYNAMIC COEFFICIENTS

```
S.O. 1081 EXTENDED AOA DATA;  CRB1 & CRB2 CHANGED 11/20/78
CLBAS              1 5 5 23
ALPHA    DEGREES 0.,5.,110.,23
.1220  .4146  .6834  .9053  .9396
1.010  1.067  1.049  1.024  .969
.927  .872  .798  .677  .546
.418  .289  .157  .025  -.116
-.257  -.402  -.547
CLSTAB  PER DEG  1 5 5 23
ALPHA    DEGREES 0.,5.,110.,23
.00699  .00694  .00676  .00637  .00571
.00513  .00503  .00486  .00463  .00438
.00416  .00393  .00371  .00348  .00324
.00300  .00300  .00300  .00300  .00300
.00300  .00300  .00300
CDBAS              1 5 5 23
ALPHA    DEGREES 0.,5.,110.,23
.035  .066  .130  .247  .382
.510  .655  .786  .911  1.011
1.128  1.245  1.352  1.405  1.451
1.493  1.523  1.542  1.570  1.585
1.600  1.583  1.567
CYB      PER DEG  1 5 5 23
ALPHA    DEGREES 0.,5.,110.,23
-.011  -.011  -.011  -.011  -.011
-.011  -.011  -.0092  -.0079  -.0065
-.0050  -.0036  -.0023  -.0008  .0006
.0020  .0030  .0030  .0030  .0030
.0030  .0030  .0030
CYDR     PER DEG  1 5 2 10
ALPHA2   DEGREES 0.,5.,45.,10
.00151  .00142  .00134  .00130  .00124
.00098  .00073  .00048  .00024  0.0
CRB1     PER DEG  1 5 5 23
ALPHA    DEGREES 0.,5.,110.,23
-.00132  -.00175  -.00236  -.00219  -.00118
-.00006  .00025  -.00010  -.00108  -.0018
-.00222  -.00241  -.00255  -.00268  -.00279
-.00291  -.00300  -.00300  -.00300  -.00300
-.00300  -.00300  -.00300
CRB2     PER DEG  1 5 5 23
ALPHA    DEGREES 0.,5.,110.,23
-.00132  -.00175  -.00236  -.00219  -.00219
-.00219  -.00219  -.00185  -.00152  -.00180
-.00222  -.00241  -.00255  -.00268  -.00279
-.00291  -.00300  -.00300  -.00300  -.00300
-.00300  -.00300  -.00300
CRP1     PER RAD  1 5 2 10
ALPHA2   DEGREES 0.,5.,45.,10
-.304  -.300  -.255  -.102  -.100
-.280  -.304  -.250  -.164  -.100
CRP2     PER RAD  1 5 2 10
ALPHA2   DEGREES 0.,5.,45.,10
-.304  -.300  -.260  -.260  -.260
-.260  -.260  -.250  -.164  -.100
CRR      PER RAD  1 5 2 10
```

TABLE 9. (CONTINUED)

```
ALPHA2   DEGREES 0.,5.,45.,10
.046  .074  .108  .170  .318
.387  .341  .204  .085  .050
CRDA     PER DEG  1 5 2 10
ALPHA2   DEGREES 0.,5.,45.,10
.000448  .000459  .000431  .000405  .000379
.000354  .000312  .000210  .000105  .000000
CRDSP    PER DEG  1 5 2 10
ALPHA2   DEGREES 0.,5.,45.,10
.000130  .000140  .000093  .000066  .000054
.000040  .000030  .000020  .000010  .000000
CRDR     PER DEG  1 5 2 10
ALPHA2   DEGREES 0.,5.,45.,10
.000199  .000165  .000135  .000116  .000092
.000069  .000052  .000035  .000017  .000000
CMBAS             1 5 5 23
ALPHA    DEGREES 0.,5.,110.,23
.000  -.013  -.027  -.033  -.050
-.068  -.093  -.144  -.196  -.242
-.263  -.285  -.318  -.381  -.430
-.475  -.501  -.532  -.571  -.616
-.658  -.695  -.729
DCM1              2 514 70
ALPHA2   DEGREES 0.,5.,45.,10
BETA     DEGREES 0.,5.,30., 7
.0000  .0000  .0000  .0000  .0000
.0000  .0000  .0000  .0000  .0000
-.0080  -.0080  -.0080  -.0138  -.0099
.0018  .0005  .0000  .0000  .0000
-.0170  -.0170  -.0170  -.0235  -.0306
-.0204  -.0160  )000  .0000  .0000
-.0312  -.0312  -.0312  -.0450  -.0580
-.0465  -.0428  -.0025  .0000  .0000
-.0455  -.0455  -.0455  -.0705  -.0800
-.0768  -.0755  -.0087  .0000  .0000
-.0565  -.0565  -.0565  -.0888  -.1000
-.0953  -.0944  -.0106  .0000  .0000
-.0674  -.0674  -.0674  -.1071  -.1200
-.1138  -.1133  -.0125  .0000  .0000
DCM2              2 514 70
ALPHA2   DEGREES 0.,5.,45.,10
BETA     DEGRFES 0.,5.,30.,7
0.0  0.0  0.0  0.0  0.0
0.0  0.0  0.0  0.0  0.0
.0080  .0080  .0080  .0138  .0099
-.0018  -.0005  .0000  .0000  .0000
.0170  .0170  .0170  .0235  .0306
.0204  .0160  .0000  .0000  .0000
.0312  .0312  .0312  .0450  .0580
.0465  .0428  .0025  .0000  .0000
.0455  .0455  .0455  .0705  .0800
.0768  .0755  .0087  .0000  .0000
.0565  .0565  .0565  .0888  .1000
.0953  .0944  .0106  .0000  .0000
.0674  .0674  .0674  .1071  .1200
.1138  .1133  .0125  .0000  .0000
```

TABLE 9. (CONCLUDED)

```
CMQ      PER RAD  1 5 2 10
ALPHA2   DEGREES 0.,5.,45.,10
-3.10  -3.41  -3.78  -3.92  -3.80
-3.62  -3.15  -3.15  -3.15  -3.15
CMAD     PER RAD  1 5 2 10
ALPHA2   DEGREES 0.,5.,45.,10
-1.30  -1.42  -1.58  -1.63  -1.59
-1.52  -1.32  -1.32  -1.32  -1.32
CMSTAB   PER DEG  1 5 5 23
ALPHA    DEGREES 0.,5.,110.,23
-.01010  -.01004  -.00981  -.00926  -.00828
-.00745  -.00733  -.00677  -.00627  -.00572
-.00519  -.00466  -.00414  -.00361  -.00308
-.00256  -.00202  -.00150  -.00097  -.00052
0.00000  0.00000  0.00000
CMDA     PER DEG  1 5 2 10
ALPHA2   DEGREES 0.,5.,45.,10
-.00105  -.00092  -.00079  -.00068  -.00066
-.00066  -.00066  -.00046  -.00066  -.00066
CMDSP    PER DEG  1 5 2 10
ALPHA2   DEGREES 0.,5.,45.,10
.000130  .000079  .000035  .000007  .00000
.000000  .000000  .000000  .000000  .000000
CNB1     PER DEG  1 5 2 10
ALPHA2   DEGREES 0.,5.,45.,10
.0022  .0022  .0021  .0013  -.0006
-.0033  -.0040  -.0038  -.0026  -.0020
CNB2     PER DEG  1 5 2 10
ALPHA2   DEGREES 0.,5.,45.,10
.0022  .0022  .0021  .0013  .0000
-.0005  -.0008  -.0011  -.0014  -.0017
CNP      PER RAD  1 5 2 10
ALPHA2   DEGREES 0.,5.,45.,10
.005  -.014  .007  .023  -.002
.055  .122  .080  .041  .000
CNR      PER RAD  1 5 2 10
ALPHA2   DEGREES 0.,5.,45.,10
-.375  -.361  -.361  -.370  -.502
-.660  -.560  -.372  -.190  .000
CNDA     PER DEG  1 5 2 10
ALPHA2   DEGREES 0.,5.,45.,10
-.000047 -.000048 -.000056 -.000067 -.000068
-.000068 -.000069 -.000070 -.000070 -.000070
CNDSP    PER DEG  1 5 2 10
ALPHA2   DEGREES 0.,5.,45.,10
.0000532 .0000433 .0000288 .0000132 .0000090
.0000044 .0000009 .0000000 .0000000 .0000000
CNDR     PER DEG  1 5 2 10
ALPHA2   DEGREES 0.,5.,45.,10
-.00090  -.00086  -.00078  -.00073  -.00065
-.00050  -.00032  -.00023  -.00014  .00000
```

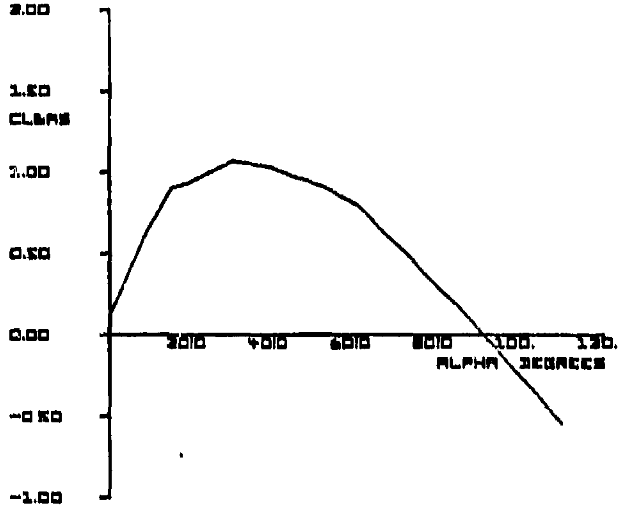

Figure 5. $C_{L_{BASIC}}(\alpha)$

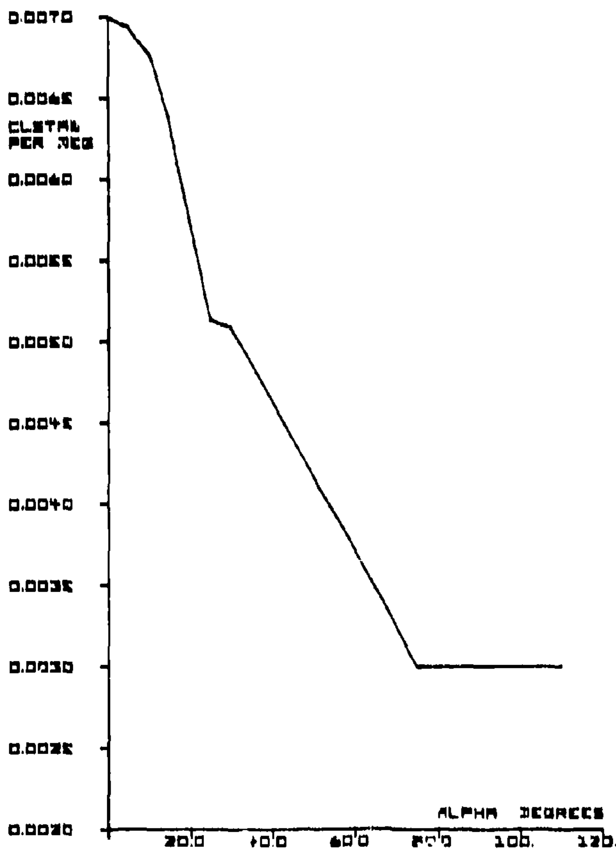

Figure 6. $C_{L_{stab}}(\alpha)$

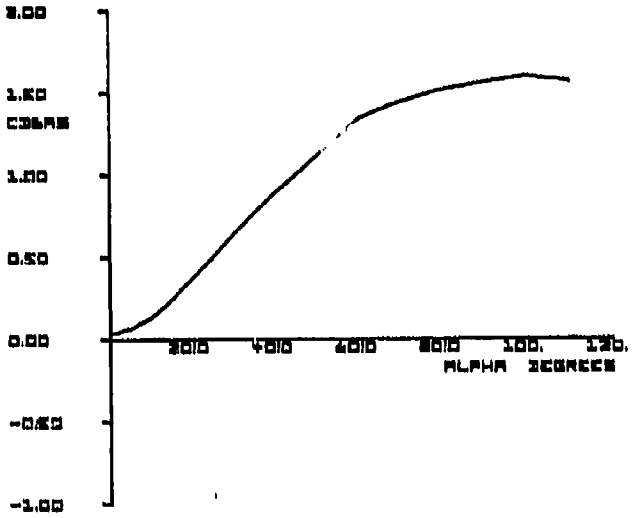

Figure 7. $C_{D_{BASIC}}(\alpha)$

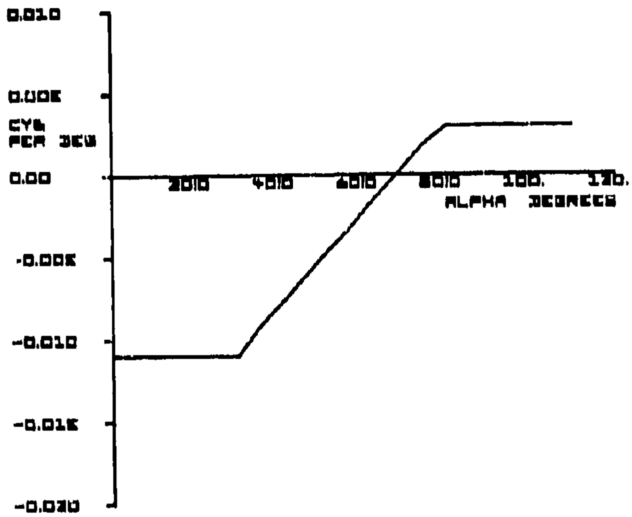

Figure 8. $C_{y_\beta}(\alpha)$

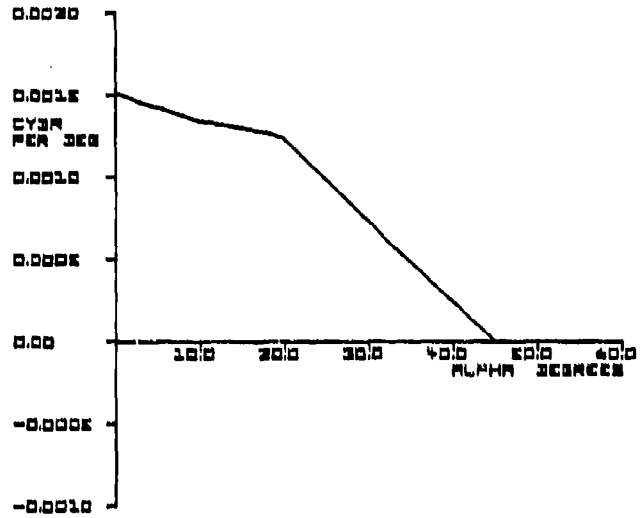

Figure 9. $C_{y_{\delta_r}}$ (α)

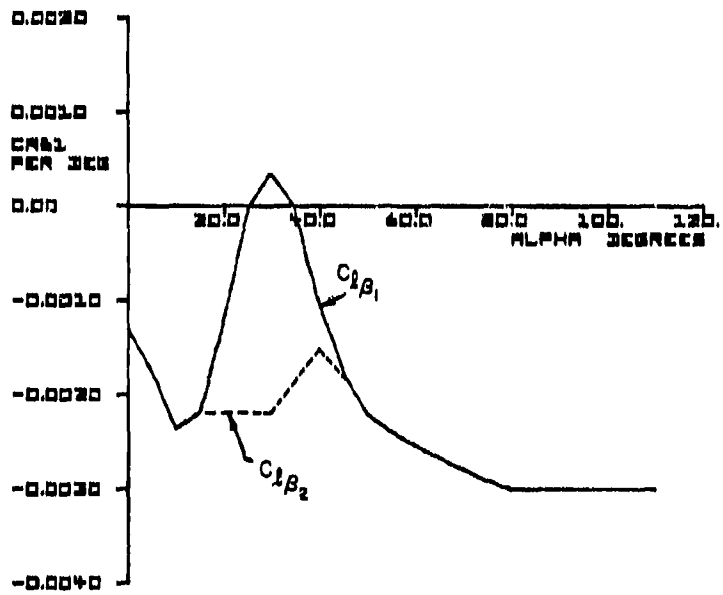

Figure 10. C_{ℓ_β} (α)

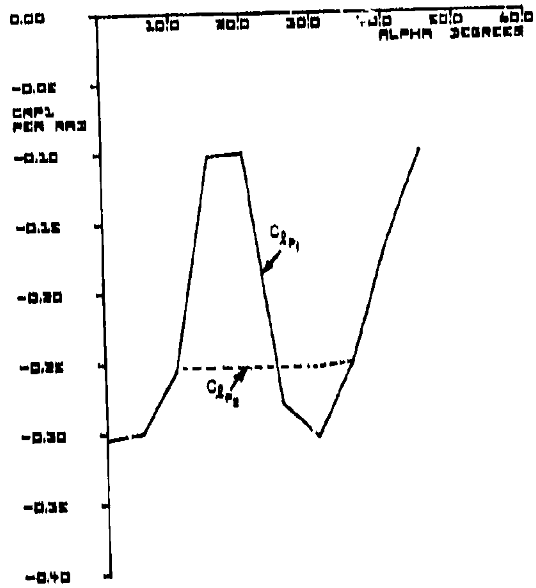

Figure 11. $C_{\ell_p}(\alpha)$

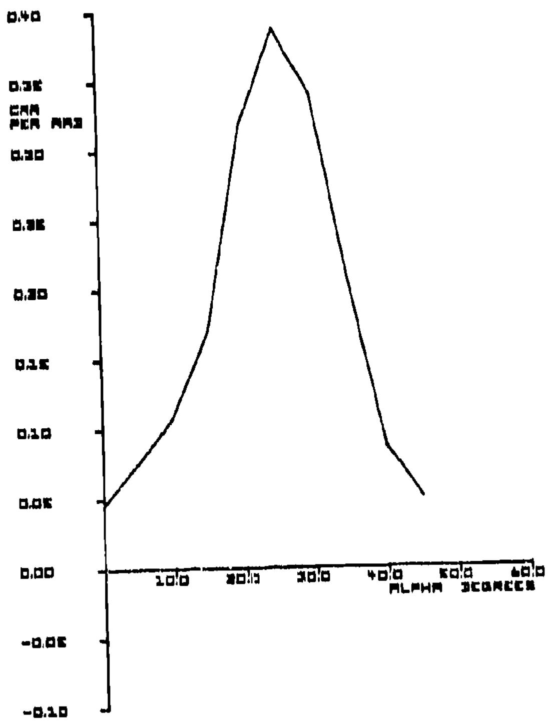

Figure 12. $C_{\ell_r}(\alpha)$

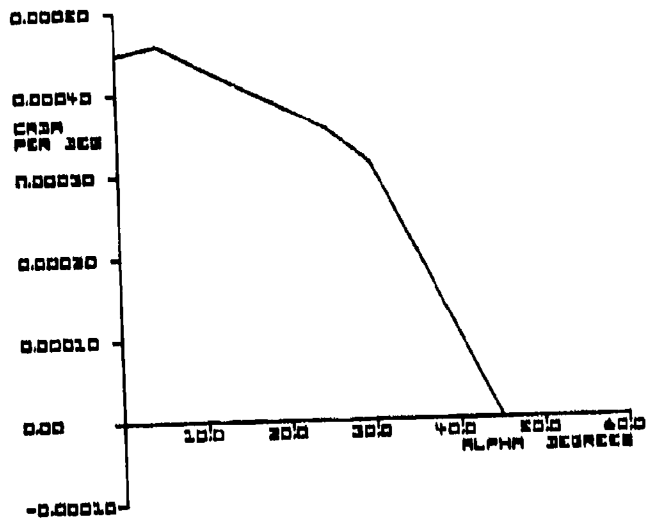

Figure 13. $C_{\ell\delta_a}(\alpha)$

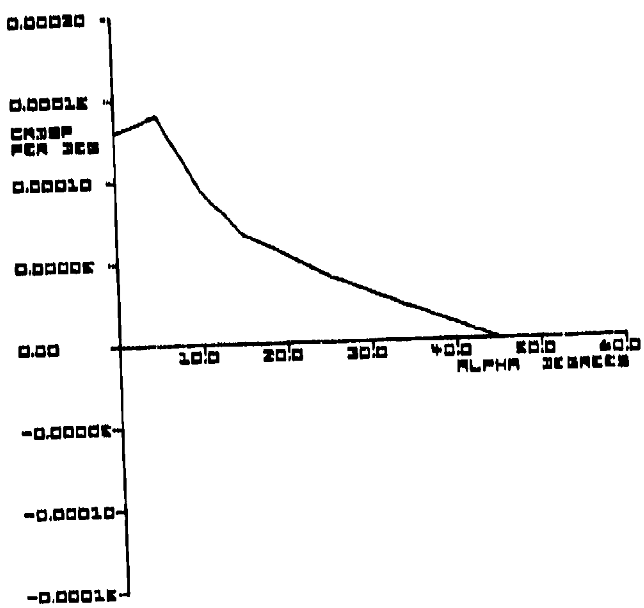

Figure 14. $C_{\ell\delta_{sp}}(\alpha)$

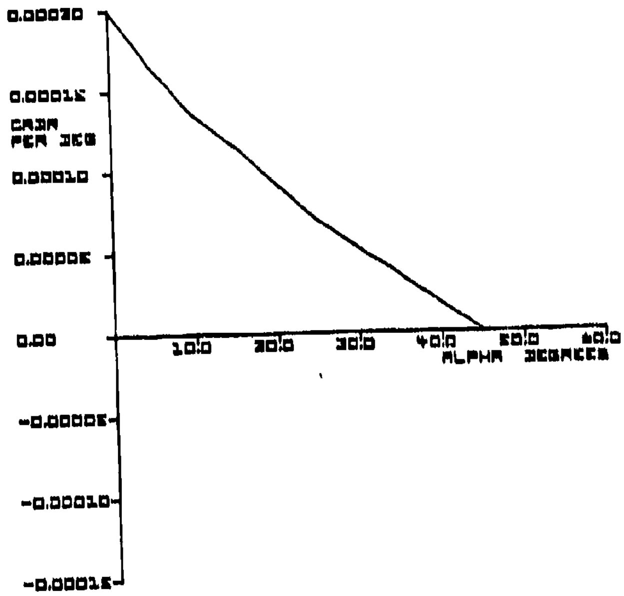

Figure 15. $C_{\ell_{\delta_r}}$ (α)

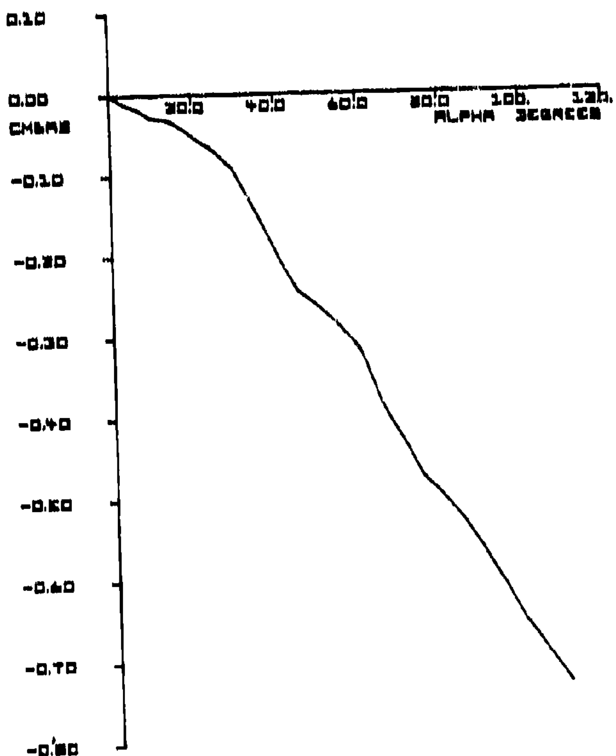

Figure 16. $C_{m_{BASIC}}$ (α)

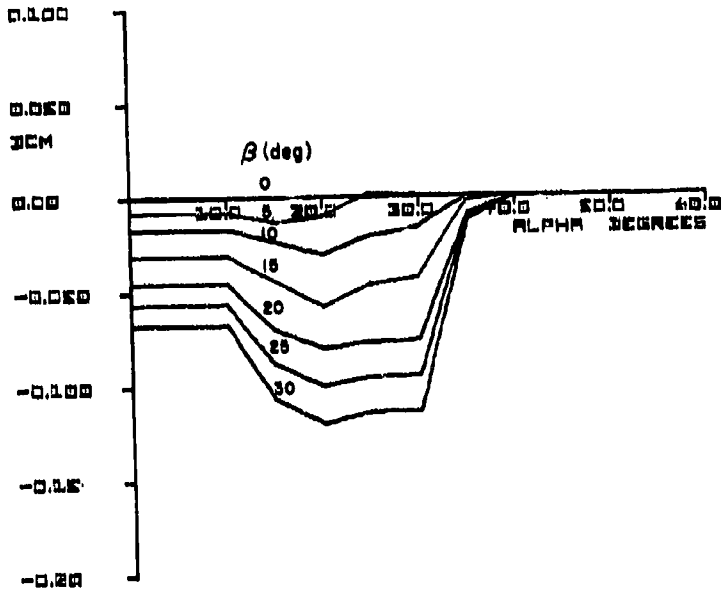

Figure 17. (a). ΔC_{m_1} $(\alpha, |\beta|)$

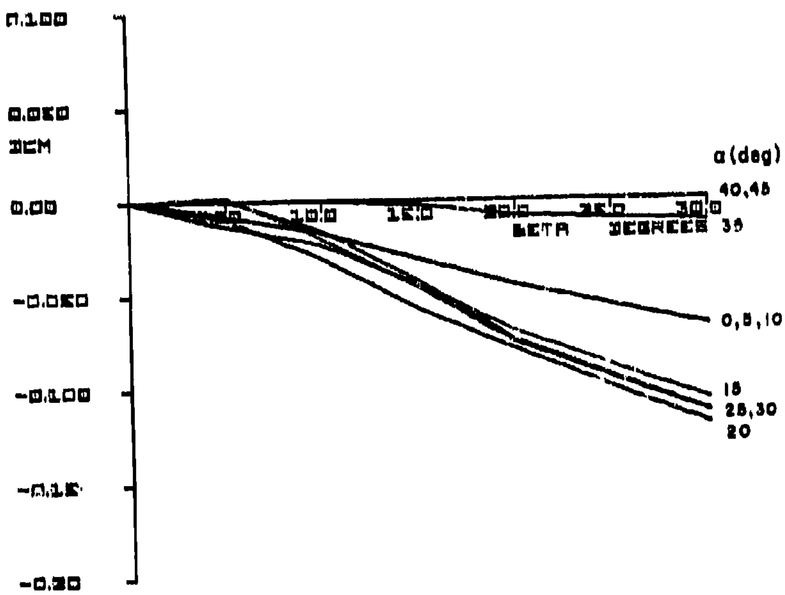

Figure 17 (b). ΔC_{m_1} $(\alpha, |\beta|)$

Note: $\Delta C_{m_2}(\alpha,\beta)$ is mirror image of $\Delta C_{m_1}(\alpha,\beta)$

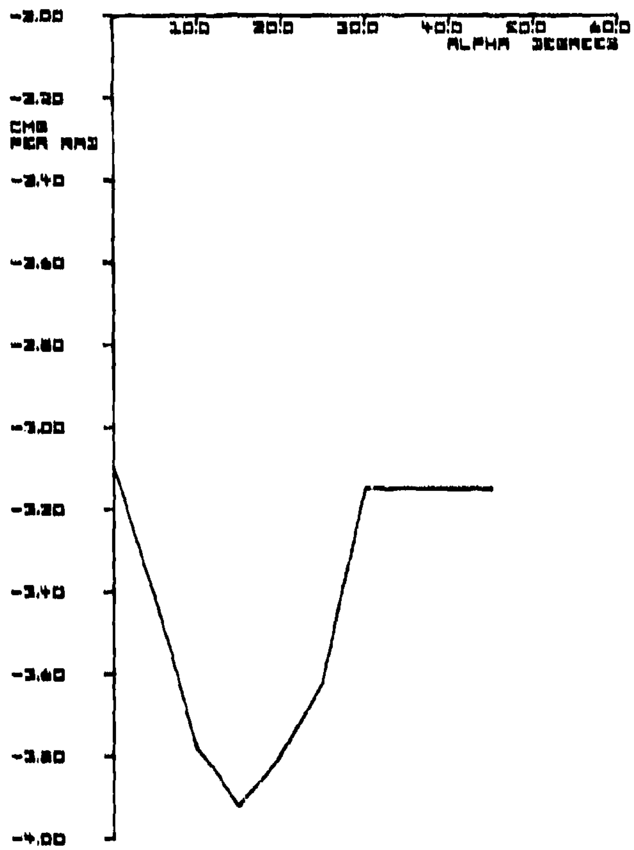

Figure 18. C_{m_q} (α)

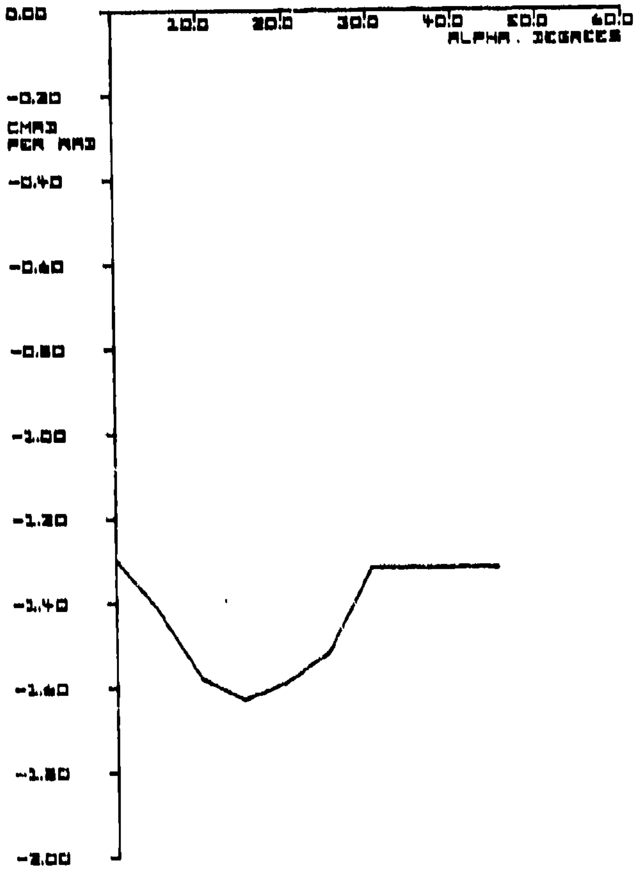

Figure 19. $C_{m_{\dot{\alpha}}}(\alpha)$

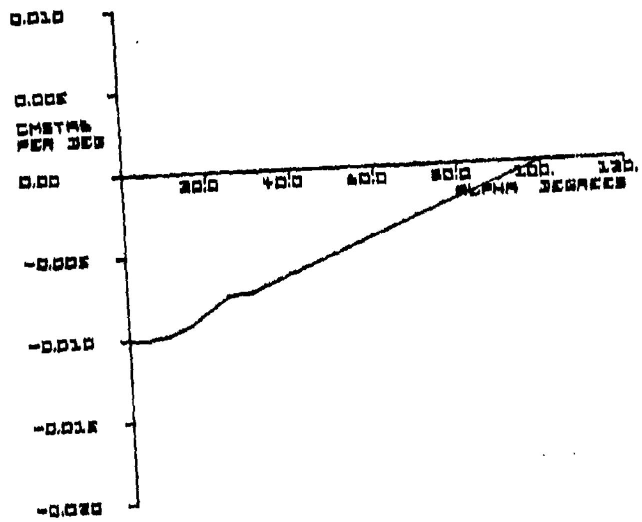

Figure 20. $C_{m_{\delta stab}}(\alpha)$

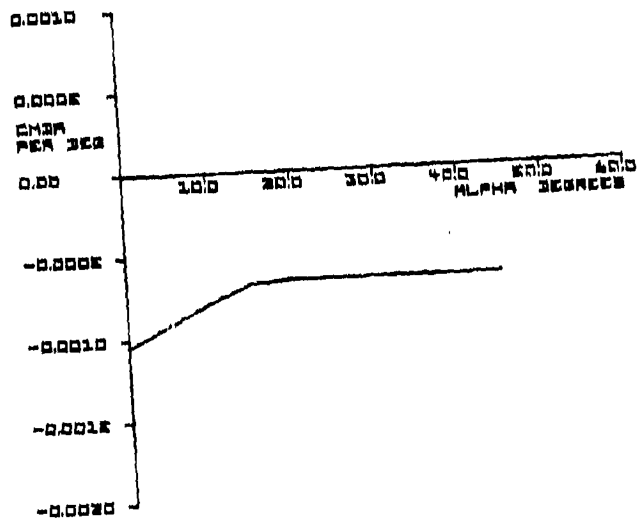

Figure 21. $C_{m_{\delta a}}(\alpha)$

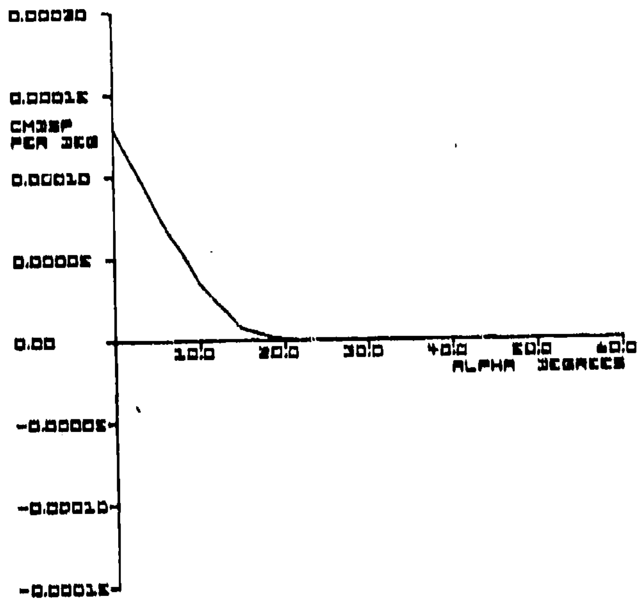

Figure 22. $C_{m_{\delta_{sp}}}(\alpha)$

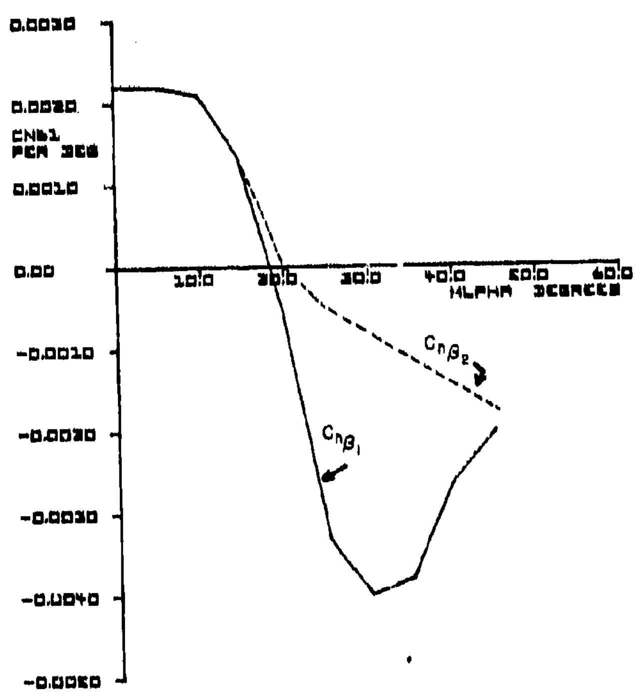

Figure 23. $C_{n_\beta}(\alpha)$

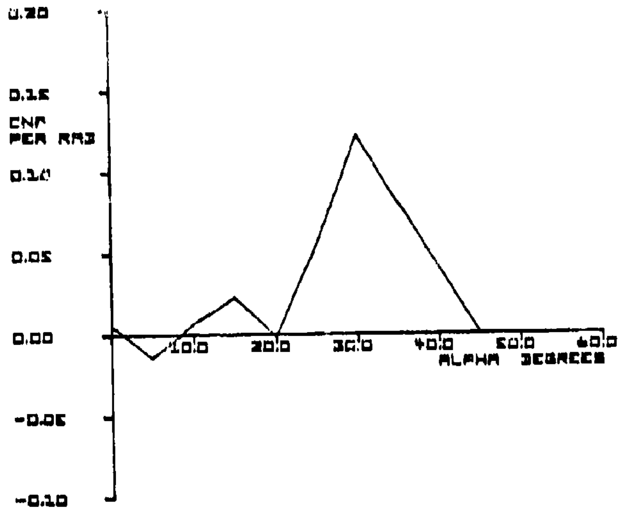

Figure 24. C_{n_p} (α)

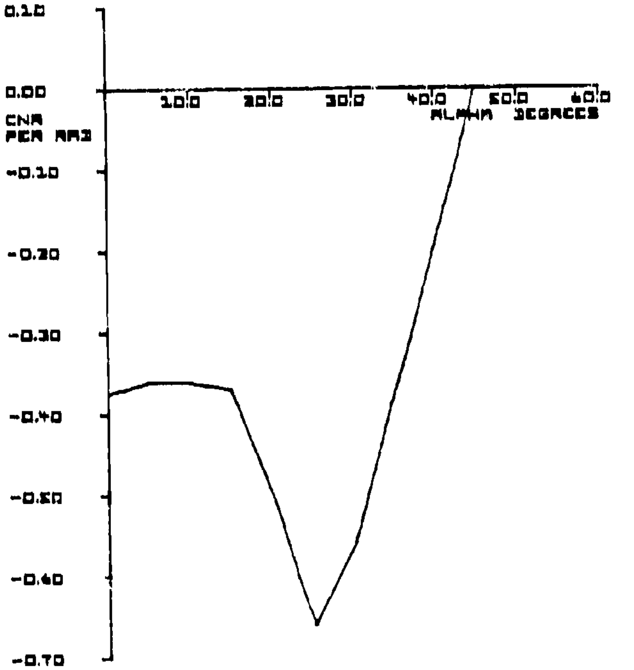

Figure 25. C_{n_r} (α)

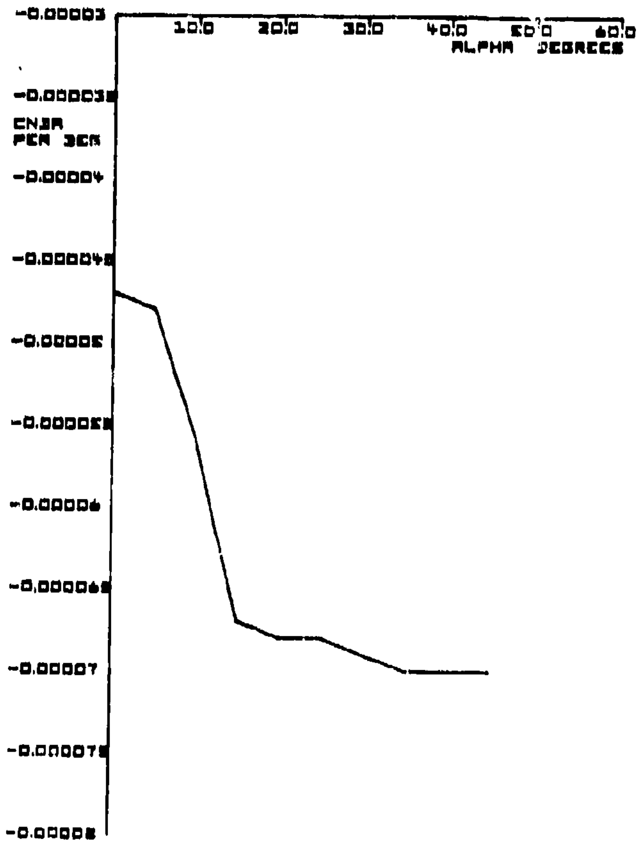

Figure 26. $Cn_{\delta_a}\ (\alpha)$

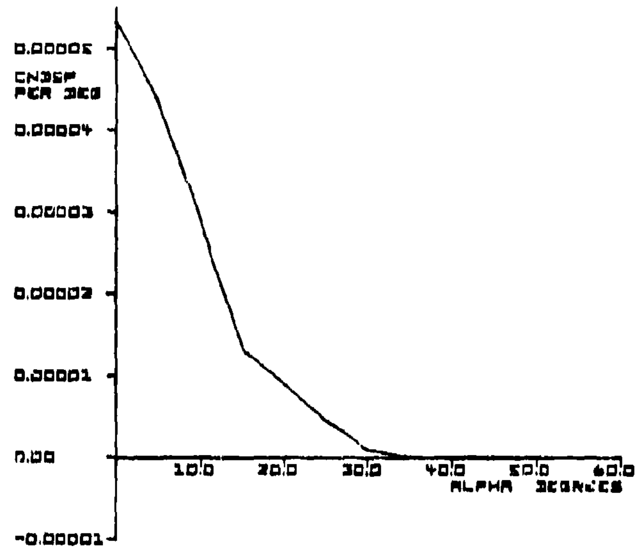

Figure 27. $C_{n_{\delta_{sp}}}(\alpha)$

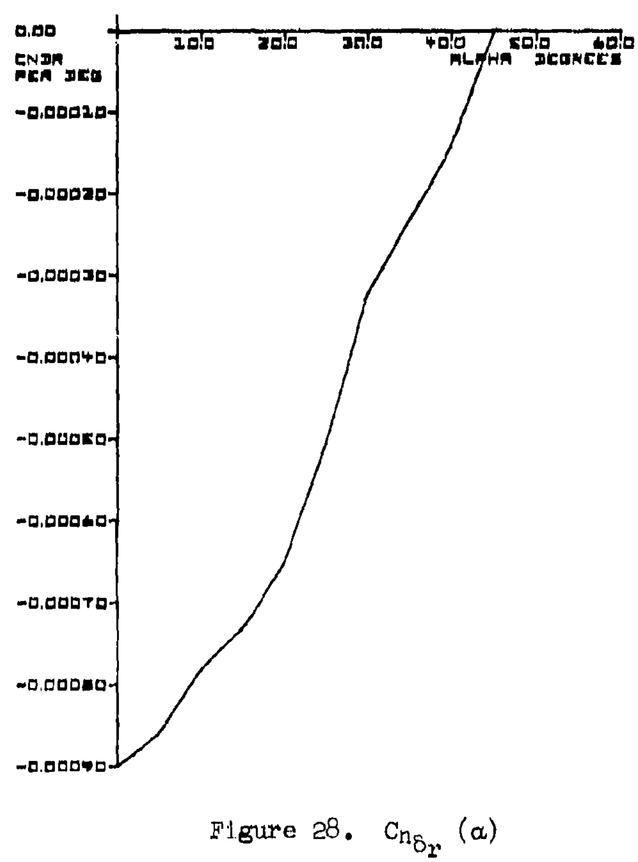

Figure 28. $C_{n_{\delta_r}}(\alpha)$

G. VALIDATION

No F-4J flight test traces of high AOA are available to compare against dynamics from the foregoing mathematical model. However, the model was originally developed for use in a moving-base piloted simulation . . which Navy F-4J pilots were given air combat maneuvering training. As a part of the checkout and acceptance tests, the simulation was flown through various offensive and defensive combat maneuvers, stalls, and departures by Navy instructor pilots who indicated it adequately represented the F-4J handling and performance. This provided the first gross validation of the aero model.

The only high-AOA flight traces available are from the F-4E stall/ post-stall flight test (Ref. 8). McDonnell Aircraft Co. indicates that all hard-wing models (no leading-edge slats) of the F-4 have approximately the same stall/departure characteristics. The Air Force (Ref. 8) noted the longer nose F-4E to have somewhat less wing rock tendency than the C and D models. The F-4J is more similar to the C and D and therefore might also have more pronounced wing rock. Also, the F-4E flight test vehicle was equipped with a spin chute, had a beefed-up aft fuselage structure to handle the spin chute loads, and had offsetting ballast in the nose. Thus its inertia characteristics are quite different from the average F-4J, as shown in the following:

	F-4E (Ref. 8)	F-4J
℄ stores	empty tank	empty tank
wing stores	pylons 1,2,8,9	pylons 2,8
W (lb	40,000	37,000
c.g. (% MAC)	28.1	29.3
I_x (slug-ft^2)	27,500	23,850
I_y (slug-ft^2)	157,000	127,400
I_z (slug-ft^2)	180,600	146,000
I_{x_z} (slug-ft^2)	5,500	2,210

This difference is assumed to have minor influence on the basic aerodynamic stall/separture characteristics as a function of AOA but a significant influence on dynamic response parameters such as dutch roll frequency and response to control inputs. With this in mind, we will proceed with a comparison of our F-4J model against the F-4E flight test results.

Reference 8 indicates that the clean aircraft exhibited lateral/directional stability breakdown in the form of a slightly divergent dutch roll (wing rock) in the vicinity of 19-22 deg AOA. As AOA was further increased the motion progressed from primarily roll to yaw (nose slice) in the region of 22-25.5 deg AOA. The dutch roll mode evaluated over the same AOA region from our 6 DOF frozen point model is shown in Fig. 29. This also indicates that at zero sideslip the dutch roll slowly becomes divergent at about 19 deg AOA. The aero data plot, Fig. 23, shows that C_{n_β} passes through zero at about 20 deg AOA, while at this same point C_{ℓ_β} (Fig. 10) is still relatively large. One would expect, then, that the dutch roll motion would be primarily rolling motion (wing rock). By 25 deg AOA C_{ℓ_β} is very small, while C_{n_β} is very large negative. Thus, one would expect the dutch roll mode to be primarily one of yaw motion (nose slice).

The root locus of Fig. 29 also indicates that the dutch roll mode is quite sensitive to sideslip in this same AOA range. Therefore, it is necessary also to look at time trace comparisons between flight test and our complete 6 DOF nonlinear aero model. Figure 30 is an F-4E time trace from Ref. 8 at 21 deg AOA and with all augmentation off. (It also has trailing-edge flaps at half deflection but they have a relatively small influence on lateral/directional stability.) The traces show the dutch roll to be a constant-amplitude, limit-cycle-like oscillation. A similar set of traces, starting at 21 deg AOA from our F-4J 6 DOF model shows an almost identical oscillation (Fig. 31). A comparison of specific traces shows the following peak-to-peak excursions.

	Flight Test	Simulation
α	21 deg	21 deg
β	11 deg	6.3 deg
φ	30 deg	21 deg
p	60 deg/sec	24 deg/sec
r	2.5 deg/sec	1.4 deg/sec
period	3 sec	6 sec
maneuver	wind-up-turn	straight/level

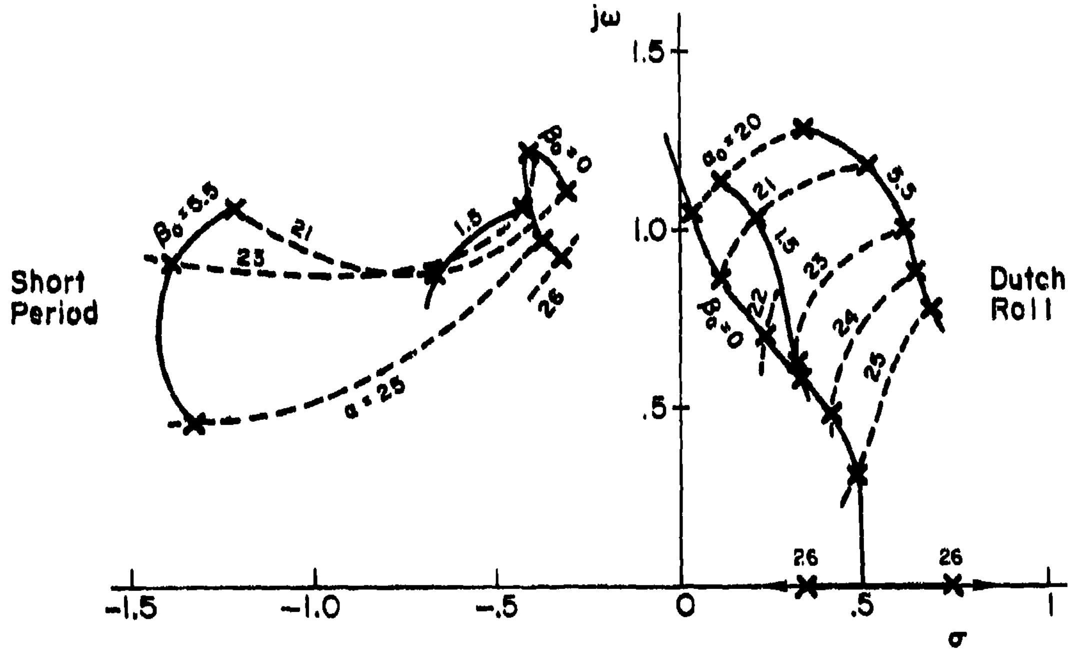

Figure 29. F-4J 6 DOF Linearized Equation; Lateral/
Longitudinal Root Migration with α and β

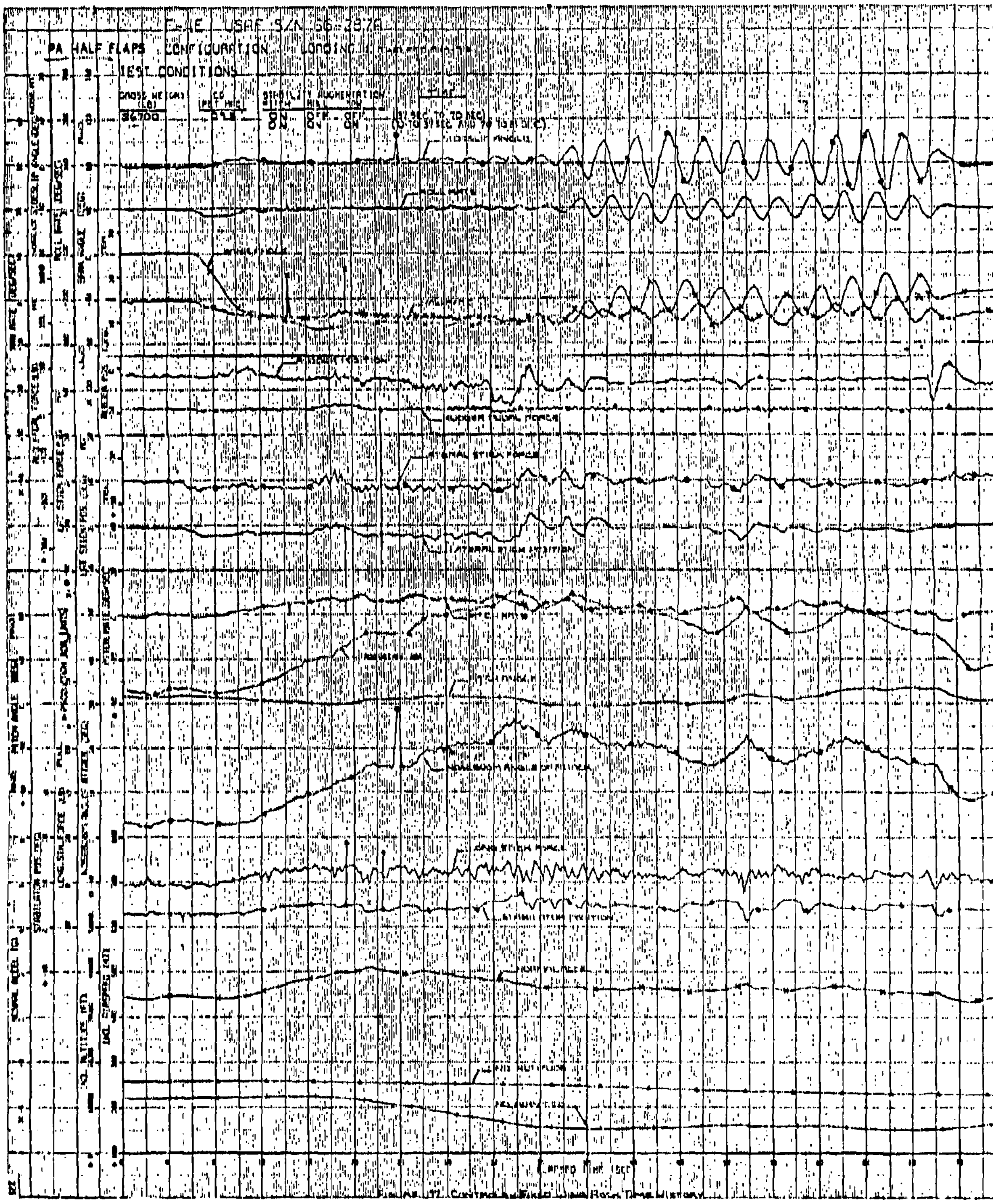

Figure 30. Controls Fixed Wing Rock
Time History (Ref. 8)

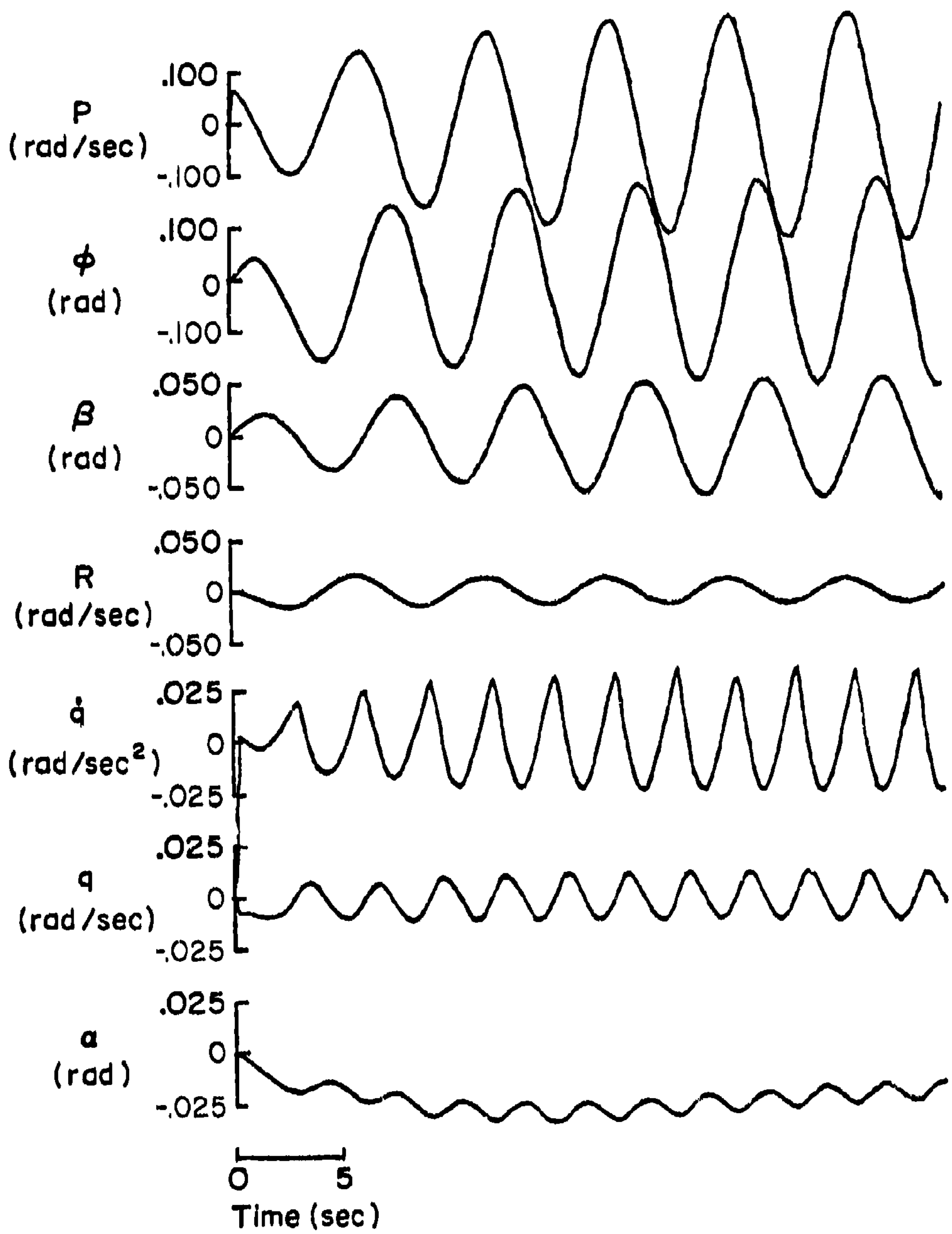

Figure 31. F-4J Open-Loop Nonlinear Airframe Response to Pulse Aileron; α_o = 21 deg, β_o = 0 deg

The absolute magnitude of motions depends upon the initial excitation and is not particularly close. However, the ratios of the motions are quite close and again tend to validate the aero model. The period of the oscillation is quite different because of the higher energy (dynamic pressure) of the flight test maneuver.

The nonlinear response traces of Fig. 31 show one additional factor. It will be noted that the longitudinal traces show a frequency which is precisely double the dutch roll frequency, while Fig. 29 predicts the longitudinal short period to be highly damped and about equal in frequency to the dutch roll. Other F-4E flight test time traces from Ref. 8 (e.g., Fig. 32) reflect the same "frequency doubling" noted in our aero model. This "frequency doubling" can only be caused by the pitching moment due to sideslip, Cm_{β}, which is quite strong and negative for the F-4 aircraft. Note in Fig. 32 that each peak in the α trace coincides with a zero crossing in β. In this set of traces the rudder activity indicates that the yaw SAS was on. A comparison set of traces from the F-4J model with pitch and yaw SAS on, starting at a trim of $\alpha_o = 23$ deg, $\beta_o = 0$ is shown in Fig. 33. Again, the motions of Figs. 32 and 33 are remarkably similar.

A final comparison between flight and simulation is shown in Fig. 34. Both aircraft depart from a wind-up turn to the left.

On the basis of the above it was considered that the aero model exhibits characteristics adequately representative of the F-4 aircraft for use in analysis and simulation of stall/departure.

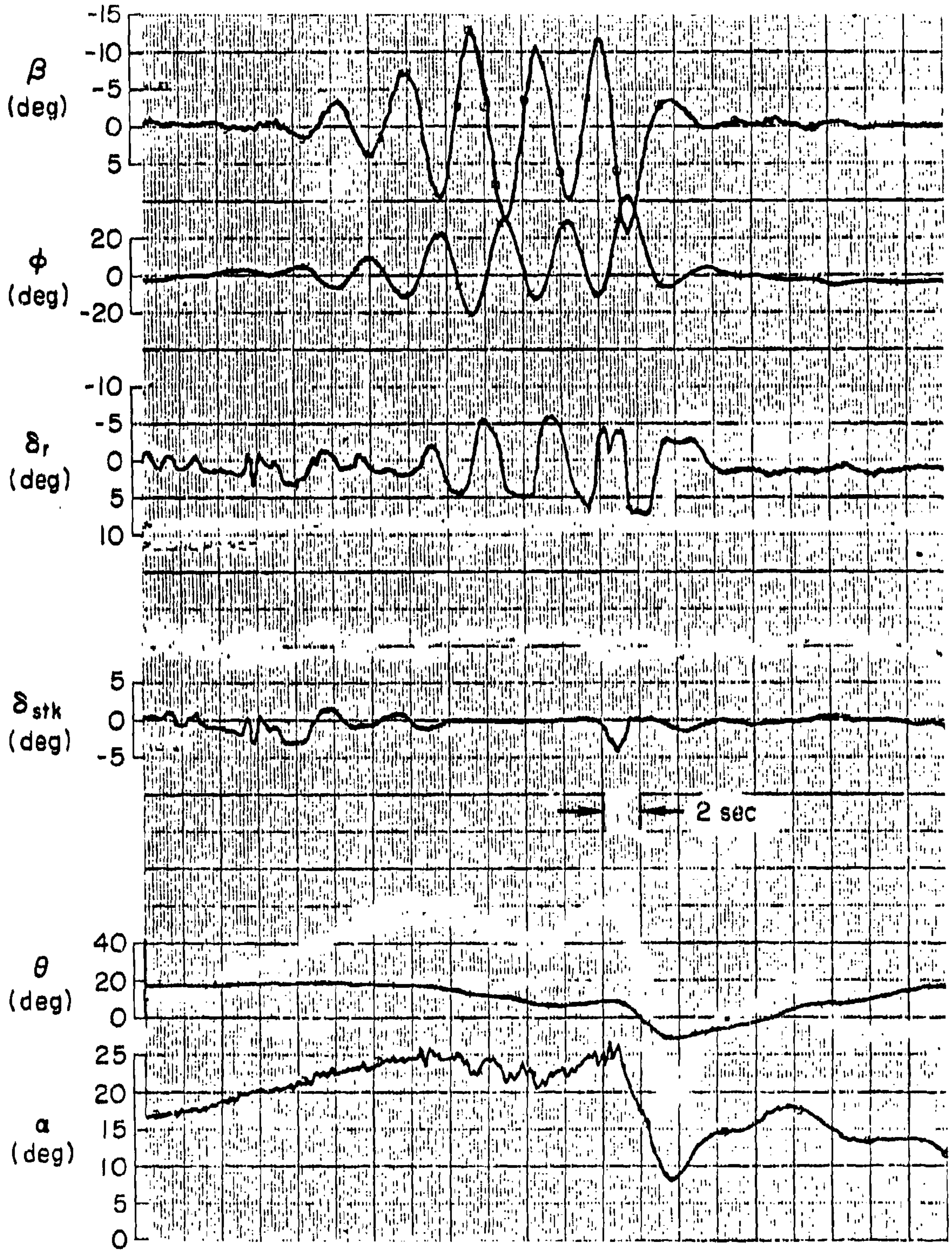

Figure 32. Pull-Up and Steady Wing Rock (From Ref. 8)

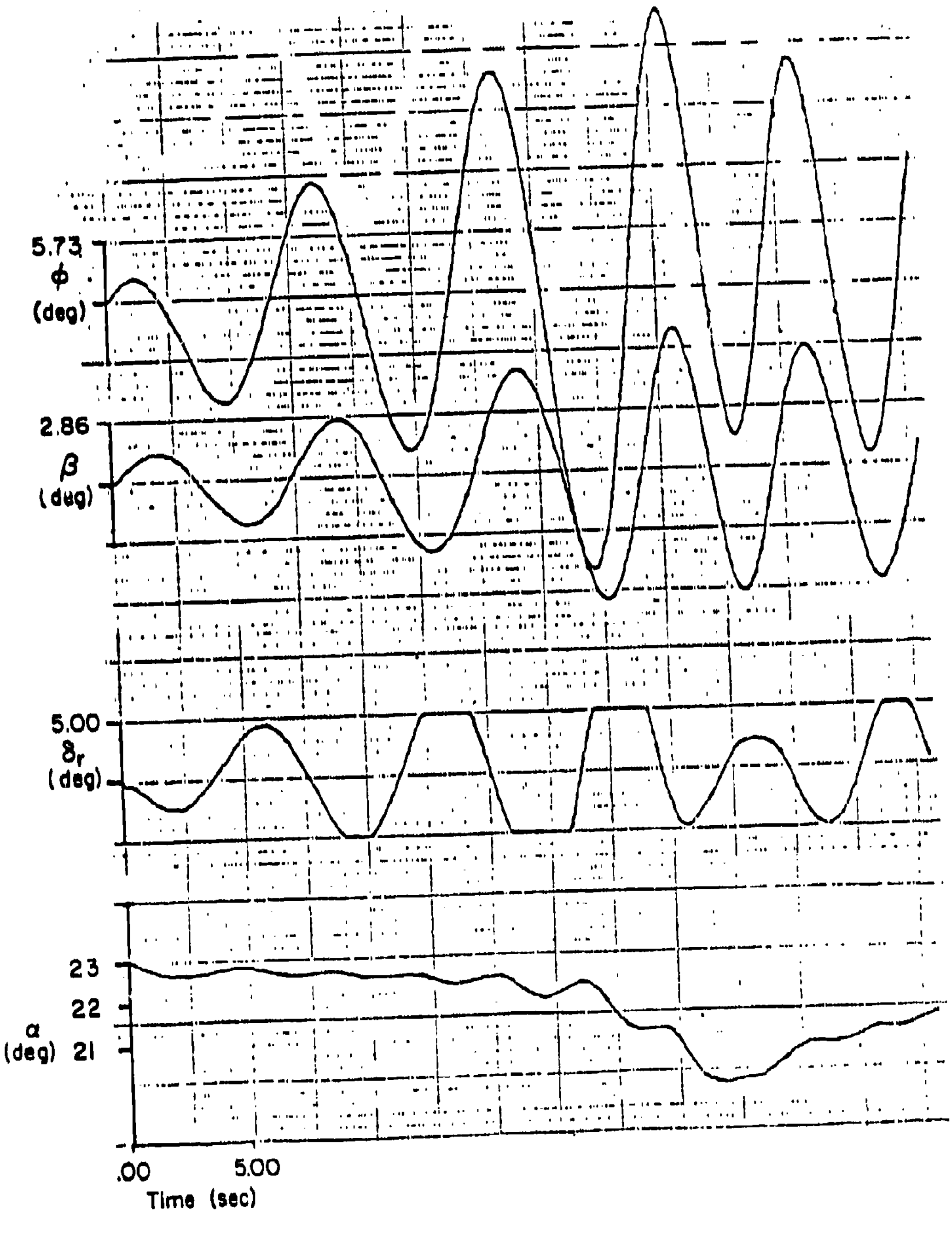

Figure 33. F-4J Wing Rock with Pitch and Yaw SAS On and α_0 = 23 deg

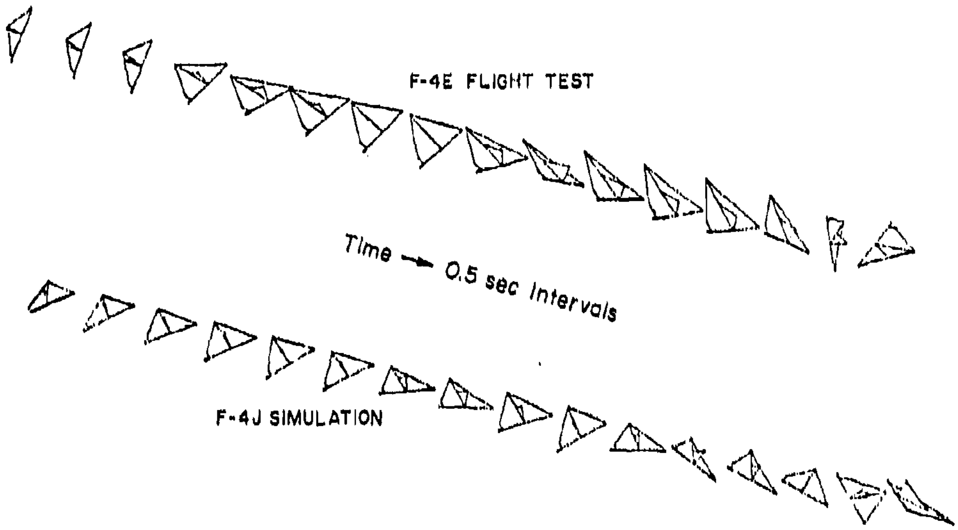

Figure 34. Departure During Left Wind-Up Turn

APPENDIX II

F-14A DATA PACKAGE

A. INTRODUCTION

This appendix documents the mathematical model used in the simulation of the F-14A aircraft. The model represents the "clean" (no slat or flap deflection) aircraft at low Mach number. All aerodynamic characteristics are for a wing sweep of 22 deg (Fig. 35) which is maintained in flight by the Mach-Sweep Programmer below M = 0.7. Aerodynamic coefficients are derived from wind tunnel data, with modifications based on parameter identification using flight test data.

The appendix is organized as follows: the equations for the aerodynamic forces and moments are presented in Section B; the origins of the individual aerodynamic coefficients is discussed in Section C; the coefficient "look-up" tables are described in Section D; the coefficient data are listed in Table 12 and plotted in Figs. 36 through 71.

The equations of motion presented in Appendix I, Section B, are applicable for this model.

B. AERODYNAMIC FORCE AND MOMENT COEFFICIENT EQUATIONS

The aerodynamic model, Table 10, is largely based on an F-14 model used on the NASA Langley Research Center Differential Maneuvering Simulator (DMS), Ref. 9. Modifications were made to incorporate additional wind tunnel data and simplify the functional dependence on sideslip angle where appropriate. The terms $\Delta C_{L_{\beta=0}}(\alpha)$ and $\Delta C_{m_{\beta=0}}(\alpha)$ were added to allow "tuning" of the model using flight-derived trim data. Similar terms were included in the lateral equations to allow inclusion of nonzero sideforce, yaw, and roll moments at $\beta = 0$. Such moments, arising from aircraft asymmetries and asymmetric vortex shedding, have been suggested as contributors to departure problems.

δ_{stab} = Positive TED	S = 565 ft^2
δ_r = Positive TEL	$\bar{c}$ = 9.80 ft
$\delta_a = \delta_{stab_{LEFT}} - \delta_{stab_{RIGHT}}$	b = 64.1 ft
	X_{REF} = 16% m.a.c.

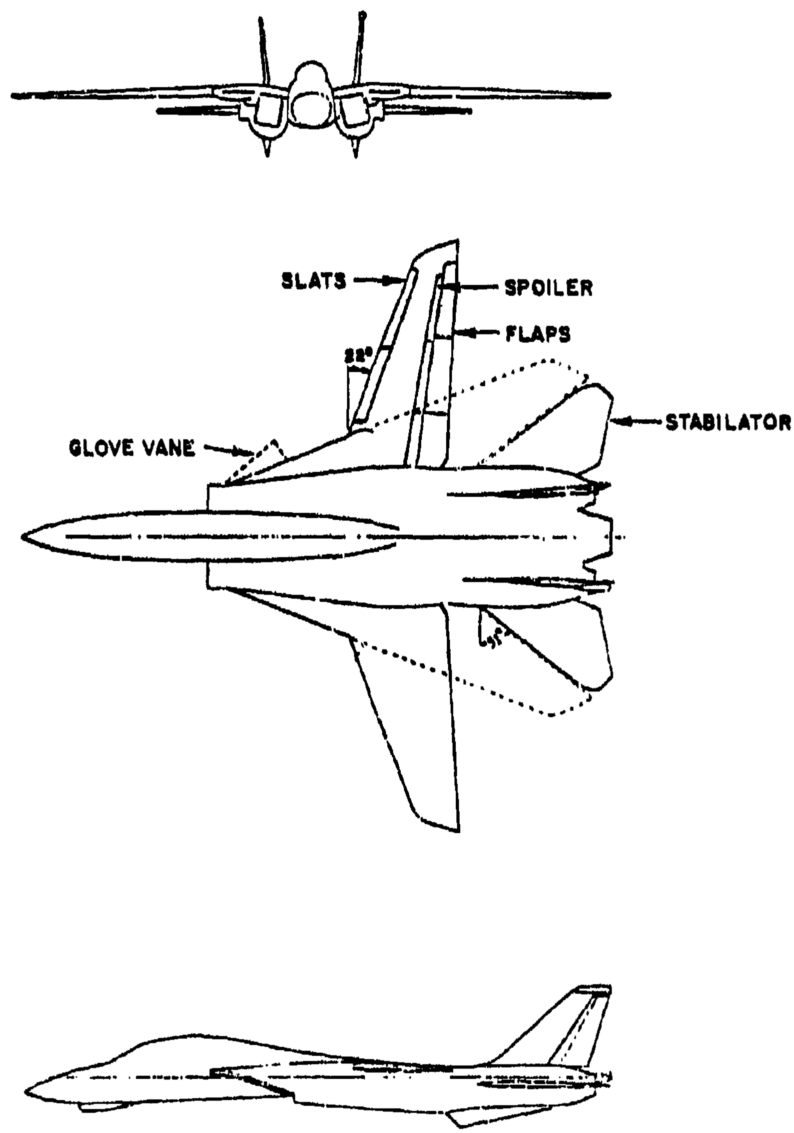

Figure 35. F-14 Aircraft Configuration

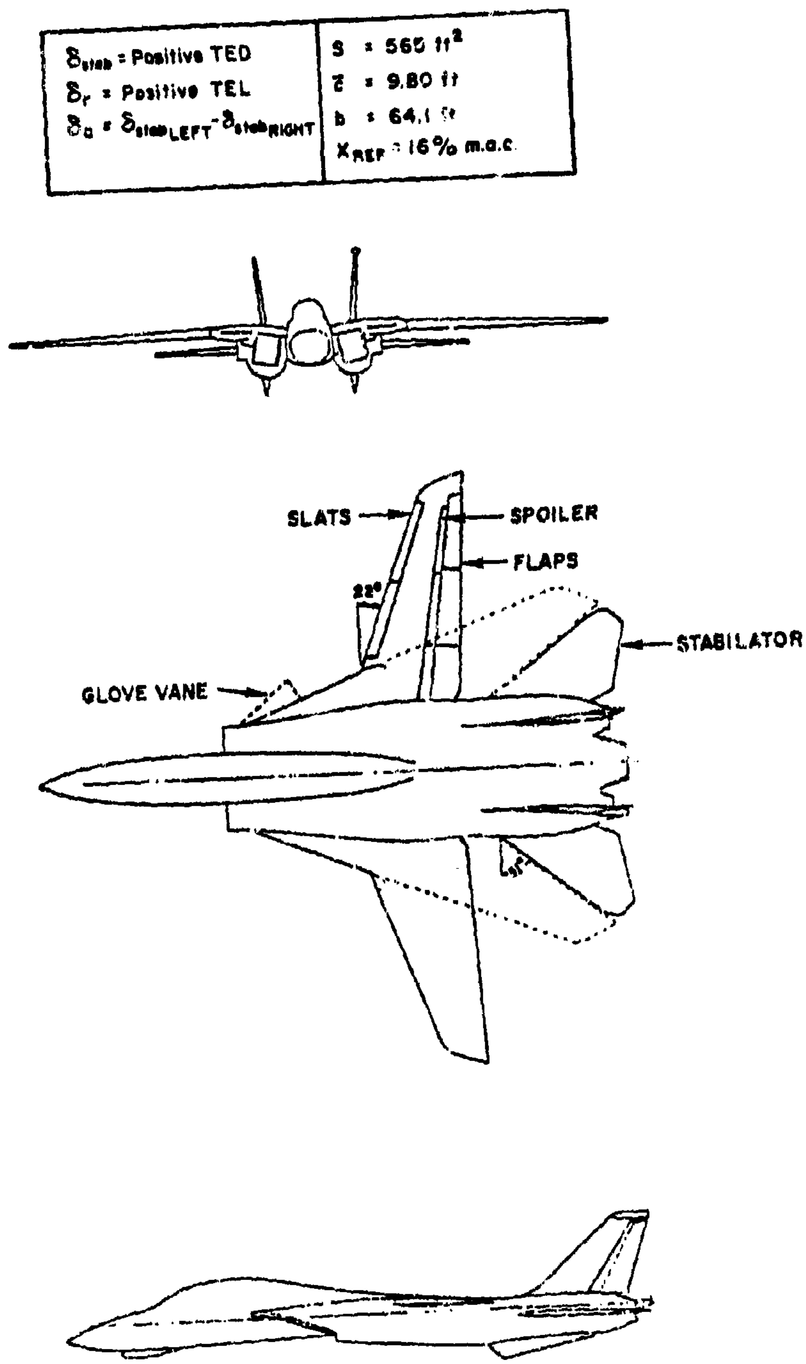

Figure 35. F-14 Aircraft Configuration

TABLE 10. F-14 AERODYNAMIC FORCE AND MOMENT EQUATIONS

(a) Aerodynamic Force Equations

$$C_L = C_{L_{BASIC}}(\alpha,\beta) + \Delta C_{L_{\beta=0}}(\alpha) + \Delta C_{L_{sp}}(\alpha)(|\delta_{sp}|/55) + \Delta C_{L_{\delta_s}}(\alpha)$$

$$\Delta C_{L_{\delta_s}}(\alpha) = C_{L_{\delta_{s_1}}}(\alpha)\delta_s \qquad (\delta_s \geq -10^\circ)$$

$$\Delta C_{L_{\delta_s}}(\alpha) = -10 C_{L_{\delta_{s_1}}}(\alpha)\delta_s + (\delta_s + 10) C_{L_{\delta_{s_2}}}(\alpha) \qquad (\delta_s < -10^\circ)$$

$$C_D = C_{D_{BASIC}}(\alpha,\beta) + \Delta C_{D_{sp}}(\alpha)(|\delta_{sp}|/55) + \Delta C_{D_{\delta_s}}(\alpha)$$

$$\Delta C_{D_{\delta_s}}(\alpha) = C_{D_{\delta_{s_1}}}(\alpha)\delta_s \qquad (\delta_s \geq -10^\circ)$$

$$\Delta C_{D_{\delta_s}}(\alpha) = -10 C_{D_{\delta_{s_1}}}(\alpha) + (\delta_s + 10) C_{D_{\delta_{s_2}}}(\alpha) \qquad (\delta_s < -10^\circ)$$

$$C_y = C_{y_{BASIC}}(\alpha,\beta) + C_{y_{\beta=0}}(\alpha) + C_{y_{\delta_a}}(\alpha)\delta_a + C_{y_{\delta_r}}(\alpha,\beta)\delta_r + C_{y_{\delta_{sp}}}(\alpha)\delta_{sp} + (b/2V_o)[C_{y_r}(\alpha)r + C_{y_p}(\alpha)p]$$

(b) Aerodynamic Moment Equations (X_{cg} in % $\bar{c}$)

$$C_m = C_{m_{BASIC}}(\alpha,\beta) + \Delta C_{m_{\beta=0}}(\alpha) + [(X_{cg} - X_{ref})/100](C_L \cos\alpha + C_D \sin\alpha) + \Delta C_{m_{sp}}(\alpha)(|\delta_{sp}|/55)$$
$$+ \Delta C_{m_{\delta_s}}(\alpha)\delta_s + (\bar{c}q/2V_o)C_{m_q}(\alpha)q$$

$$\Delta C_{m_{\delta_s}}(\alpha) = C_{m_{\delta_{s_1}}}(\alpha)\delta_s \qquad (\delta_s \geq -10^\circ)$$

$$\Delta C_{m_{\delta_s}}(\alpha) = -10 C_{m_{\delta_{s_1}}}(\alpha) + (\delta_s + 10) C_{m_{\delta_{s_2}}}(\alpha) \qquad (\delta_s < -10^\circ)$$

$$C_n = C_{n_{BASIC}}(\alpha,\beta) + \Delta C_{n_{\beta=0}}(\alpha) + \Delta C_{n_{\delta_s}}(u)\delta_s \sin(8.2\beta) + [(X_{cg} - X_{ref})/100](\bar{c}/b)C_y + C_{n_{\delta_a}}(\alpha)\delta_a$$
$$+ C_{n_{\delta_r}}(\alpha,\beta)\delta_r + C_{n_{\delta_{sp}}}(\alpha)\delta_{sp} + (b/2V_o)[C_{n_r}(\alpha)r + C_{n_p}(\alpha)p]$$

$$C_\ell = C_{\ell_{BASIC}}(\alpha,\beta) + \Delta C_{\ell_{\beta=0}}(\alpha) + C_{\ell_{\delta_a}}(\alpha,\beta)\delta_a + C_{\ell_{\delta_r}}(\alpha,\beta)\delta_r + C_{\ell_{\delta_{sp}}}(\alpha)\delta_{sp} + (b/2V_o)[C_{\ell_r}(\alpha)r + C_{\ell_p}(\alpha)p]$$

NOTE: For conciseness, δ_{stab} has been reduced to δ_s

In the DMS model the static yawing moment coefficient was treated as a function of three variables: α, β, and δ_s ($\delta_s = \delta_{stab}$). The unusual influence of stabilator deflection on directional stability arises from an interaction between the engine inlet shed vortex and the vertical and horizontal stabilizers, Ref. 10. Examination of the data indicated that this effect could be modeled as a yawing moment increment which was a function of α, δ_s, and β added to the static yawing moment $C_{n_{BASIC}}(\alpha,\beta)$. Rather than treat this increment as a three variable look-up table, it was approximated as

$$\Delta C_{n_{\delta_s}}(\alpha)\delta_s \sin (8.2\beta)$$

where $\Delta C_{n_{\delta_s}}(\alpha)$ is a one variable look-up table. The sin (8.2β) factor insures that for $\delta_s < 0$ (TEU) the effect is destabilizing for either positive or negative sideslip. The longitudinal stabilator effectiveness is nonlinear in δ_s in the DMS model. This effect was retained in the STI model but the dependence on sideslip was eliminated.

C. DATA SOURCES

The aerodynamic data package employed in the F-14 simulator was put together from several sources and then modified somewhat to obtain an acceptable match between the simulation and actual flight traces. The purpose of this section is to document the origins of the coefficients.

Although a number of high angle of attack wind tunnel tests have been conducted for the F-14, the following tests were the primary sources for the STI model:

15 March-16 April 1971, NASA Ames Research Center,
12 ft pressure tunnel

August 1971, NASA Langley Research Center,
30' × 60' (full scale) tunnel

The complete test reports were not available for these test programs. Selected ARC data were available in Ref. 10 and selected LRC data in Refs. 11, 12, and 13. The ARC data is generally considered to be the "best", primarily because the Reynolds number is higher; however, its use was limited in that Ref. 10 contained only static roll and yaw coefficients as functions of α and

β and normal force and pitching moments as a function of α only. No dynamic derivative or control effectiveness data is available from the ARC test. These were obtained from the Ref. 9 DMS simulation which was based on the LRC 30' × 60' data with some modifications based on simulation pilots' opinions. The DMS data appears to be primarily "raw" LRC wind tunnel data as it shows characteristic scatter, and coefficients (such as $C_n(\alpha,\beta)$) which are not symmetrical in β. When this data was used, coefficient values at positive and negative β's were averaged, where appropriate, to produce tables symmetrical in β. In some cases the averaged curves were further smoothed to reduce questionable scatter.

The adequacy of the wind tunnel derived aerodynamic data was validated by comparison of 6 DOF analytic models with available F-14 flight test data. On the basis of these comparisons several aerodynamic coefficients were further modified as explained in Section E.

Plots of the coefficients are shown in Figs. 36 to 71. The reference point for all moment coefficients is on the FRL at 16% MAC. The spoiler produces no effect above α = 10 deg and, since primary interest is in the high α regime, all spoiler functions are zero.

D. AERODYNAMIC COEFFICIENT DATA

For use by the simulation program all aerodynamic coefficients are represented as piece-wise linear approximations in "look-up" tables. These tables are functions either of α only or of α and β (see Table 11). In either case, the α breakpoints are every 5 deg from α = 0 to 55 deg. The β breakpoints are every 5 deg from β = 0 to ±20 deg. A listing of the computer data file containing the lookup tables is shown in Table 12. The order of the individual coefficient tables in the aerodynamic data file is as shown in Table 11. For functions of α only, α is incremented by column and then row, as indicated below:

0, 5 deg, 10 deg, 15 deg, 20 deg
25 deg, 30 deg, 35 deg, 40 deg, 45 deg
50 deg, 55 deg, 0, 0, 0

For functions of α and β, β is incremented first, then α, as follows:

Row	
1	(0, -20), (0, -15), (0, -10), (0, -5), (0, 0)
2	(0, 5), (0, 10), (0, 15), (0, 20), (5, -20)
⋮	
22	(55, 10), (55, 15), (55, 20), (0), (0)

For convenience in creating computer mnemonics, the control variable δ_{stab} has been abbreviated as δ_s in the data file and plots.

TABLE 11. ORGANIZATION OF AERODYNAMIC DATA FILE

PARAMETER	FUNCTION OF	PARAMETER UNITS	STI MNEMONIC AND ARRAY DIMENSION	NUMBER OF DATA PTS	CARD (LINE) CODE
$C_{L_{BASIC}}$	α, β	—	CLBAS(12,9)	108	STI100
$\Delta C_{L_{\beta=0}}$	α	—	DCLBO(12)	12	101
$C_{L_{\delta_{s1}}}$	α	1/deg	CLDS1(12)	12	104
$C_{L_{\delta_{s2}}}$	α	1/deg	CLDS2(12)	12	105
$\Delta C_{L_{SP}}$	α	—	DCLSP(12)	12	106
$C_{D_{BASIC}}$	α, β	—	CDBAS(12,9)	108	200
$C_{D_{\delta_{s1}}}$	α	1/deg	CDDS1(12)	12	204
$C_{D_{\delta_{s2}}}$	α	1/deg	CDDS2(12)	12	205
$\Delta C_{D_{SP}}$	α	—	DCDSP(12)	12	206
$C_{y_{BASIC}}$	α, β	—	CYBAS(12,9)	108	300
$\Delta C_{y_{\beta=0}}$	α	—	DCYBO(12)	12	301
C_{y_p}	α	1/rad	CYP(12)	12	303
C_{y_r}	α	1/rad	CYR(12)	12	304
$C_{y_{\delta_a}}$	α	1/deg	CYDA(12)	12	305
$C_{y_{SP}}$	α	1/deg	CYDSP(12)	12	306
$C_{y_{\delta_r}}$	α, β	1/deg	CY[illegible](12,9)	108	307
$C_{\ell_{BASIC}}$	α, β	—	CRBAS(12,9)	108	400
$\Delta C_{\ell_{\beta=0}}$	α	—	DCRBO(12)	12	401
C_{ℓ_p}	α	1/rad	CRP(12)	12	403
C_{ℓ_r}	α	1/rad	CRR(12)	12	404
$C_{\ell_{\delta_a}}$	α, β	1/deg	CRDA(12,9)	108	405
$C_{\ell_{\delta SP}}$	α	1/deg	CRDSP(12)	12	406
$C_{\ell_{\delta_r}}$	α, β	1/deg	CRDR(12,9)	108	407
$C_{m_{BASIC}}$	α, β	—	CMBAS(12,9)	108	500
$\Delta C_{m_{\beta=0}}$	α	—	DCMBO(12)	12	501
C_{m_q}	α	1/rad	CMQ(12)	12	503
$C_{m_{\delta_{s1}}}$	α	1/deg	CMDS1(12)	12	504
$C_{m_{\delta_{s2}}}$	α	1/deg	CMDS2(12)	12	505
$\Delta C_{m_{SP}}$	α	—	DCMSP(12)	12	506
$C_{n_{BASIC}}$	α, β	—	CNBAS(12,9)	108	600
$\Delta C_{n_{\beta=0}}$	α	—	DCNBO(12)	12	601
$\Delta C_{n_{\delta_s}}$	α	1/deg	DCNDS(12)	12	602
C_{n_p}	α	1/rad	CNP(12)	12	603
C_{n_r}	α	1/rad	CNR(12)	12	604
$C_{n_{\delta_a}}$	α	1/deg	CNDA(12)	12	605
$C_{n_{\delta SP}}$	α	1/deg	CNDSP(12)	12	606
$C_{n_{\delta_r}}$	α, β	1/deg	CNDR(12,9)	108	607

TABLE 12. AERODYNAMIC DATA FILE

$C_{L_{BASIC}}$

```
0.6145000E-01  0.1470500E+00  0.1098500E+00  0.1455500E+00  0.7760000E-01
0.1455500E+00  0.1098500E+00  0.1470500E+00  0.6145000E-01  0.5286301E+00
0.5746194E+00  0.6024052E+00  0.6185578E+00  0.5813407E+00  0.6185578E+00
0.6024052E+00  0.5746194E+00  0.5286301E+00  0.9215569E+00  0.9808749E+00
0.1001756E+01  0.1019454E+01  0.1012943E+01  0.1019454E+01  0.1001756E+01
0.9808749E+00  0.9215569E+00  0.1213586E+01  0.1244889E+01  0.1284404E+01
0.1276219E+01  0.1278946E+01  0.1276219E+01  0.1284404E+01  0.1244889E+01
0.1213586E+01  0.1439421E+01  0.1515402E+01  0.1563296E+01  0.1569673E+01
0.1603160E+01  0.1569673E+01  0.1563296E+01  0.1515402E+01  0.1439421E+01
0.1640450E+01  0.1698947E+01  0.1740003E+01  0.1766289E+01  0.1774422E+01
0.1766289E+01  0.1740003E+01  0.1698947E+01  0.1640450E+01  0.1720108E+01
0.1790446E+01  0.1852892E+01  0.1898136E+01  0.1927053E+01  0.1898136E+01
0.1852892E+01  0.1790446E+01  0.1720108E+01  0.1733031E+01  0.1770326E+01
0.1840752E+01  0.1870520E+01  0.1930109E+01  0.1870520E+01  0.1840752E+01
0.1770326E+01  0.1733031E+01  0.1666409E+01  0.1691728E+01  0.1712288E+01
0.1748122E+01  0.1771812E+01  0.1748122E+01  0.1712288E+01  0.1691728E+01
0.1666409E+01  0.1567197E+01  0.1610224E+01  0.1617188E+01  0.1652013E+01
0.1668984E+01  0.1652013E+01  0.1617188E+01  0.1610224E+01  0.1567197E+01
0.1476011E+01  0.1499908E+01  0.1521349E+01  0.1546793E+01  0.1580945E+01
0.1546793E+01  0.1521349E+01  0.1499908E+01  0.1476011E+01  0.1346354E+01
0.1385247E+01  0.1394564E+01  0.1417692E+01  0.1427369E+01  0.1417692E+01
0.1394564E+01  0.1385247E+01  0.1346354E+01  0.0000000E+00  0.0000000E+00
```

$\Delta C_{L_{\beta=0}}$

```
0.,0.,0.,0.,0.,
0.,0.,0.,0.,0.,
0.,0.,0.,0.,0.,
```

$C_{L_{\delta_{S_1}}}$

```
.0165,.0125,.0135,.0150,.0165,
.0145,.0130,.0115,.0045,.0060,
.0070,.0065,0.,0.,0.
```

$C_{L_{\delta_{S_2}}}$

```
.0065,.0095,.0115,.0125,.0120,
.0125,.0125,.0135,.0120,.0110,
.0080,.0055,0.,0.,0.
```

$\Delta C_{L_{SP}}$

```
0.,0.,0.,0.,0.,
0.,0.,0.,0.,0.,
0.,0.,0.,0.,0.,
```

$C_{D_{BASIC}}$

```
0.1700000E-01  0.1705000E-01  0.2160000E-01  0.2295000E-01  0.2520000E-01
0.2295000E-01  0.2160000E-01  0.1705000E-01  0.1700000E-01  0.4338825E-01
0.4781333E-01  0.5320554E-01  0.5617464E-01  0.5818861E-01  0.5617464E-01
0.5320554E-01  0.4781333E-01  0.4338825E-01  0.1407652E+00  0.1565048E+00
0.1624715E+00  0.1677752E+00  0.1678456E+00  0.1677752E+00  0.1624715E+00
0.1565048E+00  0.1407652E+00  0.3116691E+00  0.3275625E+00  0.3448796E+00
0.3454817E+00  0.3463160E+00  0.3454817E+00  0.3448796E+00  0.3275625E+00
0.3116691E+00  0.5123598E+00  0.5432075E+00  0.5629274E+00  0.5651420E+00
0.5772239E+00  0.5651420E+00  0.5629274E+00  0.5432075E+00  0.5123598E+00
0.7522102E+00  0.7825773E+00  0.8042048E+00  0.8174002E+00  0.8211373E+00
0.8174002E+00  0.8042048E+00  0.7825773E+00  0.7522102E+00  0.9869851E+00
0.1031058E+01  0.1068497E+01  0.1095831E+01  0.1113046E+01  0.1095831E+01
0.1068497E+01  0.1031058E+01  0.9869851E+00  0.1211406E+01  0.1243747E+01
0.1294586E+01  0.1321289E+01  0.1362586E+01  0.1321289E+01  0.1294586E+01
0.1243747E+01  0.1211406E+01  0.1398217E+01  0.1424750E+01  0.1448008E+01
0.1483166E+01  0.1504872E+01  0.1483166E+01  0.1448008E+01  0.1424750E+01
0.1398217E+01  0.1563307E+01  0.1612557E+01  0.1625533E+01  0.1664035E+01
0.1683551E+01  0.1664035E+01  0.1625533E+01  0.1612557E+01  0.1563307E+01
0.1748774E+01  0.1782309E+01  0.1814706E+01  0.1849619E+01  0.1890475E+01
0.1849619E+01  0.1814706E+01  0.1782309E+01  0.1748774E+01  0.1905706E+01
0.1963867E+01  0.1982491E+01  0.2021536E+01  0.2034659E+01  0.2021536E+01
0.1982491E+01  0.1963867E+01  0.1905706E+01  0.0000000E+00  0.0000000E+00
```

$C_{D_{\delta_{S_1}}}$

```
-.0012,.0003,.0018,.0040,.0062,
.0075,.0095,.0105,.0075,.0090,
.0125,.0140,0.,0.,0.
```

$C_{D_{\delta_{S_2}}}$

```
-.0033,-.0025,-.0010,.0005,.0020,
.0040,.0060,.0085,.0095,.0110,
```

TABLE 12. (CONTINUED)

```
.0105,.0090,0.,0.,0.
```

$C_{D_{\delta_{S2}}}$

```
0.,0.,0.,0.,0.,
0.,0.,0.,0.,0.,
0.,0.,0.,0.,0.,
```

$\Delta C_{D_{SP}}$

```
 0.2941500E+00  0.2176000E+00  0.1462000E+00  0.6380000E-01  0.0000000E+00
-0.6380000E-01 -0.1462000E+00 -0.2176000E+00 -0.2941500E+00  0.3005500E+00
 0.2218000E+00  0.1464500E+00  0.7015000E-01  0.0000000E+00 -0.7015000E-01
-0.1464500E+00 -0.2218000E+00 -0.3005500E+00  0.2885500E+00  0.2037000E+00
 0.1410000E+00  0.6940000E-01  0.0000000E+00 -0.6940000E-01 -0.1410000E+00
-0.2037000E+00 -0.2885500E+00  0.2463000E+00  0.1678000E+00  0.1124000E+00
 0.5945000E-01  0.0000000E+00 -0.5945000E-01 -0.1124000E+00 -0.1678000E+00
-0.2463000E+00  0.2049000E+00  0.1587000E+00  0.1083000E+00  0.5500000E-01
 0.0000000E+00 -0.5500000E-01 -0.1083000E+00 -0.1587000E+00 -0.2049000E+00
 0.1895500E+00  0.1527500E+00  0.1177500E+00  0.6045000E-01  0.0000000E+00
-0.6045000E-01 -0.1177500E+00 -0.1527500E+00 -0.1895500E+00  0.2146500E+00
 0.1781500E+00  0.1331000E+00  0.7580000E-01  0.0000000E+00 -0.7580000E-01
-0.1331000E+00 -0.1781500E+00 -0.2146500E+00  0.2386000E+00  0.1866500E+00
 0.1460500E+00  0.7135000E-01  0.0000000E+00 -0.7135000E-01 -0.1460500E+00
-0.1866500E+00 -0.2386000E+00  0.2566000E+00  0.2026000E+00  0.1450500E+00
 0.7680000E-01  0.0000000E+00 -0.7680000E-01 -0.1450500E+00 -0.2026000E+00
-0.2566000E+00  0.2676000E+00  0.2223500E+00  0.1607500E+00  0.9275000E-01
 0.0000000E+00 -0.9275000E-01 -0.1607500E+00 -0.2223500E+00 -0.2676000E+00
 0.2737000E+00  0.2207500E+00  0.1515000E+00  0.7865000E-01  0.0000000E+00
-0.7865000E-01 -0.1515000E+00 -0.2207500E+00 -0.2737000E+00  0.2491500E+00
 0.1915000E+00  0.1315000E+00  0.7155000E-01  0.0000000E+00 -0.7155000E-01
-0.1315000E+00 -0.1915000E+00 -0.2491500E+00  0.0000000E+00  0.0000000E+00
```

$C_{y_{BASIC}}$

```
0.,0.,0.,0.,0.,
0.,0.,0.,0.,0.,
0.,0.,0.,0.,0.,
```

$\Delta C_{y_{\beta=0}}$

```
0.1490,.2686,.1250,.1596,.3264,
.3800,.6799,.5603,.9302,.1392,
-.0696,-.3818,0.,0.,0.,
```

C_{y_P}

```
.5684,.5356,.4996,.6782,.5295,
.2712,-.7340,-1.3173,-2.0531,-.7688,
-.2885,-.1206,0.,0.,0.,
```

C_{y_r}

```
-.00095,-.0010,-.00085,-.00065,-.0003
.0001,.0006,.0016,.0024,.0025
.00255,.00265,0.,0.,0.
```

$C_{y_{\delta_a}}$

```
0.,0.,0.,0.,0.,
0.,0.,0.,0.,0.,
0.,0.,0.,0.,0.,
```

$C_{y_{SP}}$

```
.00480,.00520,.00560,.005[illegible],.00560,
.00560,.00560,.00520,.004[illegible],.00450,
.00485,.00520,.00530,.00[illegible],.00530,
.00520,.00485,.00450,.00[illegible],.00450,
.00480,.00495,.00510,.004[illegible],.00480,
.00450,.00420,.00370,.004[illegible],.00430,
.00450,.00470,.00450,.004[illegible],.00400,
.00370,.00330,.00355,.00380,.00400,
.00420,.00400,.00380,.00355,.003[illegible],
.00280,.00305,.00330,.00350,.003[illegible],
.00350,.00330,.00305,.00280,.002[illegible],
.00250,.00270,.00290,.00310,.002[illegible],
.00270,.00250,.00230,.00160,.00180,
.00200,.00220,.00240,.00220,.00200,
.00180,.00160,.00100,.00110,.00120,
.00135,.00150,.00135,.00120,.00110,
.00100,.00030,.00035,.00040,.00045,
.00050,.00045,.00040,.00035,.00030,
0.,0.,0.,0.,0.,
0.,0.,0.,0.,0.,
0.,0.,0.,0.,0.,
0.,0.,0.,0.,0.,
```

$C_{y_{\delta_r}}$

TABLE 12. (CONTINUED)

0.9500000E-02	0.8000000E-02	0.6000000E-02	0.3000000E-02	0.0000000E+00	
-0.3000000E-02	-0.6000000E-02	-0.8000000E-02	-0.9500000E-02	0.2050000E-01	
0.1700000E-01	0.1350000E-01	0.6500000E-02	0.0000000E+00	-0.6500000E-02	
-0.1350000E-01	-0.1700000E-01	-0.2050000E-01	0.3100000E-01	0.2600000E-01	
0.2100000E-01	0.1050000E-01	0.0000000E+00	-0.1050000E-01	-0.2100000E-01	
-0.2600000E-01	-0.3100000E-01	0.4700000E-01	0.3650000E-01	0.2650000E-01	
0.1350000E-01	0.0000000E+00	-0.1350000E-01	-0.2650000E-01	-0.3650000E-01	
-0.4700000E-01	0.5500000E-01	0.4100000E-01	0.2700000E-01	0.1600000E-01	
0.0000000E+00	-0.1600000E-01	-0.2700000E-01	-0.4100000E-01	-0.5500000E-01	
0.5250000E-01	0.3933333E-01	0.2616667E-01	0.1483333E-01	0.0000000E+00	
-0.1483333E-01	-0.2616667E-01	-0.3933333E-01	-0.5250000E-01	0.4900000E-01	
0.3766667E-01	0.2533333E-01	0.1366667E-01	0.0000000E+00	-0.1366667E-01	$C_{\ell_{BASIC}}$
-0.2533333E-01	-0.3766667E-01	-0.4900000E-01	0.4750000E-01	0.3600000E-01	
0.2450000E-01	0.1250000E-01	0.0000000E+00	-0.1250000E-01	-0.2450000E-01	
-0.3600000E-01	-0.4750000E-01	0.5200000E-01	0.3900000E-01	0.2550000E-01	
0.1300000E-01	0.0000000E+00	-0.1300000E-01	-0.2550000E-01	-0.3900000E-01	
-0.5200000E-01	0.6100000E-01	0.4600000E-01	0.3050000E-01	0.1500000E-01	
0.0000000E+00	-0.1500000E-01	-0.3050000E-01	-0.4600000E-01	-0.6100000E-01	
0.6450000E-01	0.4850000E-01	0.3300000E-01	0.1650000E-01	0.0000000E+00	
-0.1650000E-01	-0.3300000E-01	-0.4850000E-01	-0.6450000E-01	0.6500000E-01	
0.4950000E-01	0.3350000E-01	0.1650000E-01	0.0000000E+00	-0.1650000E-01	
-0.3350000E-01	-0.4950000E-01	-0.6500000E-01	0.0000000E+00	0.0000000E+00	
0.,0.,0.,0.,0.,					
0.,0.,0.,0.,0.,					$\Delta C_{\ell_{\beta=0}}$
0.,0.,0.,0.,0.,					
-0.4016,-.4057,-.2000,-.080,-.080,					
-.2000,-.2700,-.2283,-.1863,-.1104,					C_{ℓ_p}
-.0361,-.0891,0,0,0,					
0.0080,.0552,.0838,.0789,.2310,					
.2834,.3200,.3200,.2545,.0725,					C_{ℓ_r}
-.0434,-.0588,0,0,0,					
0.7900000E-03	0.7900000E-03	0.7900000E-03	0.7900000E-03	0.7900000E-03	
0.7900000E-03	0.7900000E-03	0.7900000E-03	0.7900000E-03	0.7900000E-03	
0.7900000E-03	0.7900000E-03	0.7900000E-03	0.7900000E-03	0.7900000E-03	
0.7900000E-03	0.7900000E-03	0.7900000E-03	0.7900000E-03	0.7900000E-03	
0.7900000E-03	0.7900000E-03	0.7900000E-03	0.7900000E-03	0.7900000E-03	
0.7900000E-03	0.7900000E-03	0.6200000E-03	0.6600000E-03	0.7125000E-03	
0.7775000E-03	0.8050000E-03	0.7775000E-03	0.7125000E-03	0.6600000E-03	
0.6200000E-03	0.4825000E-03	0.5750000E-03	0.6600000E-03	0.7475000E-03	
0.7550000E-03	0.7475000E-03	0.6600000E-03	0.5750000E-03	0.4825000E-03	
0.3100000E-03	0.4650000E-03	0.5300000E-03	0.6050000E-03	0.6450000E-03	$C_{\ell_{\delta_a}}$
0.6050000E-03	0.5300000E-03	0.4650000E-03	0.3100000E-03	0.2350000E-03	
0.3475000E-03	0.3900000E-03	0.4400000E-03	0.4850000E-03	0.4400000E-03	
0.3900000E-03	0.3475000E-03	0.2350000E-03	0.1675000E-03	0.2200000E-03	
0.2175000E-03	0.2150000E-03	0.2350000E-03	0.2150000E-03	0.2175000E-03	
0.2200000E-03	0.1675000E-03	0.9250000E-04	0.1425000E-03	0.1225000E-03	
0.1400000E-03	0.1200000E-03	0.1400000E-03	0.1225000E-03	0.1425000E-03	
0.9250000E-04	0.1725000E-03	0.1375000E-03	0.1150000E-03	0.1175000E-03	
0.1400000E-03	0.1175000E-03	0.1150000E-03	0.1375000E-03	0.1725000E-03	
0.1450000E-03	0.1375000E-03	0.1825000E-03	0.2425000E-03	0.2200000E-03	
0.2425000E-03	0.1825000E-03	0.1375000E-03	0.1450000E-03	0.1750000E-03	
0.2100000E-03	0.2775000E-03	0.3300000E-03	0.3500000E-03	0.3300000E-03	
0.2775000E-03	0.2100000E-03	0.1750000E-03	0.0000000E+00	0.0000000E+00	
0.,0.,0.,0.,0.,					
0.,0.,0.,0.,0.,					$C_{\ell_{\delta_{SP}}}$
0.,0.,0.,0.,0.,					
0.9600000E-04	0.1040000E-03	0.1120000E-03	0.1120000E-03	0.1120000E-03	
0.1120000E-03	0.1120000E-03	0.1040000E-03	0.9600000E-04	0.9000000E-04	
0.9700000E-04	0.1040000E-03	0.1060000E-03	0.1080000E-03	0.1060000E-03	$C_{\ell_{\delta_r}}$
0.1040000E-03	0.9700000E-04	0.9000000E-04	0.8400000E-04	0.9000000E-04	
0.9600000E-04	0.9900000E-04	0.1020000E-03	0.9900000E-04	0.9600000E-04	
0.9000000E-04	0.8400000E-04	0.7400000E-04	0.8000000E-04	0.8600000E-04	

TABLE 12. (CONTINUED)

0.9000000E-04	0.9400000E-04	0.9000000E-04	0.8600000E-04	0.8000000E-04	
0.7400000E-04	0.6600000E-04	0.7100000E-04	0.7600000E-04	0.8000000E-04	
0.8400000E-04	0.8000000E-04	0.7600000E-04	0.7100000E-04	0.6600000E-04	
0.5600000E-04	0.6100000E-04	0.6600000E-04	0.7000000E-04	0.7400000E-04	
0.7000000E-04	0.6600000E-04	0.6100000E-04	0.5600000E-04	0.4500000E-04	
0.5000000E-04	0.5400000E-04	0.5800000E-04	0.6200000E-04	0.5800000E-04	
0.5400000E-04	0.5000000E-04	0.4600000E-04	0.3200000E-04	0.3600000E-04	
0.4000000E-04	0.4400000E-04	0.4800000E-04	0.4400000E-04	0.4000000E-04	
0.3600000E-04	0.3200000E-04	0.2000000E-04	0.2200000E-04	0.2400000E-04	$C_{l_{\delta_r}}$
0.2700000E-04	0.3000000E-04	0.2700000E-04	0.2400000E-04	0.2200000E-04	
0.2000000E-04	0.6000000E-05	0.7000000E-05	0.8000000E-05	0.9000000E-05	
0.1000000E-04	0.9000000E-05	0.8000000E-05	0.7000000E-05	0.6000000E-05	
0.0000000E+00	0.0000000E+00	0.0000000E+00	0.0000000E+00	0.0000000E+00	
0.0000000E+00	0.0000000E+00	0.0000000E+00	0.0000000E+00	0.0000000E+00	
0.0000000E+00	0.0000000E+00	0.0000000E+00	0.0000000E+00	0.0000000E+00	
0.0000000E+00	0.0000000E+00	0.0000000E+00	0.0000000E+00	0.0000000E+00	
0.6052187E-01	0.6540000E-01	0.6888437E-01	0.7097500E-01	0.7167188E-01	
0.7097500E-01	0.6888437E-01	0.6540000E-01	0.6052187E-01	0.2583125E-01	
0.3173750E-01	0.3595625E-01	0.3848750E-01	0.3933125E-01	0.3848750E-01	
0.3595625E-01	0.3173750E-01	0.2583125E-01	-0.4367188E-01	-0.2247500E-01	
-0.7334375E-02	0.1750000E-02	0.4778125E-02	0.1750000E-02	-0.7334375E-02	
-0.2247500E-01	-0.4367188E-01	-0.1495656E+00	-0.1033000E+00	-0.7025313E-01	
-0.5042500E-01	-0.4381563E-01	-0.5042500E-01	-0.7025313E-01	-0.1033000E+00	
-0.1495656E+00	-0.1772469E+00	-0.1244188E+00	-0.8668438E-01	-0.6404375E-01	
-0.5649687E-01	-0.6404375E-01	-0.8668438E-01	-0.1244188E+00	-0.1772469E+00	
-0.2248094E+00	-0.1879937E+00	-0.1616969E+00	-0.1459187E+00	-0.1406594E+00	$C_{m_{BASIC}}$
-0.1459187E+00	-0.1616969E+00	-0.1879937E+00	-0.2248094E+00	-0.2387250E+00	
-0.2321625E+00	-0.2274750E+00	-0.2246625E+00	-0.2237250E+00	-0.2246625E+00	
-0.2274750E+00	-0.2321625E+00	-0.2387250E+00	-.300	-.300	
-.300	-.300	-.300	-.300	-.300	
-.300	-.300	-0.3490531E+00	-0.3721313E+00	-0.3886156E+00	
-0.3985063E+00	-0.4018031E+00	-0.3985063E+00	-0.3886156E+00	-0.3721313E+00	
-0.3490531E+00	-0.4248187E+00	-0.4461250E+00	-0.4613438E+00	-0.4704750E+00	
-0.4735188E+00	-0.4704750E+00	-0.4613438E+00	-0.4461250E+00	-0.4248187E+00	
-0.4808313E+00	-0.5169250E+00	-0.5427063E+00	-0.5581750E+00	-0.5633313E+00	
-0.5581750E+00	-0.5427063E+00	-0.5169250E+00	-0.4808313E+00	-0.5400406E+00	
-0.5832000E+00	-0.6140281E+00	-0.6325250E+00	-0.6386906E+00	-0.6325250E+00	
-0.6140281E+00	-0.5832000E+00	-0.5400406E+00	0.0000000E+00	0.0000000E+00	
-.055,-.055,-.055,-.055,-.055					
-.055,-.055,-.055,-.055,-.055					$\Delta C_{m_{\beta=0}}$
-.055,-.055,-.055,-.055,-.055					
-15.424,-14.129,-17.967,-22.807,-21.078,					
-19.629,-15.185,-1.886,-7.707,-5.479,					C_{m_q}
-13.113,-10.298,0,0,0,					
-.009,-.0115,-.0140,-.0155,-.0160,					
-.0160,-.0160,-.0145,-.0145,-.0145,					$C_{m_{\delta_{s_1}}}$
-.0145,-.0120,0.,0.,0.					
-.0195,-.0185,-.0185,-.0190,-.0190,					
-.0170,-.0133,-.0075,-.0010,.0040,					$C_{m_{\delta_{s_2}}}$
.0060,.0005,0.,0.,0.					
0.,0.,0.,0.,0.,					
0.,0.,0.,0.,0.,					$\Delta C_{m_{sp}}$
0.,0.,0.,0.,0.,					
-0.4000000E-01	-0.3050000E-01	-0.2150000E-01	-0.1000000E-01	0.0000000E+00	
0.1000000E-01	0.2150000E-01	0.3050000E-01	0.4000000E-01	-0.3900000E-01	
-0.3000000E-01	-0.2150000E-01	-0.1000000E-01	0.0000000E+00	0.1000000E-01	
0.2150000E-01	0.3000000E-01	0.3900000E-01	-0.3600000E-01	-0.2750000E-01	$C_{n_{BASIC}}$
-0.1900000E-01	-0.9500000E-02	0.0000000E+00	0.9500000E-02	0.1900000E-01	
0.2750000E-01	0.3600000E-01	-0.8500000E-02	-0.7500000E-02	-0.6000000E-02	
-0.3000000E-02	0.0000000E+00	0.3000000E-02	0.6000000E-02	0.7500000E-02	

TABLE 12. (CONCLUDED)

$C_{n_{BASIC}}$

```
 0.8500000E-02  0.1000000E-01  0.7000000E-02  0.4000000E-02  0.2000000E-02
 0.0000000E+00 -0.2000000E-02 -0.4000000E-02 -0.7000000E-02 -0.1000000E-01
 0.2550000E-01  0.1700000E-01  0.9000000E-02  0.4500000E-02  0.0000000E+00
-0.4500000E-02 -0.9000000E-02 -0.1700000E-01 -0.2550000E-01  0.3800000E-01
 0.2800000E-01  0.1800000E-01  0.1100000E-01  0.0000000E+00 -0.1100000E-01
-0.1800000E-01 -0.2800000E-01 -0.3800000E-01  0.4050000E-01  0.3150000E-01
 0.2300000E-01  0.1450000E-01  0.0000000E+00 -0.1450000E-01 -0.2300000E-01
-0.3150000E-01 -0.4050000E-01  0.4050000E-01  0.2950000E-01  0.1900000E-01
 0.8500000E-02  0.0000000E+00 -0.8500000E-02 -0.1900000E-01 -0.2950000E-01
-0.4050000E-01  0.4150000E-01  0.3150000E-01  0.2150000E-01  0.1300000E-01
 0.0000000E+00 -0.1300000E-01 -0.2150000E-01 -0.3150000E-01 -0.4150000E-01
 0.3600000E-01  0.2800000E-01  0.2050000E-01  0.1450000E-01  0.0000000E+00
-0.1450000E-01 -0.2050000E-01 -0.2800000E-01 -0.3600000E-01  0.2600000E-01
 0.2200000E-01  0.1750000E-01  0.1450000E-01  0.0000000E+00 -0.1450000E-01
-0.1750000E-01 -0.2200000E-01 -0.2600000E-01  0.0000000E+00  0.0000000E+00
```

$\Delta C_{n_{\beta=0}}$

```
0.,0.,0.,0.,0.
0.,0.,0.,0.,0.
0.,0.,0.,0.,0.,
```

$\Delta C_{n_{\delta_s}}$

```
.000117,.000117,.00015,.000183,.000217,
.000250,.000267,.000133,.000083,.000050,
.000050,.000050,0.,0.,0.,
```

C_{n_p}

```
-0.0333,-.0947,-.1068,-.1189,-.131
-.080,-.0116,.1421,.1007,-.0298,
-.0958,-.0134,0,0,0,
```

C_{n_r}

```
-0.1154,-.1256,-.1380,-.2048,-.1897,
-.1918,-.1972,-.2911,-.1449,-.0458,
.0455,-.0441,0,0,0,
```

$C_{n_{\delta_a}}$

```
.00025,.00025,.000175,.000075,-.00005,
-.000225,-.000375,-.000525,-.00070,-.000825
-.00085,-.000725,0.,0.,0.
```

$C_{n_{SP}}$

```
0.,0.,0.,0.,0.,
0.,0.,0.,0.,0.,
0.,0.,0.,0.,0.,
```

$C_{n_{\delta_r}}$

```
-.00103,-.00115,-.00127,-.00142,-.00158,
-.00142,-.00127,-.00115,-.00103,-.00107,
-.00118,-.00130,-.00140,-.00150,-.00140
-.00130,-.00118,-.00107,-.00102,-.00114,
-.00127,-.00135,-.00144,-.00135,-.00127,
-.00114,-.00102,-.00085,-.00102,-.00120,
-.00130,-.00140,-.00130,-.00120,-.00102,
-.00085,-.00063,-.00085,-.00107,-.00120,
-.00134,-.00120,-.00107,-.00085,-.00063,
-.00048,-.00066,-.00084,-.00098,-.00112,
-.000[illegible]8,-.00084,-.00066,-.00048,-.00042,
-.00054,-.00067,-.00072,-.00077,-.00072,
-.00067,-.00054,-.00042,-.00033,-.00035,
-.00037,-.00044,-.00052,-.00044,-.00037,
-.00035,-.00033,-.00020,-.00020,-.00020,
-.00024,-.00029,-.00024,-.00020,-.00020,
-.00020,-.00004,-.00004,-.00004,-.00007,
-.00011,-.00007,-.00004,-.00004,-.00004,
.00000,.00000,.00000,.00000,.00000,
.00000,.00000,.00000,.00000,.00000,
.00000,.00000,.00000,.00000,.00000
.00000,.00000,.00000,.00000,.00000
```

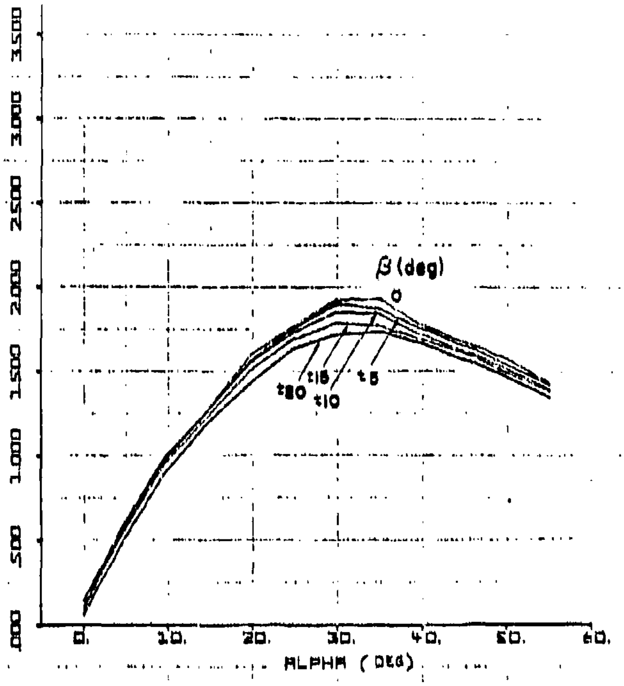

Figure 36. $C_{L_{BASIC}}(\alpha,\beta)$

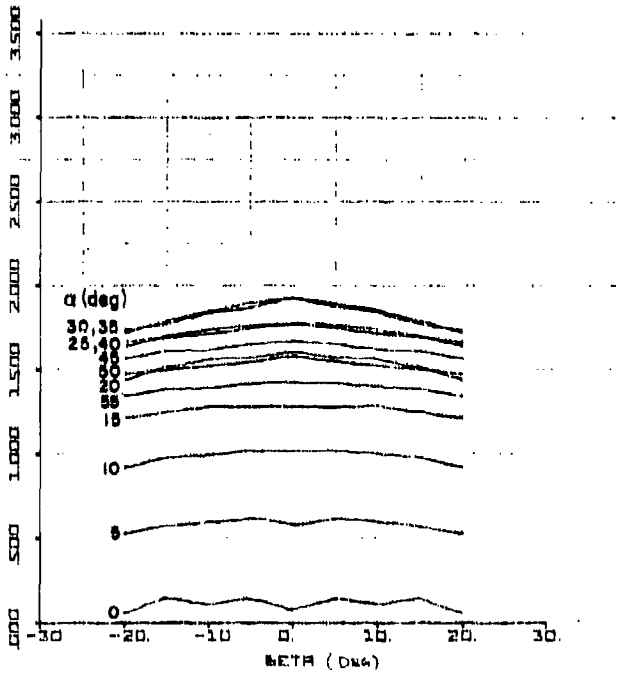

Figure 37. $C_{L_{BASIC}}(\alpha,\beta)$

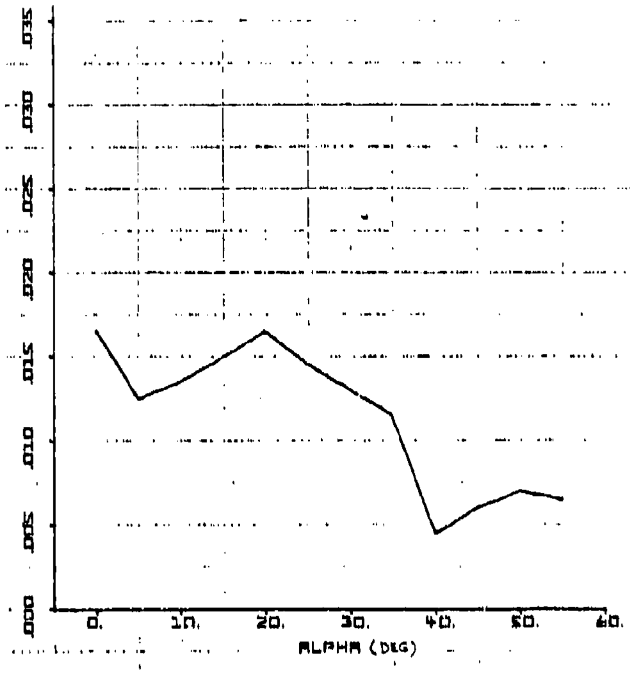

Figure 38. $C_{L\delta_{s_1}}(\alpha)$ - 1/deg

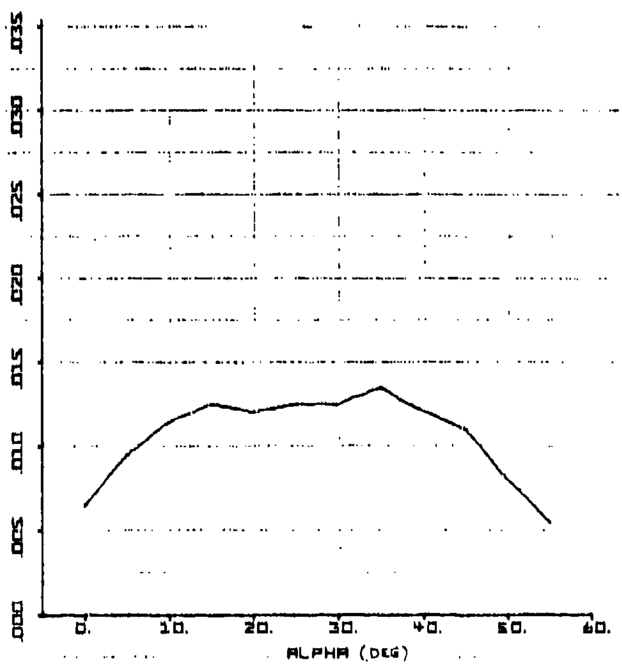

Figure 39. $C_{L\delta_{s_2}}(\alpha)$ - 1/deg

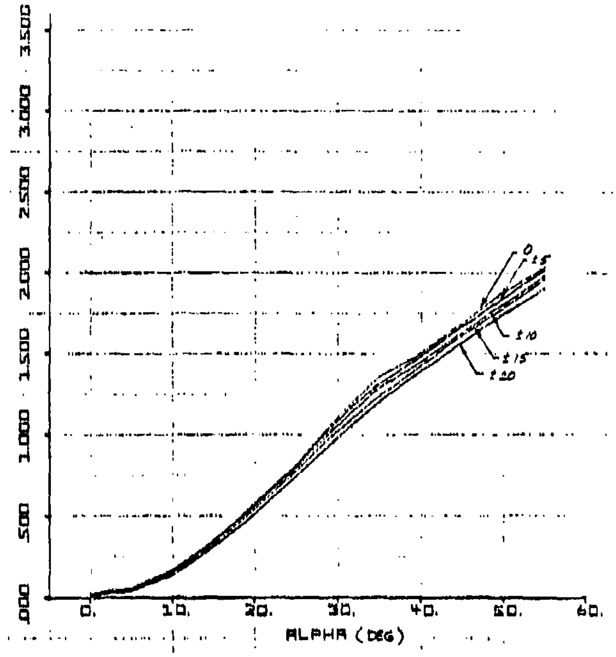

Figure 40. $C_{D_{BASIC}}(\alpha,\beta)$

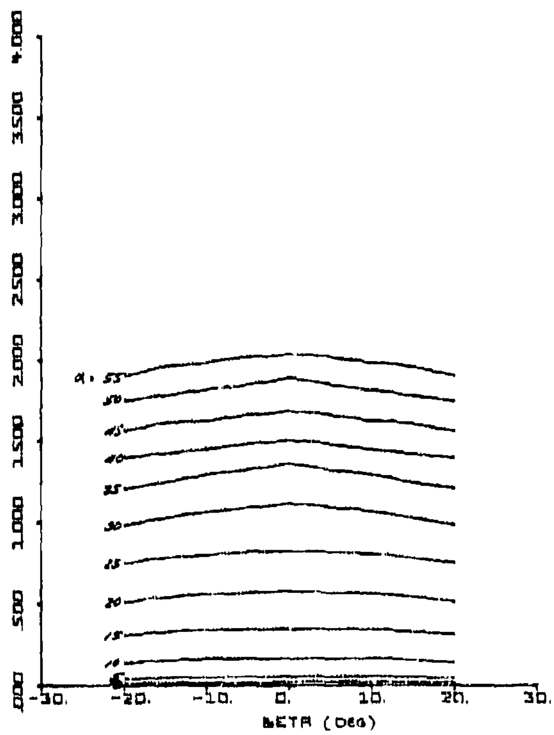

Figure 41. $C_{D_{BASIC}}(\alpha,\beta)$

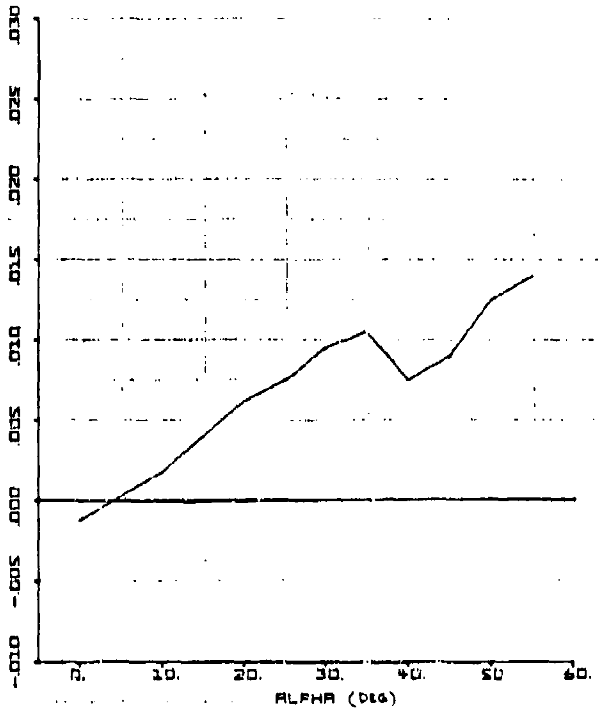

Figure 42. $C_{D\delta_{s_1}}(\alpha)$ - 1/deg

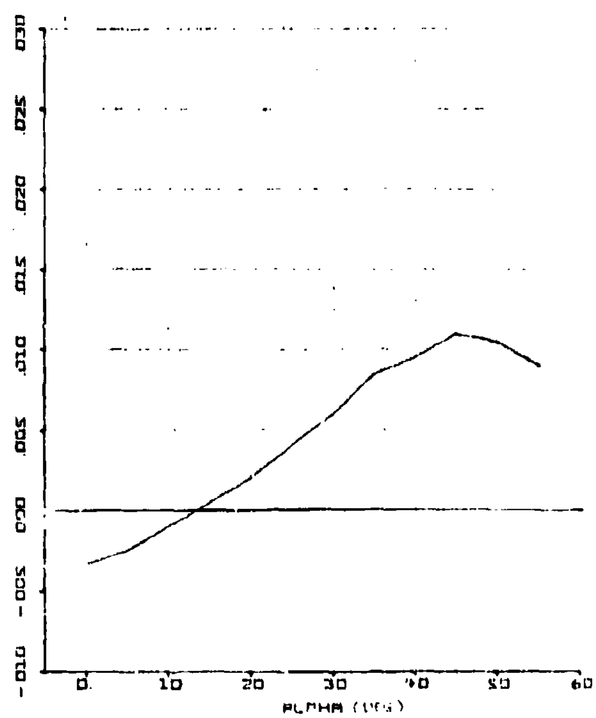

Figure 43. $C_{D\delta_{s_2}}(\alpha)$ - 1/deg

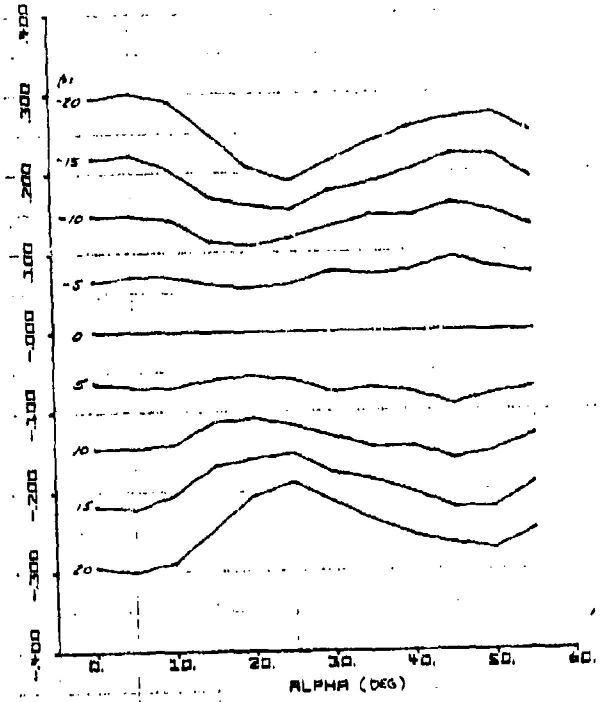

Figure 44. $C_{Y_{BASIC}}(\alpha,\beta)$

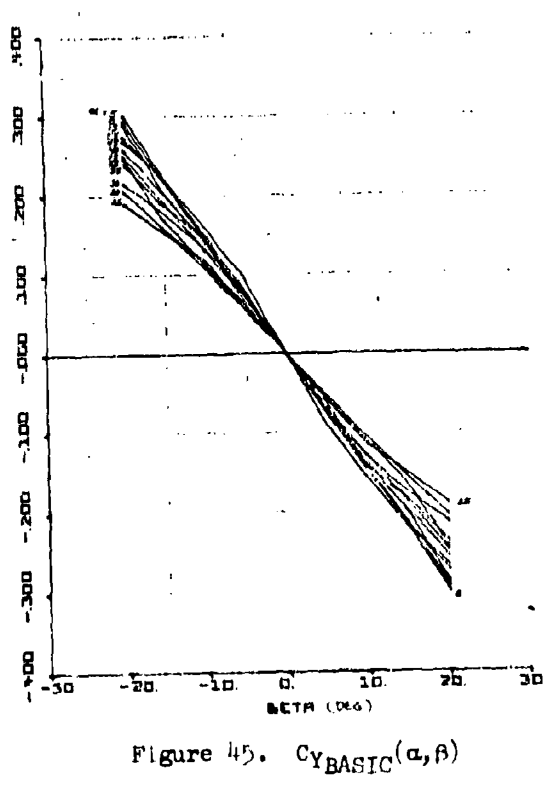

Figure 45. $C_{Y_{BASIC}}(\alpha,\beta)$

Figure 46. $C_{Y_p}(\alpha)$ - 1/rad

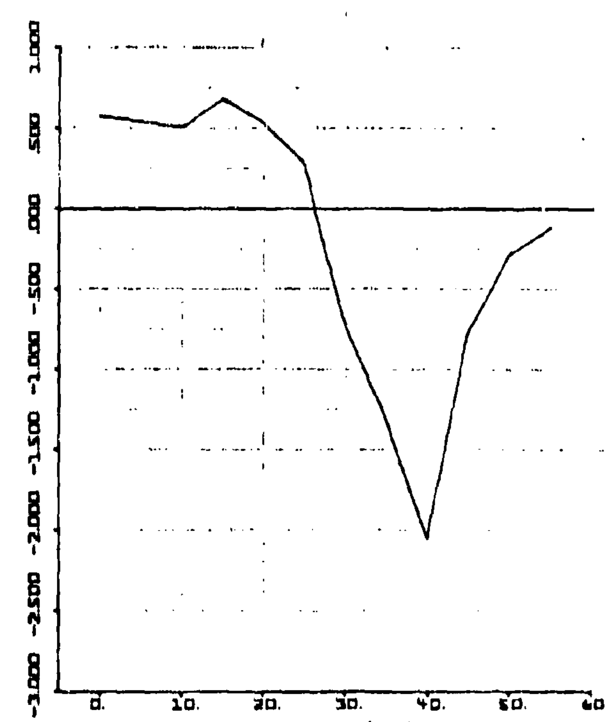

Figure 47. $C_{Y_r}(\alpha)$ - 1/rad

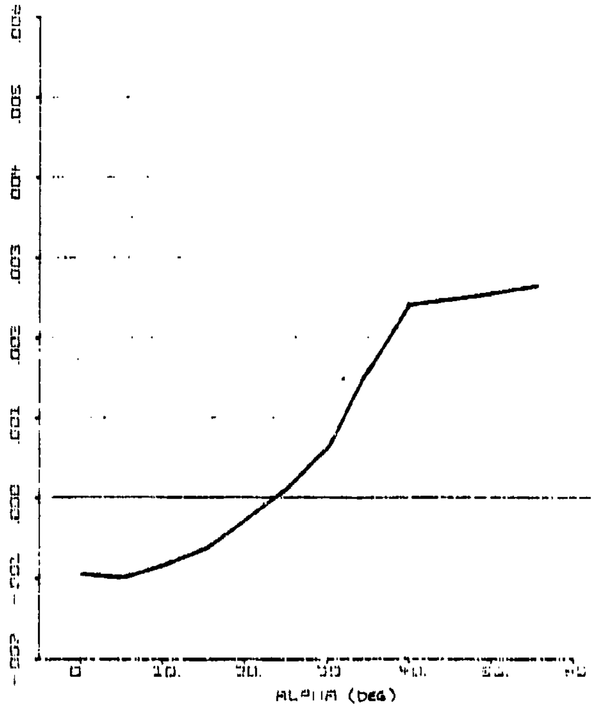

Figure 48. $C_{Y_{\delta a}}(\alpha)$ - 1/deg

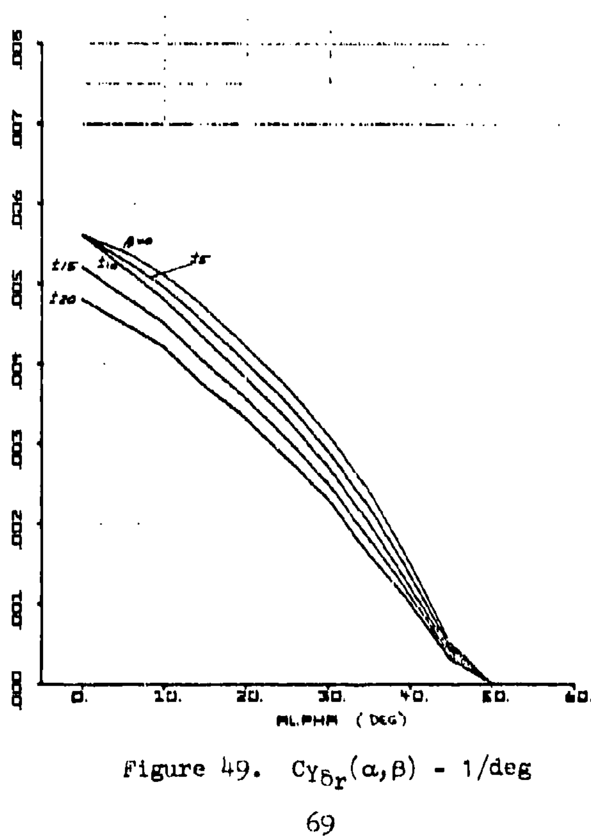

Figure 49. $C_{Y_{\delta r}}(\alpha,\beta)$ - 1/deg

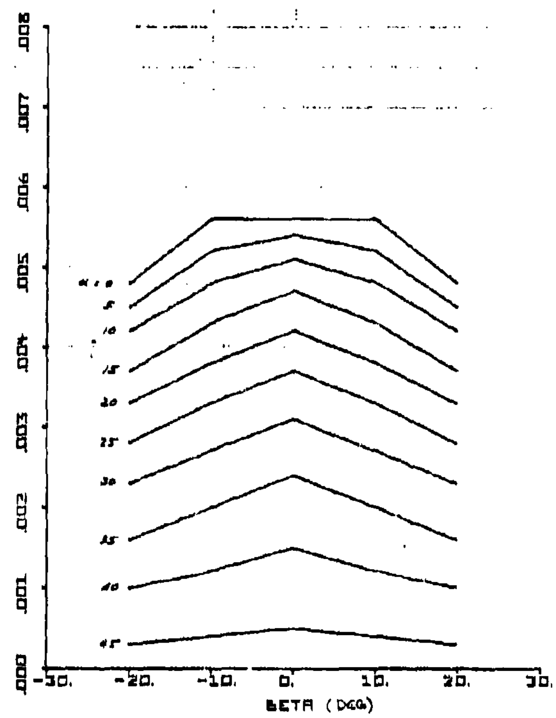

Figure 50. $Cy_{\delta_r}(\alpha, \beta)$ - 1/deg

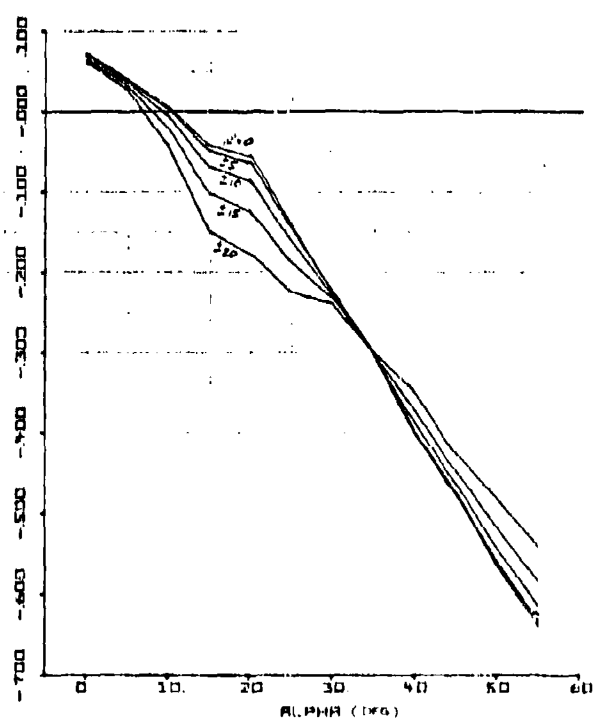

Figure 51. $Cm_{BASIC}(\alpha, \beta)$

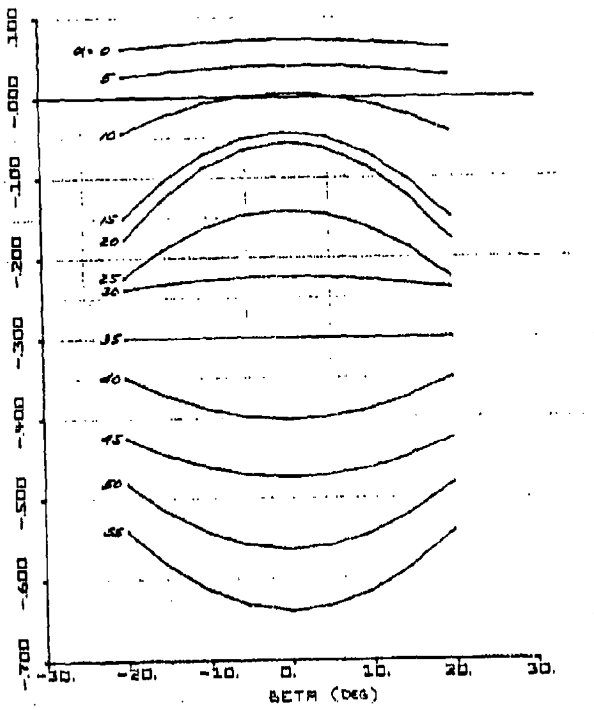

Figure 52. $Cm_{BASIC}(\alpha,\beta)$

Figure 53. $Cm_q(\alpha)$ - 1/rad

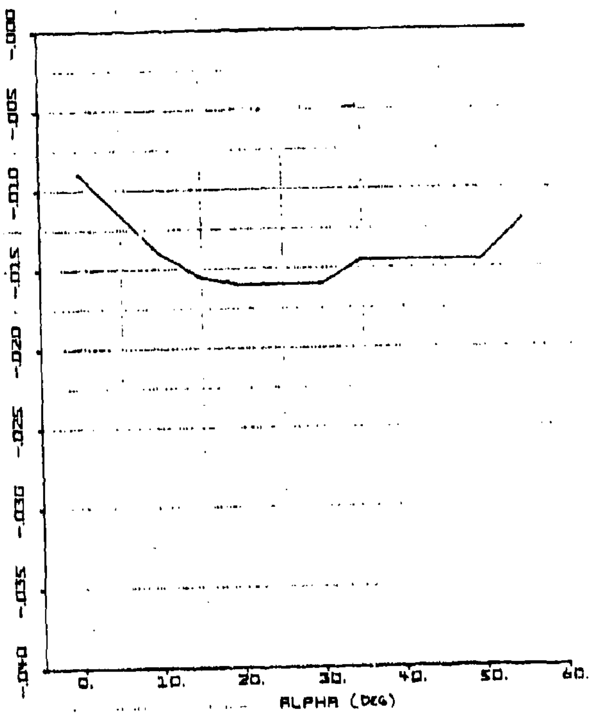

Figure 54. $C_{m_{\delta_{s_1}}}(\alpha)$ - 1/deg

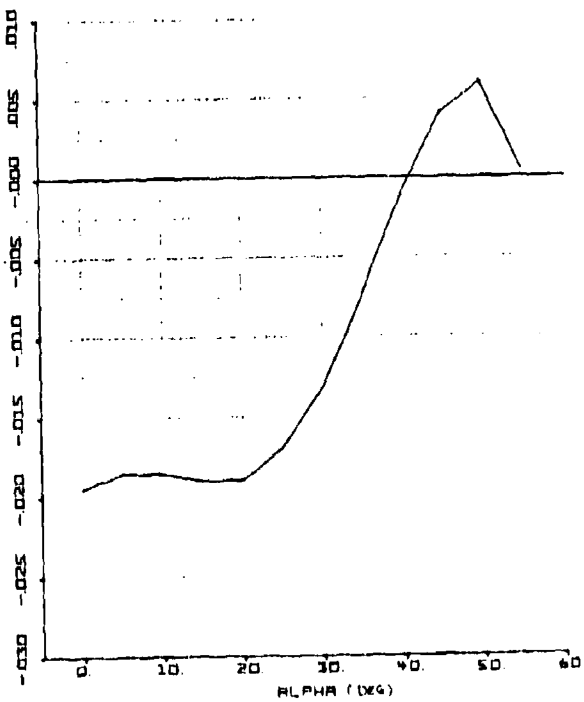

Figure 55. $C_{m_{\delta_{s_2}}}(\alpha)$ - 1/deg

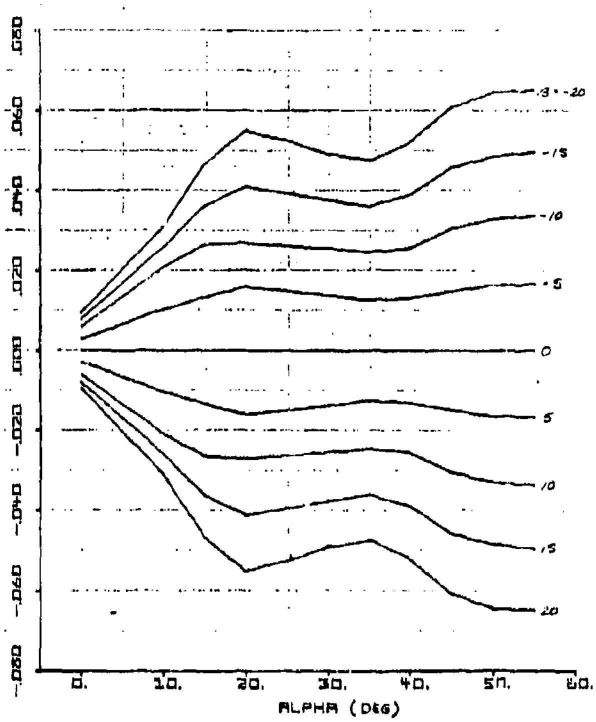

Figure 56. $C_{\ell_{BASIC}}(\alpha,\beta)$ - 1/deg

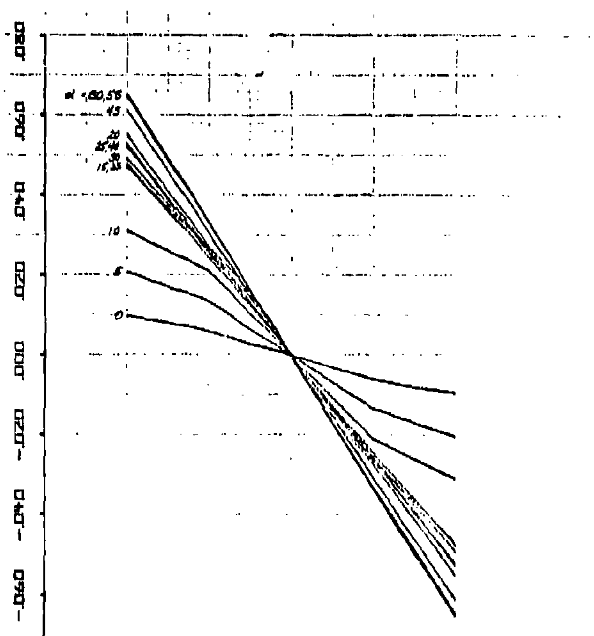

Figure 57. $C_{\ell_{BASIC}}(\alpha,\beta)$

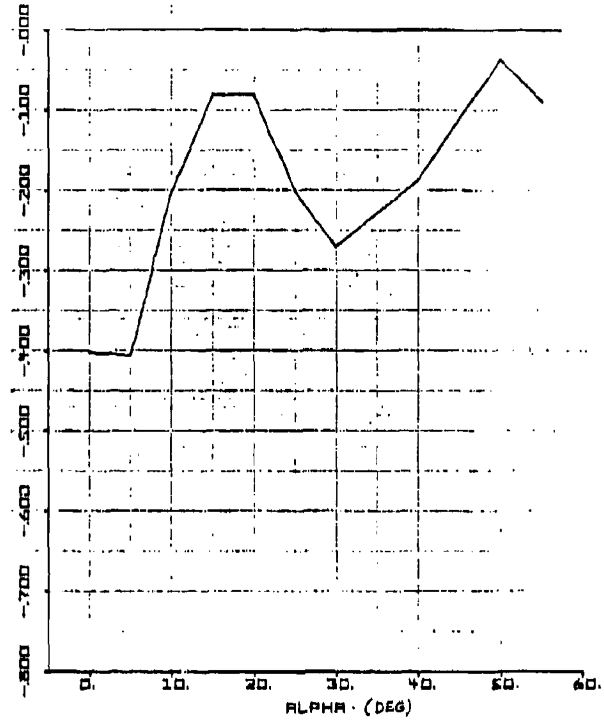

Figure 58. $C_{\ell_p}(\alpha)$ - 1/rad

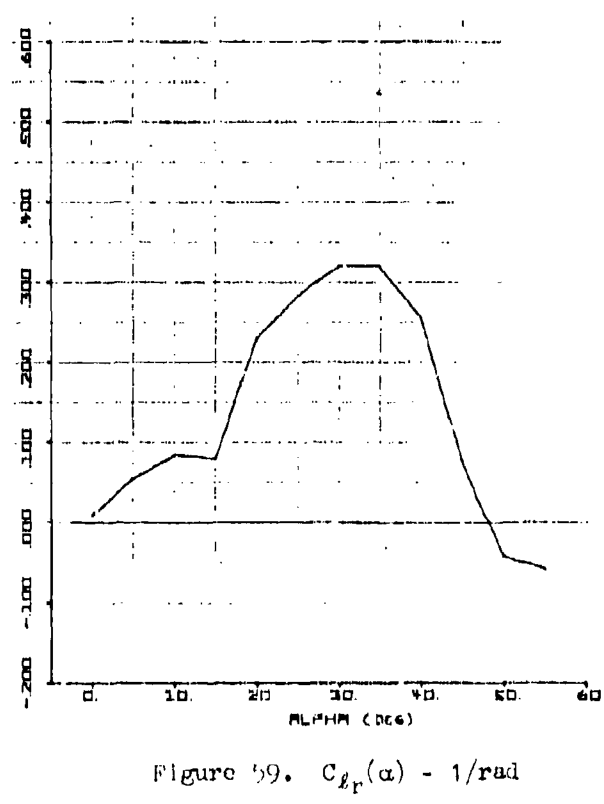

Figure 59. $C_{\ell_r}(\alpha)$ - 1/rad

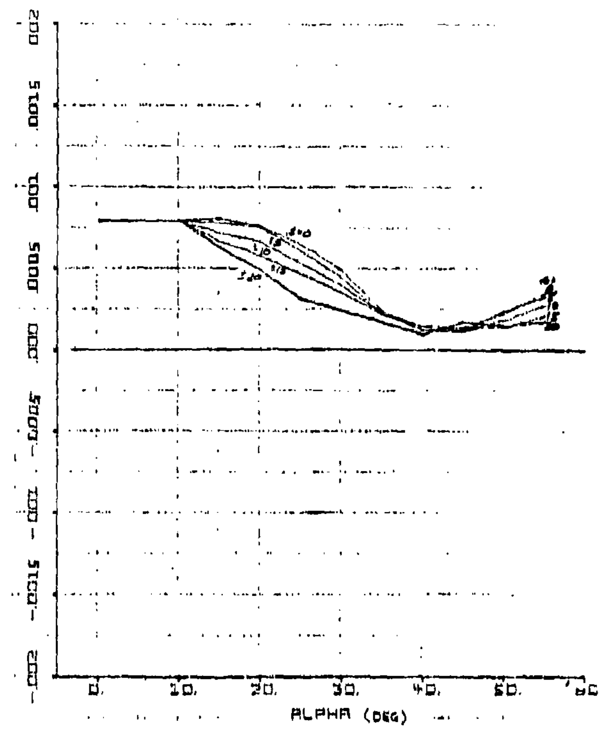

Figure 60. $C_{\ell_{\delta_a}}(\alpha,\beta)$ - 1/deg

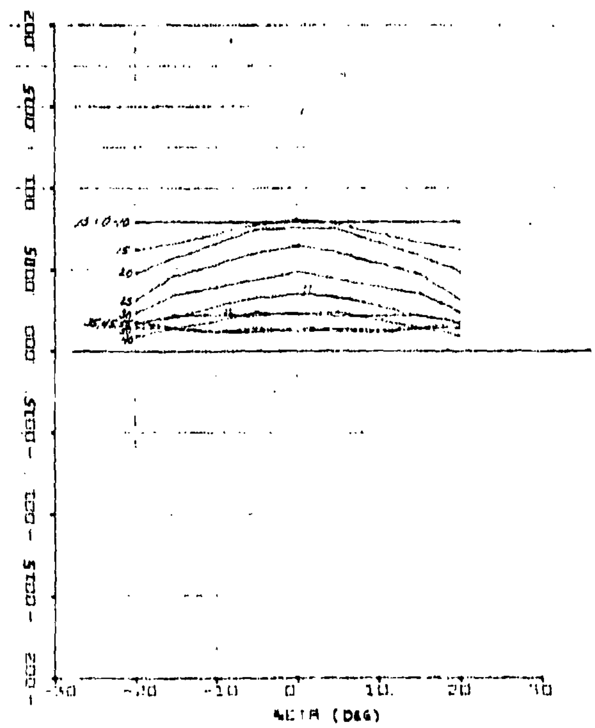

Figure 61. $C_{\ell_{\delta_a}}(\alpha,\beta)$ - 1/deg

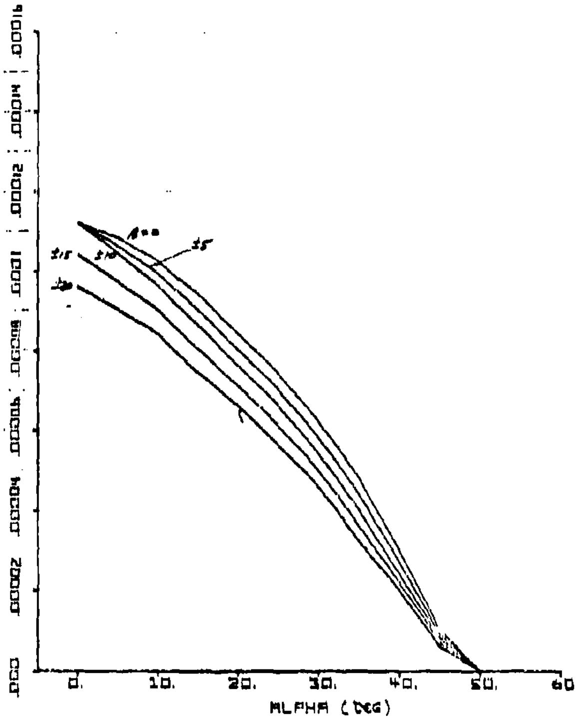

Figure 62. $C_{\ell\delta_r}(\alpha,\beta)$ - 1/deg

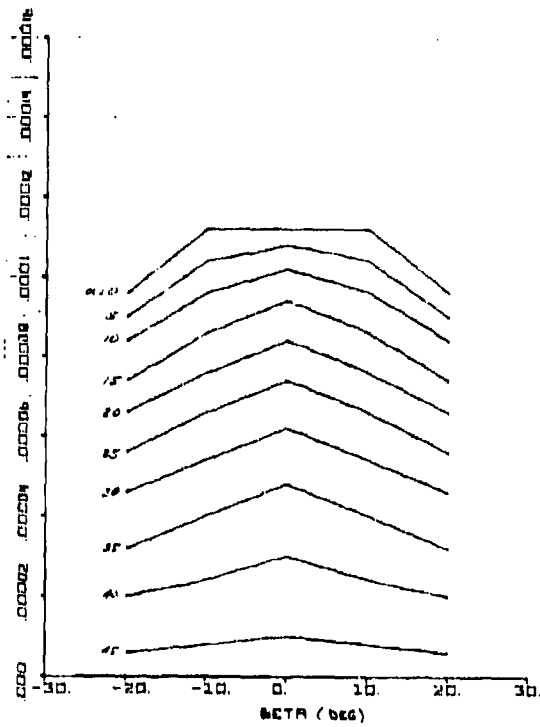

Figure 63. $C_{\ell\delta_r}(\alpha,\beta)$ - 1/deg

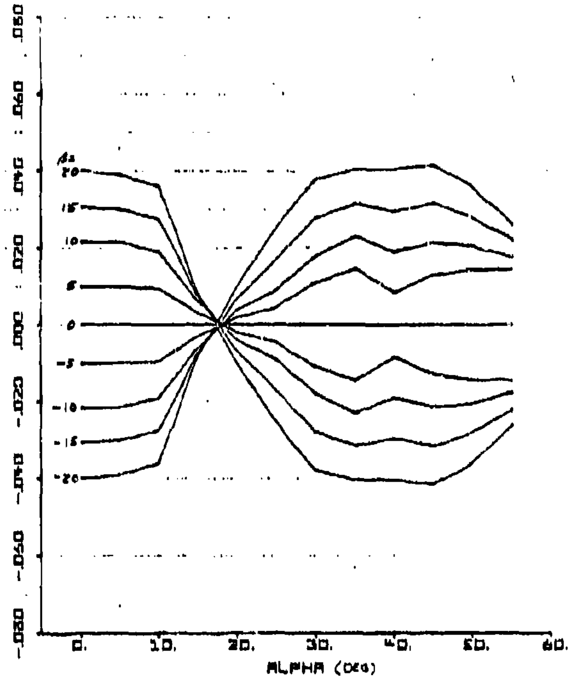

Figure 64. $Cn_{BASIC}(\alpha,\beta)$

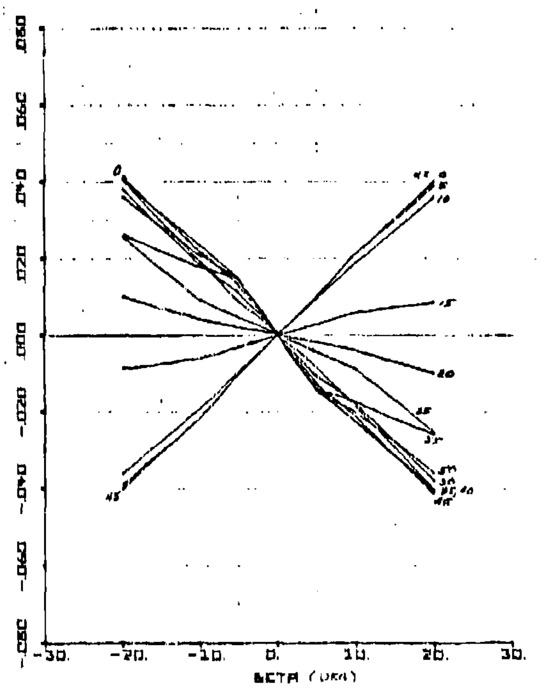

Figure 65. $Cn_{BASIC}(\alpha,\beta)$

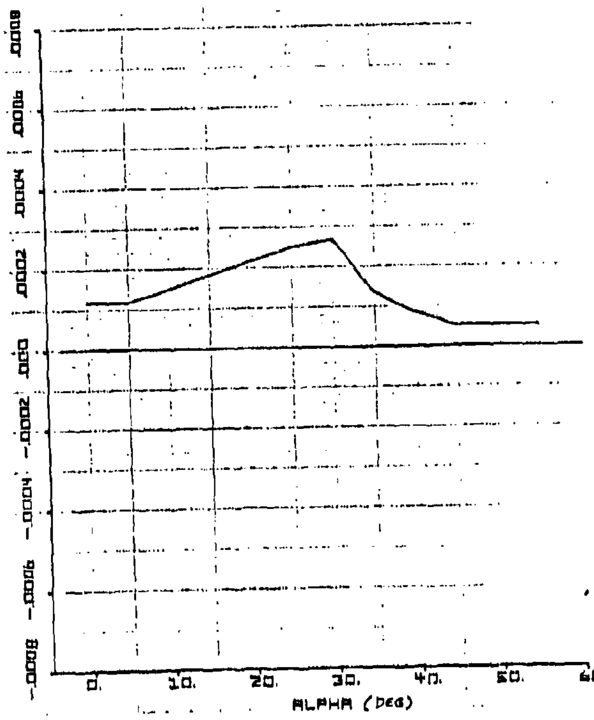

Figure 66. $\Delta Cn\delta_{\beta}(\alpha)$ - 1/deg

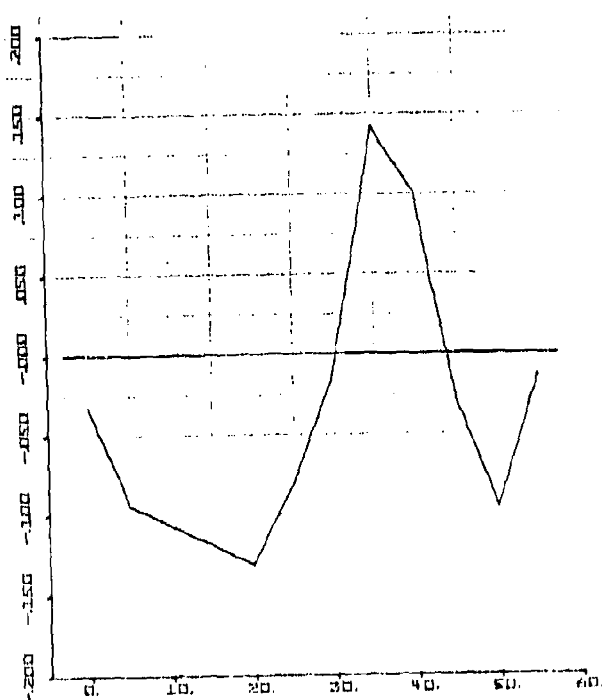

Figure 67. $C_{n_p}(\alpha)$ - 1/rad

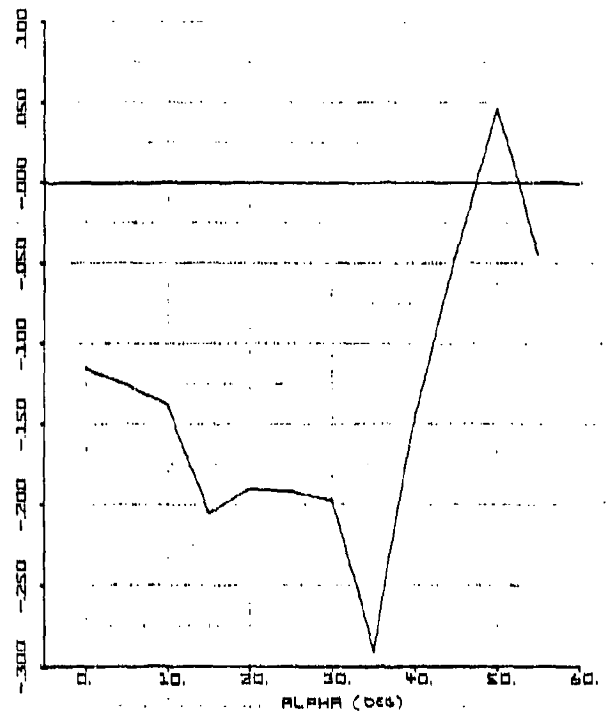

Figure 68. $C_{n_r}(\alpha)$ - 1/rad

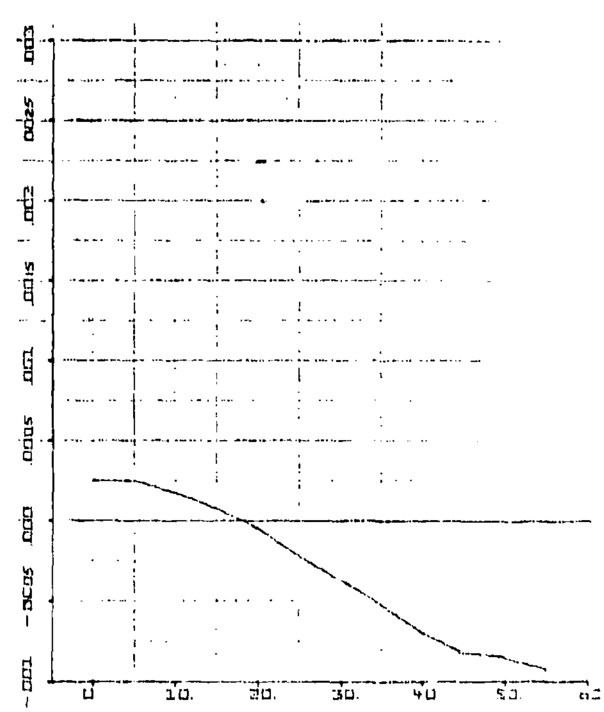

Figure 69. $C_{n_{\delta_a}}(\alpha)$ - 1/deg

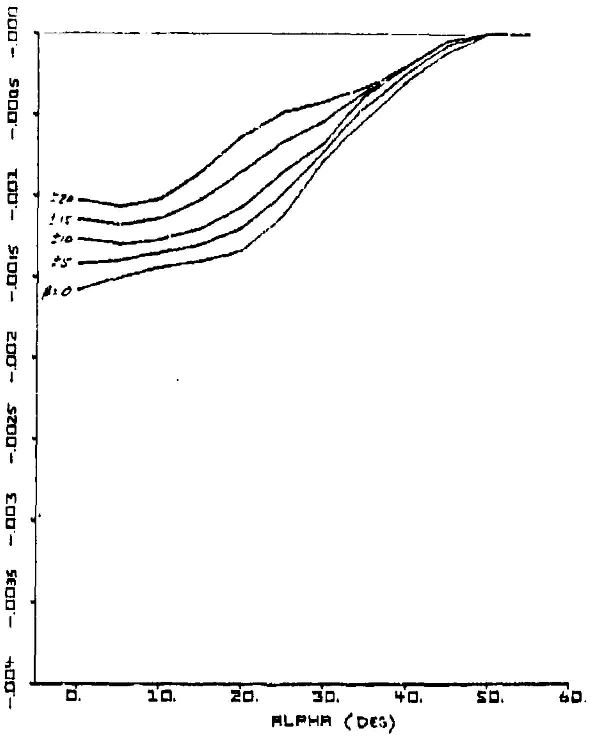

Figure 70. $C_{n_{\delta_r}}(\alpha,\beta)$ - 1/deg

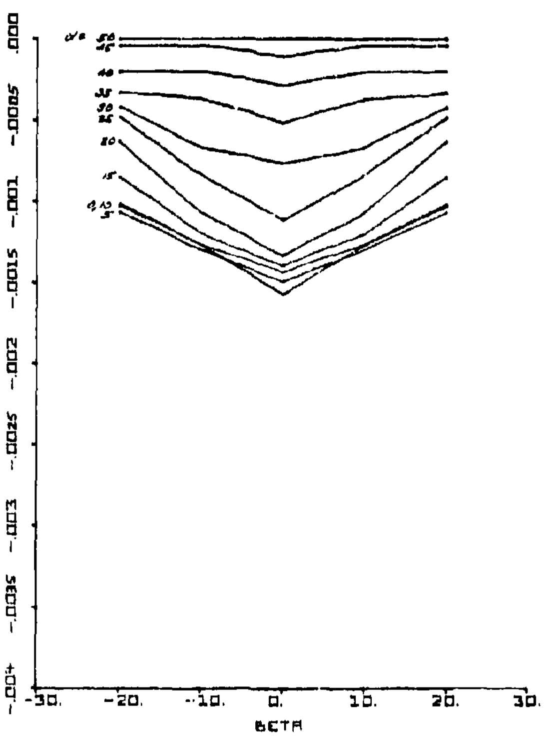

Figure 71. $C_{n_{\delta_r}}(\alpha,\beta)$ - 1/deg

E. VALIDATION

This section documents the validation of the F-14 high angle-of-attack aero model against flight test data. Basically, it was necessary to determine whether the simulation model would produce the high α dynamic phenomena of the unslatted F-14A, specifically:

- Mildly divergent dutch roll in the AOA range 12 to 22 deg
- Wing rock when AOA is maintained in the 12 to 25 deg range at low Mach Number
- Roll reversal starting at α = 18 deg when differential tail is used to roll the aircraft

1. Validation Methods

Two basic methods were available for comparing the simulation model with the flight test data. First, simulation time response traces were compared directly to the flight test traces. This approach had limited success, since the STI unpiloted time-domain simulation program does not have provision for non-zero acceleration initial conditions (i.e., the aircraft is assumed to start from a steady trim condition) and does not have the capability to reproduce the complex control inputs of the flight traces.

The second method involved extracting values of damping ratio, ζ, and frequency, ω, by locally approximating oscillations in the flight traces with a second-order linear-system response. In regions where the control inputs were fixed or could be related to identifiable feedback loops, flight-derived ζ and ω values could be compared to open-or closed-loop roots obtained from small-perturbation linearization of the simulation model. This second method was particularly useful, since the lateral oscillatory response was of primary interest and the linear response parameters ζ and ω can be directly related to the aircraft's stability and control derivatives through literal approximate factors, Ref. 1. The approximate factors were rewritten for body-centerline-axis stability derivatives, Table 13, rather than the usual stability-axis factors, so that the response parameters could be related directly to the aerodynamic model body axis moment coefficients. Thus the significant stability and control derivatives for a given response parameter could be determined and modified to match the flight test result. Such parameter modifications made by linear analysis were then checked by extracting ζ and ω values from non-linear simulation time responses.

TABLE 13. APPROXIMATE FACTORS FOR KEY LATERAL-DIRECTIONAL PARAMETERS AT HIGH AOA USING BODY CENTERLINE AXIS DERIVATIVES ($\gamma_o = 0, \beta_o \approx 0$)

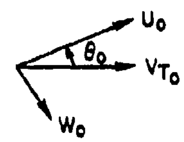

$$\omega_d^2 \doteq N'_\beta - L'_\beta \tan\theta_o$$

$$2\zeta_d\omega_d \doteq -Y_v - L'_p + \left(N'_p - \frac{g}{V_{T_o}}\right)\frac{1}{\tan\theta_o}$$

$$\frac{1}{T_R} \doteq -\frac{N'_\beta}{N'_\beta - L'_\beta \tan\theta_o}\left\{-L'_p + \frac{L'_\beta}{N'_\beta}\left(N'_p - \frac{g}{V_{T_o}} + N'_r \tan\theta_o\right)\right\}$$

$$\frac{1}{T_s} \doteq \frac{T_R}{\omega_d^2}\frac{g}{V_{T_o}}\left\{L'_\beta(N'_r - N'_p \tan\theta_o) - N'_\beta(L'_r - L'_p \tan\theta_o)\right\}$$

2. Flight Test Conditions and Configurations

F-14 flight test data covering the high-α region was obtained from the manufacturer, Ref. 15. From this data six flight test runs (Table 14) were found which were suitable for comparison with the STI simulation. Three different aircraft were involved in these tests. One flight, No. 199, was only used for comparison with the simulation trim routine.

Reproductions of the flight test traces are shown in Figs. 74, 75, 78, 80, 82, and 84. Aircraft 2 and 3 had flight-test nose booms with angle-of-attack and sideslip-angle sensors. The α traces for Flights 230-5 and 230-6 (Aircraft 3) are "raw" noseboom α (denoted α_{IND} on the traces). Noseboom α is related to true α by

$$\alpha_{TRUE} = .8561\ \alpha_{NOSEBOOM} + .178\ \text{deg}$$

TABLE 14. FLIGHT TEST CONDITIONS AND AIRCRAFT CONFIGURATIONS

AIRCRAFT NO.	FLIGHT NO.	TIME SLICE (sec)	ALTITUDE ($ft \times 10^{-3}$)	V_{TRUE} (kt)	α_{TRUE} (deg)	GROSS WEIGHT ($lbs \times 10^{-3}$)	X_{cg} (percent MAC)
2	199	$0 \rightarrow 30$	35	$250 \rightarrow 170$	$10 \rightarrow 38$	47	13.8
3	243	$33 \rightarrow 50$	20	$120 \rightarrow 140$	18 ± 2	47	14.0
1X	234-1	$15 \rightarrow 28$	16	$150 \rightarrow 140$	15 ± 2	53	14.0
1X	236-1	$35 \rightarrow 55$	17	$260 \rightarrow 195$	$13 \rightarrow 28$	54	12.7
2	230-5	$12 \rightarrow 25$	$25 \rightarrow 22$	360	29 ± 1	50	12.5
2	230-6	$20 \rightarrow 40$	18	140	$18 \rightarrow 35$	50	13.0

Aircraft 1X had no nose boom and hence no sideslip sensor. Angle of attack was measured by the ARI nose probe and denoted α_{ARI} on the traces. The nose-probe α is related to true α by

$$\alpha_{TRUE} = .8122 \, \alpha_{NOSEPROBE} + .797 \text{ deg}$$

The simulation model was designed to represent the "clean" (flaps and slats retracted) F-14 at low Mach number and forward wing sweep (22 deg), Fig. 35. The flight test runs used for validation match these conditions as closely as possible, specifically:

- Flaps and slats are retracted except for $\delta_{flap} = -2$ deg on Flight No. 236-1
- Mach number below $M = .35$
- Wing sweep, $\Lambda = 19$–20 deg
- Glove vane and speed brakes retracted
- No external stores

The maneuvers were performed at $n_z \doteq 1$ g, either by maintaining speed and AOA constant and exciting lateral motions with a doublet, or in a "1 g stall" in which angle of attack is steadily increased as speed is decreased. Longitudinal acceleration, $\dot{V}_T$, varied from 0 to −0.4 g, and large negative flight path angles were reached at higher angles of attack. Fairly large excursions in mean bank angle occurred in some runs, but lateral accelerations were generally small. True AOA ranged from 13 deg to 32 deg, which covers the range of interest for high AOA phenomena on this aircraft.

At low speeds the lateral SAS gains are scheduled with AOA (Figs. 72 and 73) such that:

• yaw SAS off	$\alpha > 10^\circ$
• $\delta_{latstick} \rightarrow \delta_r$ phased in	$10^\circ < \alpha < 20^\circ$
• Roll SAS and command augmentation phased out	$20^\circ < \alpha < 31^\circ$

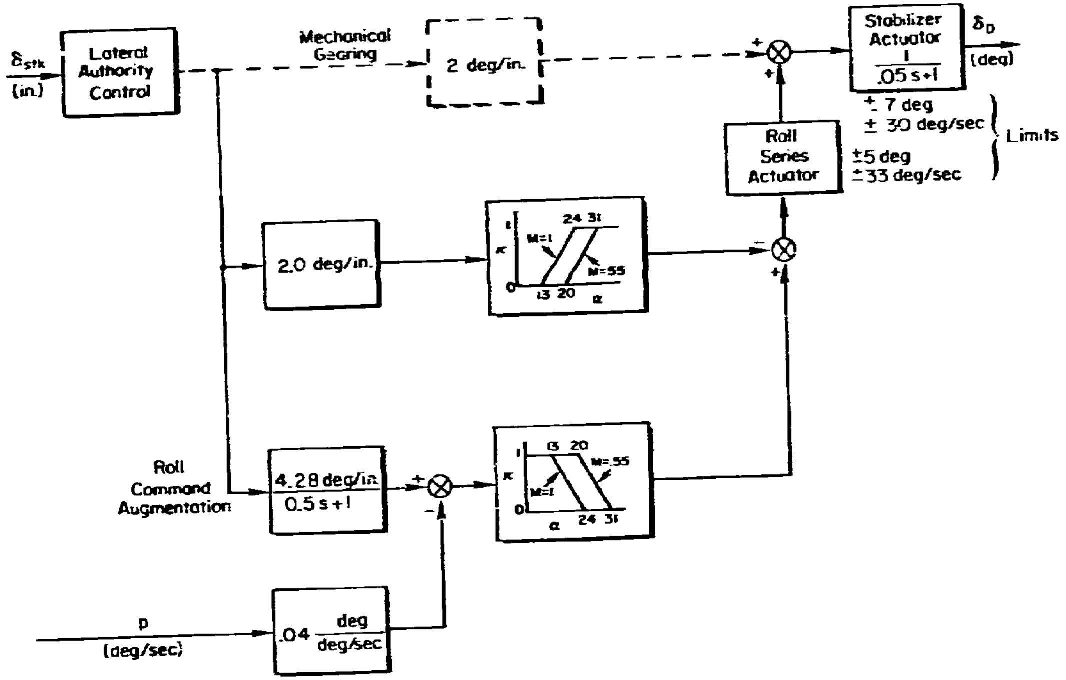

Figure 72. Roll CAS Block Diagram

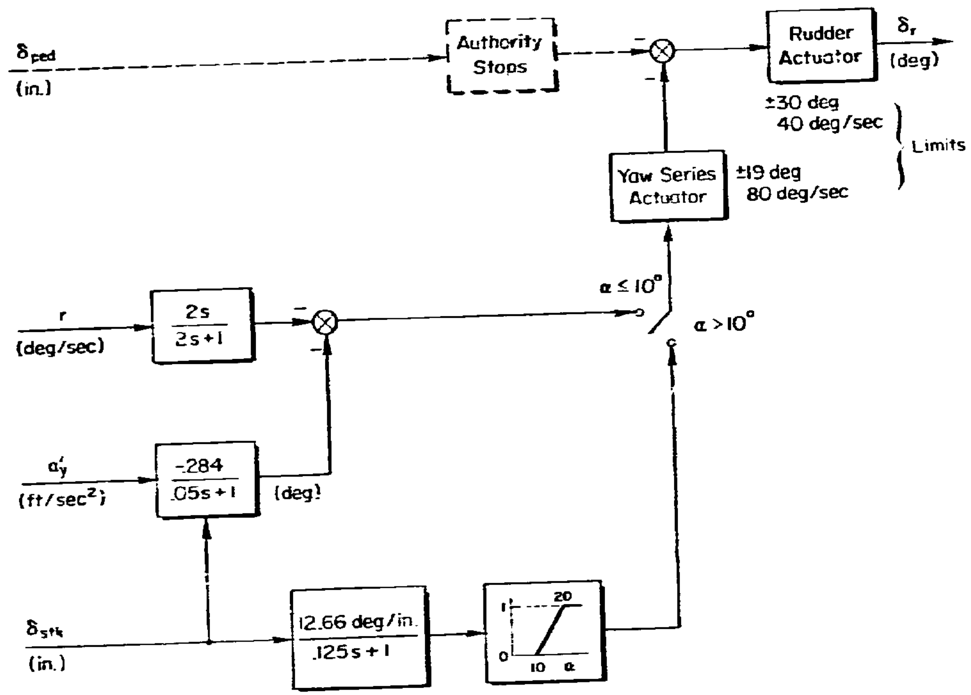

Figure 73. Yaw SAS Block Diagram

Where α as used in Figs. 72 and 73 is the angle of attack as measured by the ARI nose probe. According to this schedule the yaw SAS should be off for all cases. However, Flight No. 243 appears to have the yaw SAS on as will be discussed later. Flights with roll SAS and ARI on were included.

3. Flight Test Comparisons and Derivative Modifications to Match "Wing Rock"

Flight 199 (Aircraft No. 2)

Flight 199, Fig. 74, is a 1-g stall maneuver in which angle of attack is increased steadily from 10 deg to almost 40 deg with a ramp (TEU) horizontal stabilizer input. This maneuver was used to check the simulation trim values. At a given speed, 1-g trim values of α and δ_{stab} from the simulation were compared to the flight α and δ_{stab} traces. Initial comparison using the original wind tunnel derived aerodynamic model gave good comparison with flight α but the flight δ_{stab} traces indicated a more trailing-edge-up deflection. The original simulation C_m (α,β) was based on the LRC wind tunnel data (which differed from the ARC data by an essentially constant nose up increment). A $\Delta C_{m_{\beta=0}}(\alpha)$ increment of $-.055$ was added to the simulation to bring the pitching moment into line with the ARC data. This change resulted in a better match of the δ_{stab} trace, as shown by the circled points in Fig. 74.

Flight 243 (Aircraft No. 3)

In the time "slice" of interest (t = 33-50 sec) AOA is maintained at 18 ± 2 deg, Fig. 75. In this AOA region the gain schedule implies that the yaw SAS and ARI are off and that the roll SAS is on. However, comparison of the yaw rate and rudder position traces indicates that the rudder is correlated with yaw rate at approximately the magnitude and phase angle that would result from the yaw damper. The rudder pedal and lateral stick are both effectively zeroed, and thus the aircraft response can be considered the free response of the augmented airframe.

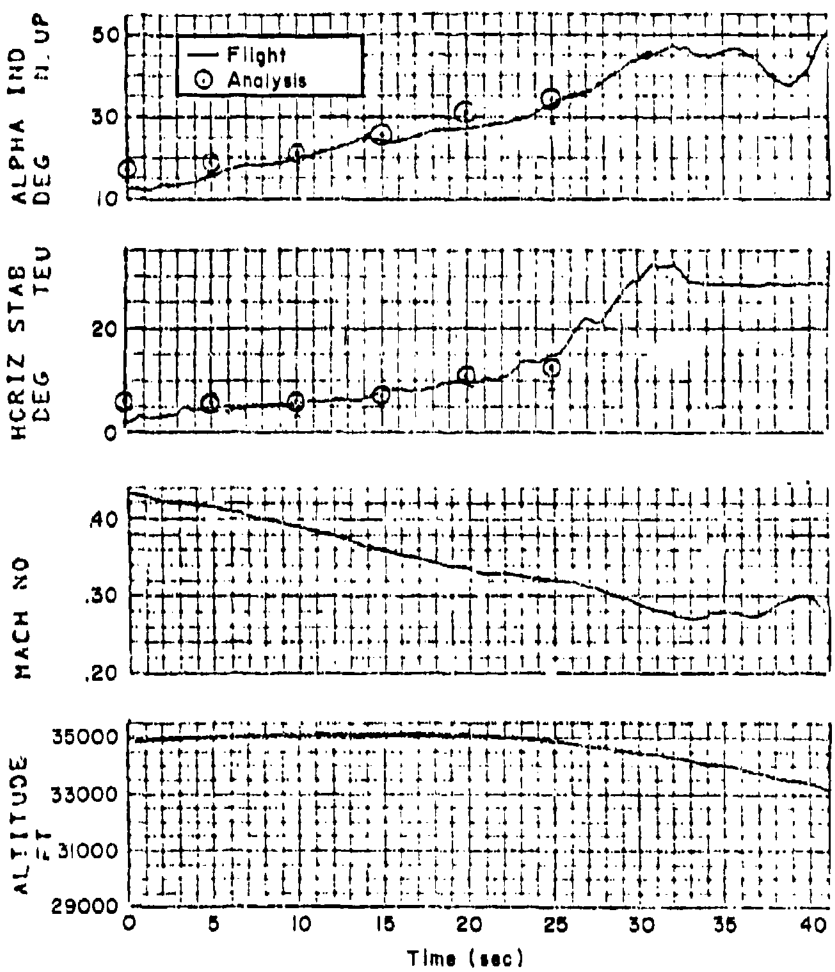

Figure 74. Flight 199 Traces

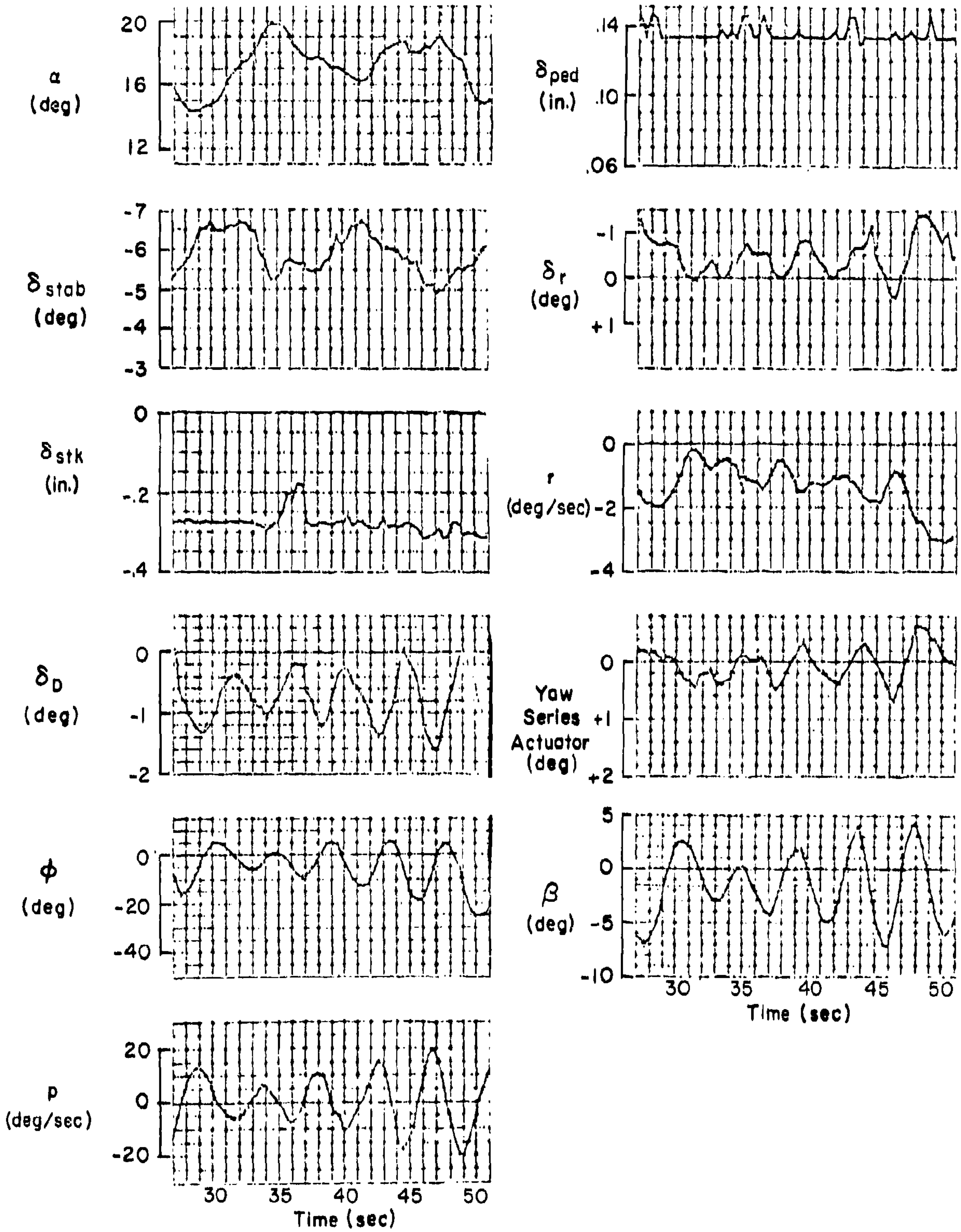

Figure 75. Flight 243 Traces

The aircraft exhibits a divergent "wing rock" oscillation. The fact that the envelope appears to grow linearly with time rather than exponentially indicates a somewhat nonlinear response; however, approximate values of damping ratio and frequency can be extracted as:

$$\zeta \doteq -.05$$

$$\omega \doteq 1.4 \text{ rad/sec}$$

The dutch roll root obtained from linear analysis using the original (wind tunnel derived) aerodynamic data is stable and about 15 percent lower in frequency than the flight value. This is shown (both SAS off and SAS on) in Fig. 76. The body-axis approximate factors, Table 13, evaluated with the original aerodynamic data yield

$$\omega_d \doteq \left(-\tan\theta_o \, L'_\beta\right)^{1/2}$$

$$\doteq \left(-\tan\theta_o \, \frac{\bar{q}SB}{I_x} \, C_{\ell_\beta}\right)^{1/2}$$

$$= 1.21 \text{ rad/sec}$$

$$\zeta_d\omega_d = \frac{1}{2}\left[-Y_v - L'_p + \frac{1}{\tan\theta_o}\left(N'_p - \frac{g}{VT_o}\right)\right]$$

$$= \frac{1}{2}\,(.0475 + .5738 - .0978 - .3510)$$

$$= .0863$$

These approximations are within 4 percent of the values obtained by numerical factorization of the characteristic equation. It can be seen that either an increase in dihedral effect, C_{ℓ_β}, or a decrease in roll moment of inertia, I_x, would increase the dutch roll frequency. A reduction in the magnitude of the roll damping, $C\ell_p$, or a more positive value of the cross coupling parameter, C_{n_p}, would reduce the dutch roll damping. Such changes were made iteratively using the approximate factors for guidance until the dutch roll reasonably approximated the observed frequency and divergence rate.

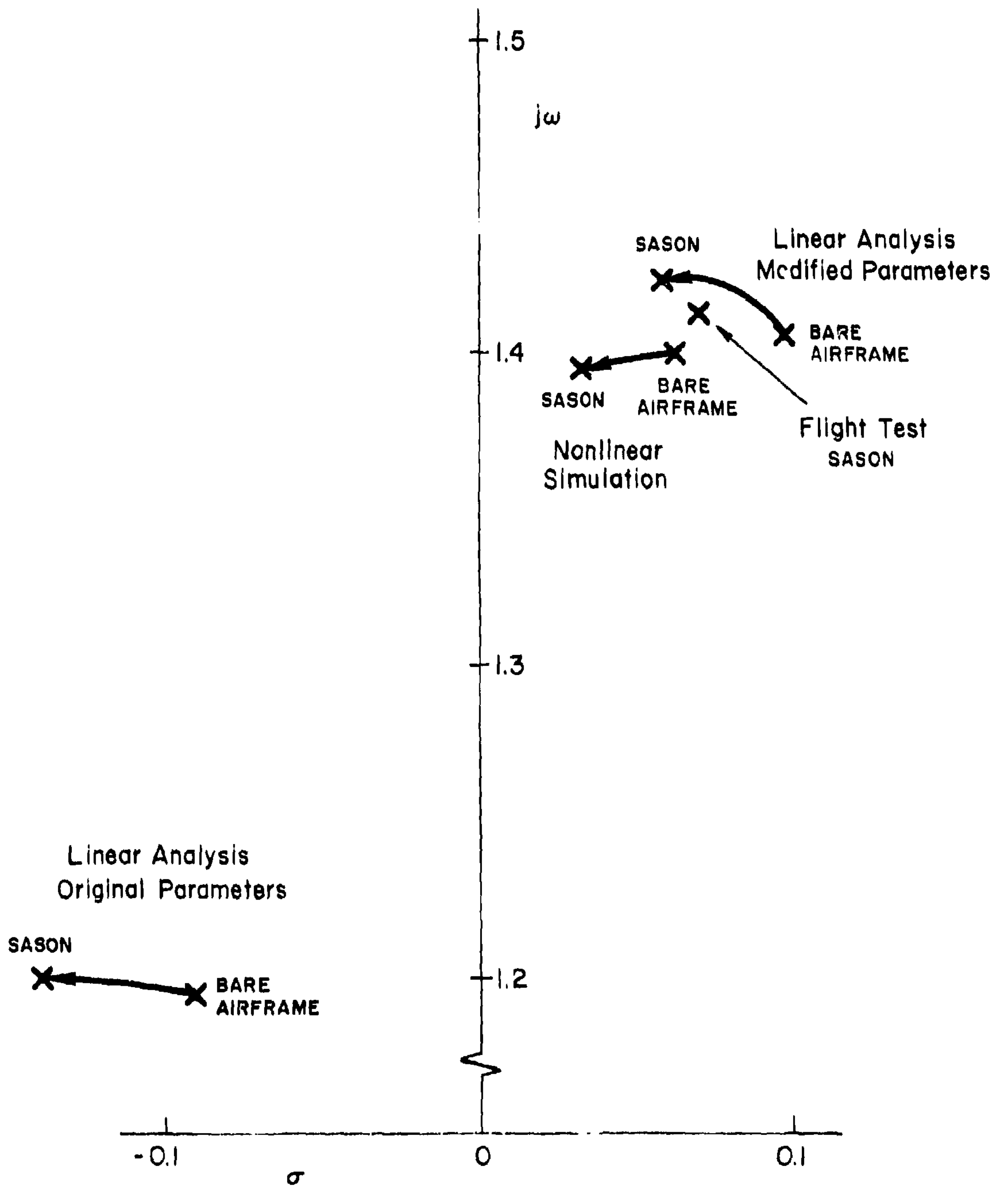

Figure 76. Comparison of Oscillation Root from Simulation with Flight Test for Flight No. 243

These changes produced a small-perturbation (linear) dutch roll root at $[\zeta_d, \omega_d] = [-.071, 1.41]$ for the bare airframe, and $[\zeta_d, \omega_d] = [-.041, 1.43]$, SAS on, which can be compared with the flight-derived root in Fig. 76.

To check possible nonlinear effects the airframe alone digital simulation was run, Fig. 77, with the final modified parameters. The approximate ζ and ω in response to a pulse rudder were extracted as for the flight test data. This resulted in $[\zeta,\omega] \doteq [-.045, 1.4]$ for the bare airframe Actually the frequency started at about 1.45 rad/sec and decreased to about 1.35 rad/sec as the amplitude of oscillation increased. With the SAS on the root moves to $[\zeta,\omega] = [-.024, 1.40]$.

Flight 234-1 (Aircraft 1X)

The Flight 234-1 maneuver was performed at an approximately constant AOA, α_o = 15 deg, Fig. 78. In the time slice of interest, t = 15 to 28 seconds, the yaw SAS is off per the α schedule, as can be confirmed from the rudder position trace. The ARI is scheduled at 60 percent but has no effect since the lateral stick is fixed. The roll SAS which would normally be on at this AOA has been switched off, as can be seen from the roll series actuator trace. Thus from t = 19 to 28 seconds the response is that of the bare airframe. This shows an oscillating divergence (dutch roll) with $[\zeta,\omega] = [-.07, 1.4$ rad/sec].

Calculation of the dutch roll root using the original (wind tunnel) aerodynamic data again produced a stable mode. Estimates of parameter changes required to match the flight test divergence indicated that a level of roll damping comparable to the final Flight 243 match, $C_{\ell_p} = -.08$ 1/rad, was required. When this C_{ℓ_p} value was used in the nonlinear simulation of the bare airframe, Fig. 79, the approximate damping ratio and frequency were found to be $[\zeta,\omega] = [-.058, 1.43]$.

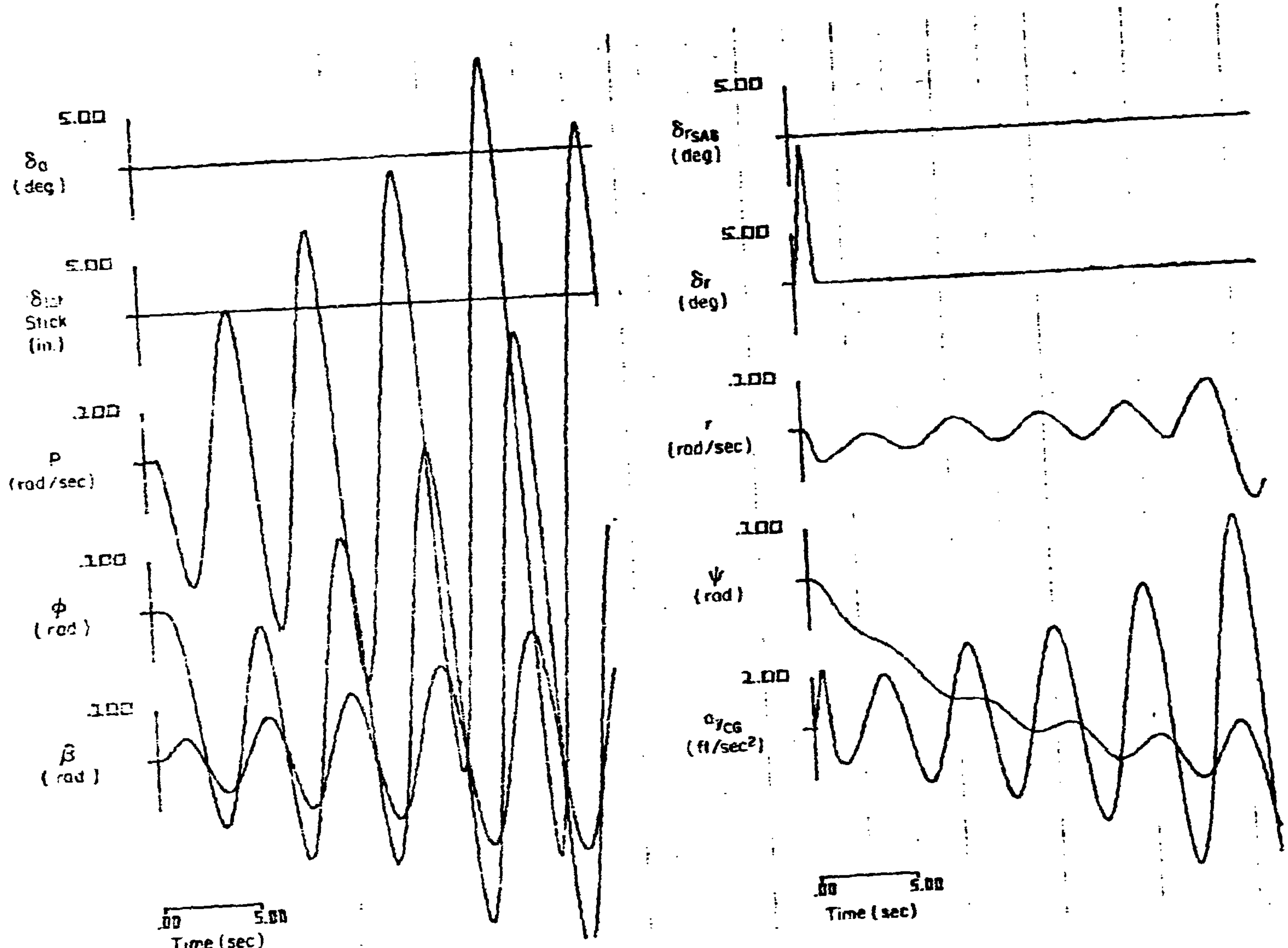

Figure 77. Non-Linear Simulation of Bare Airframe, Flight 243

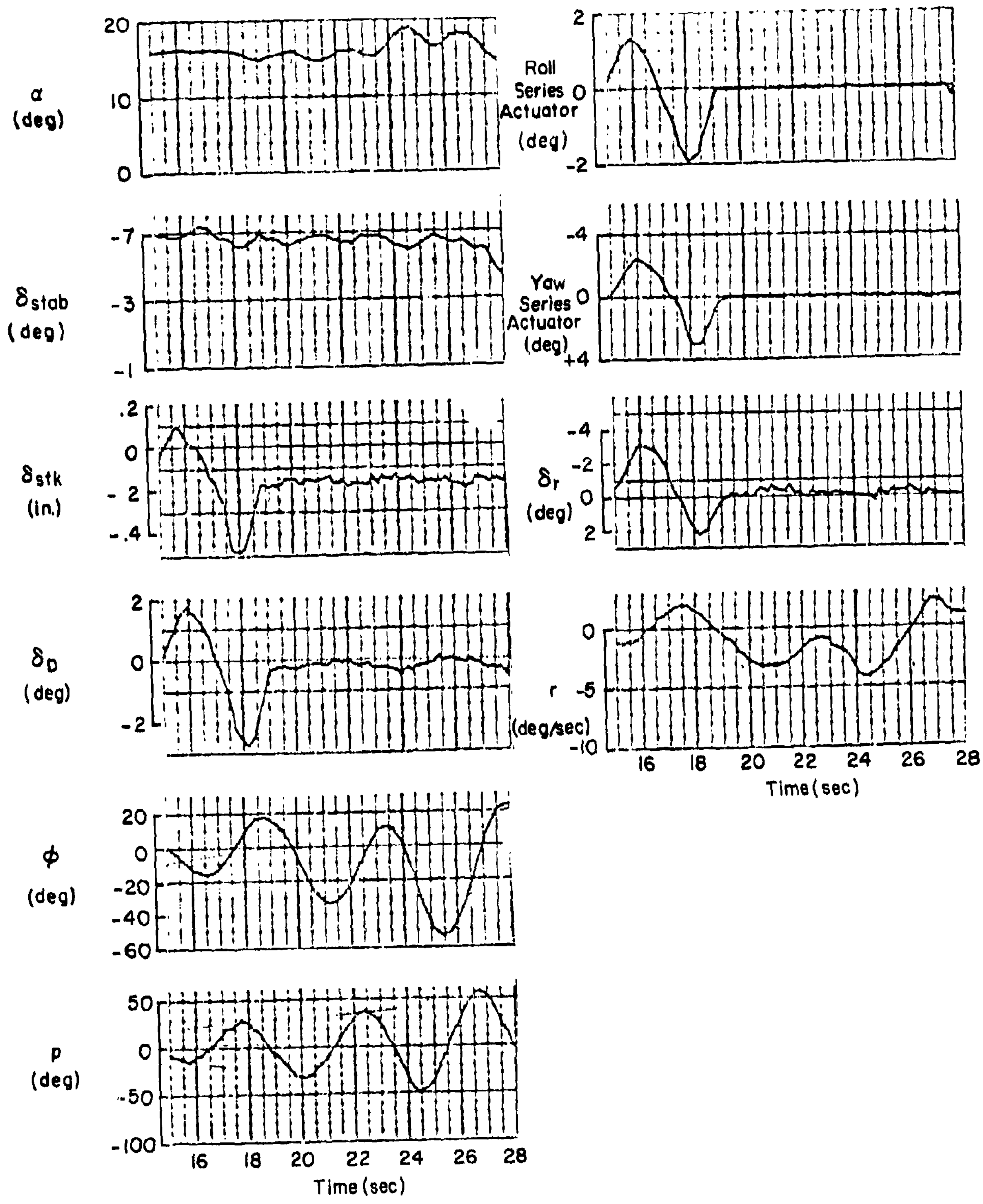

Figure 78. Flight 234-1 Traces

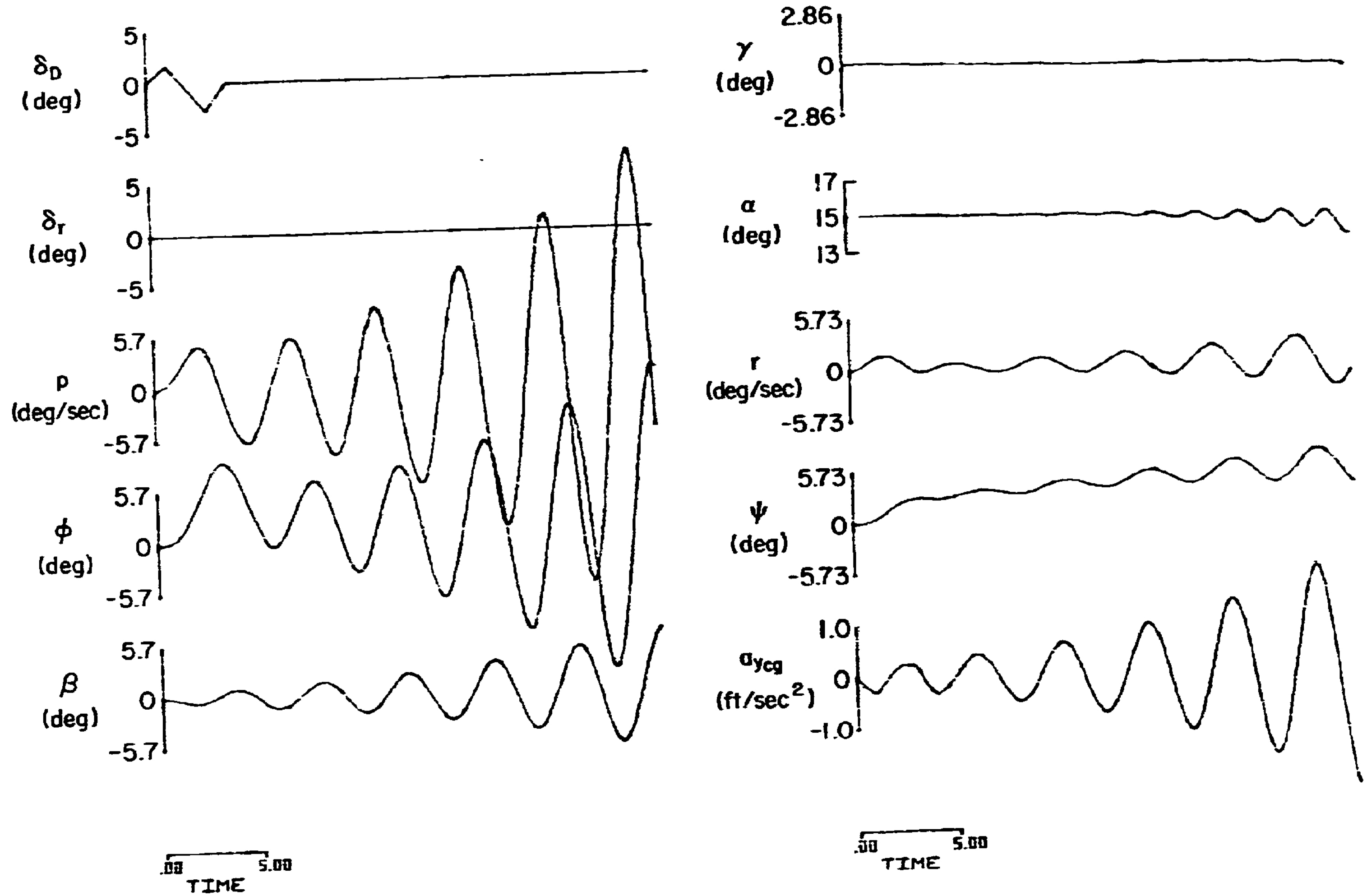

Figure 79. Bare Airframe Nonlinear Simulation
Time Responses for Flight 234-1

Flight 236-1 (Aircraft 1X)

The Flight 236-1 maneuver was a 1 g stall in which angle of attack was steadily increased from $\alpha = 13$ to 28 deg in the time slice examined, Fig. 80. The roll SAS has been switched off, as seen from the roll series actuator trace and the lateral stick is fixed, thus the differential tail is zeroed. The yaw SAS is also off per the α schedule. Between $t = 35$ and 40 sec the lateral stick and rudder are used to excite a rolling oscillation. The lateral stick is then centered and held fixed. A rudder pedal input is made at $t = 43$ sec. Also note that the rudder apparently was used to counter some other disturbance since the aircraft is rolling to the right and the rudder input is trailing-edge left. Thus the rudder input and other disturbance may contaminate the response sufficiently to alter the apparent ζ and ω values. As in the Flight 243 trace, the envelope of the bank-angle oscillation appears to grow linearly with time rather than logarithmically, but an estimate of the response parameters gives $[\zeta,\omega] = [-.085,\ 1.30 \text{ rad/sec}]$.

Matching of this flight condition was done directly from nonlinear simulation time responses, Fig. 81. Matching frequency required a 30 percent increase in I_x (at this heavy weight the aircraft has approximately 4,000 lb of fuel in the wings) and matching the divergence rate required reducing the roll damping below the level of the wind-tunnel data in the $20 < \alpha < 30$ deg region (again similar to the C_{ℓ_p} reduction required at $15 < \alpha < 20$ deg). The final simulation time response shows a nonlogarithmic φ envelope, similar to the flight traces, which is possibly a nonlinear effect of the time-varying α. Oscillation frequency derived from the simulation φ trace varies from 1.40 rad/sec at low amplitude to 1.1 rad/sec at large amplitude. Damping ratio varies from $-.11$ to $-.085$.

Flight 230-5

In the time slice examined, the angle-of-attack was roughly constant at $\alpha = 29$ deg, Fig. 82. Although there is considerable stick activity, the roll SAS and command augmentation is almost phased out at this AOA and thus the differential stabilizer is essentially zeroed. The large-amplitude rudder oscillation is due primarily to the lateral stick deflection acting through

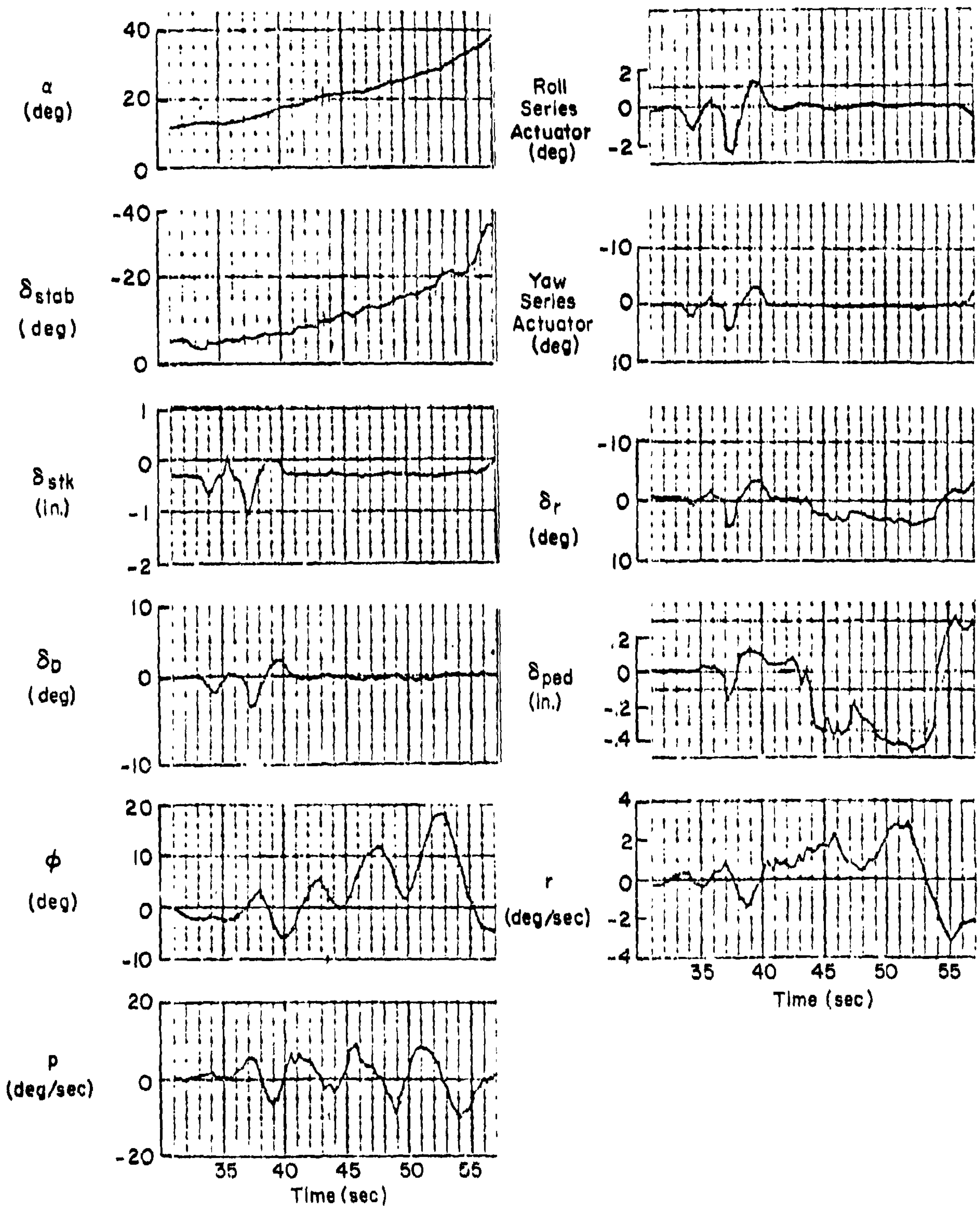

Figure 80. Flight 236-1 Traces

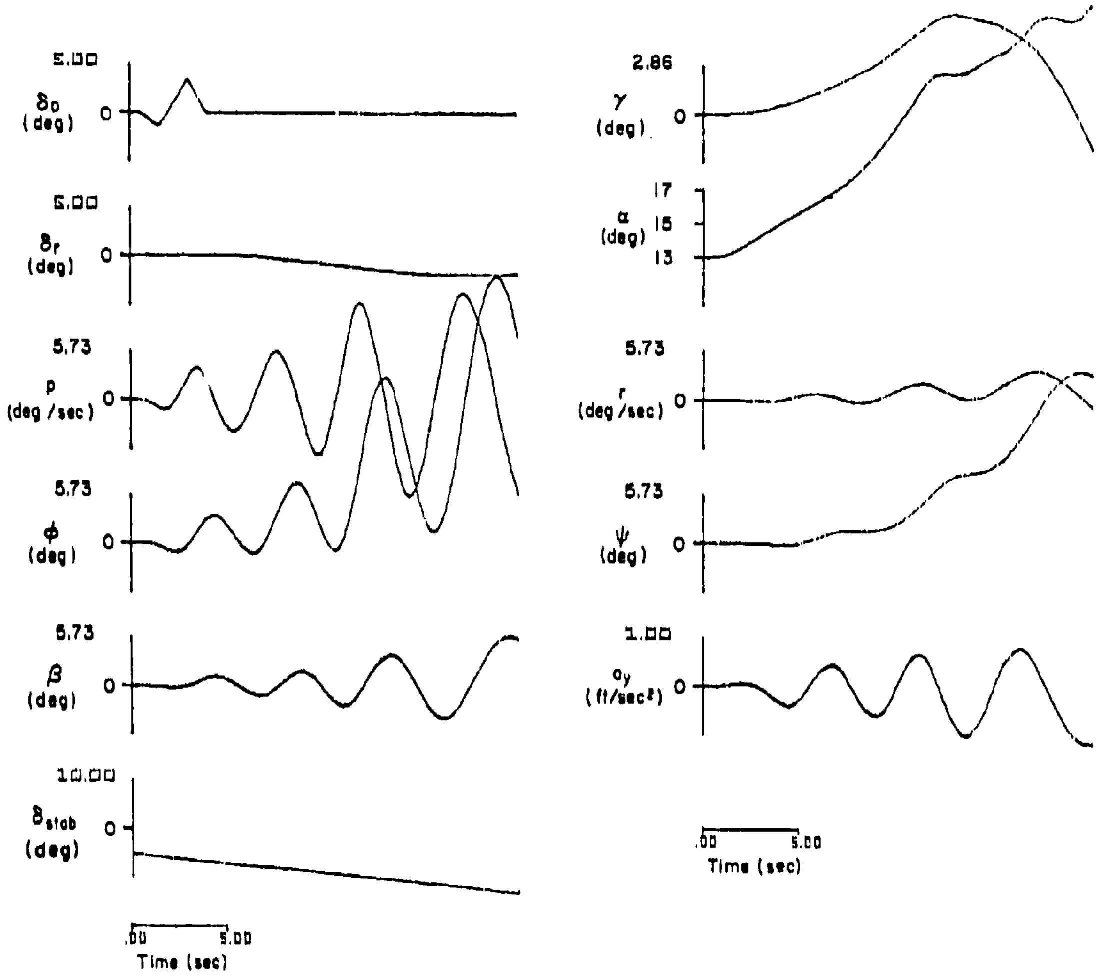

Figure 81. Bare Airframe Simulation Time Responses for Flight 236-1

the stick-to-rudder interconnect (SRI). From an examination of the rudder and roll traces it cannot be determined immediately if the pilot was attempting to excite the roll with the rudder or was feeding p, φ, or both to rudder to damp the oscillation. The latter possibility can be checked by considering a system survey (root locus and Bode-siggie; see Part I, Section II) for $\varphi \rightarrow \delta_r$ loop closure as shown in Fig. 83. It can be seen that at gains on the order of those observed in the flight traces, $K_{\varphi_p} \doteq 1$ deg/deg, the dutch roll is stable but a divergent first-order root appears. Since no aperiodic divergence is apparent in the flight traces, it would seem likely that the rudder input is an open-loop excitation. From the flight traces, the frequency is $\omega \doteq 1.4$-1.6 rad/sec and $|\varphi/\delta_r\,(j\omega)| = .6$ to 1.0 (-4.4 dB to 0 dB). This is in reasonable agreement with the open-loop Bode plot of Fig. 83 indicating that the rudder effectiveness is reasonable at this angle of attack, $\alpha \doteq 29$ deg.

Flight 230-6

From t = 20 to 40 seconds, AOA is increased rapidly with a ramp stabilator input, Fig. 84. The rudder and lateral stick are essentially zero during most of this time. There is no evidence of a divergent lateral oscillation, which is in general agreement with the simulation which indicates a stable airframe in this angle-of-attack region ($\alpha > 25$ deg). The simulation yields

α	ζ_d	ω_d
25	+.097	1.22 rad/sec
30	+.244	.93 rad/sec

4. Roll Reversal Validation

Figure 85 shows the migration of the ω_φ root with AOA. It can be seen that between $\alpha = 15$ and 20 deg ω_φ becomes real with one zero in the right half-plane. This produces an initial open-loop roll opposite to that commanded with lateral stick. It also results in a first-order lateral-directional divergence if the $\varphi \rightarrow \delta_D$ loop is closed, Fig. 86. This behavior can be traced to the change from proverse to adverse yaw at $\alpha = 18$ deg shown in the $C_{n_{\delta_D}}$ vs. α plot of Fig. 87.

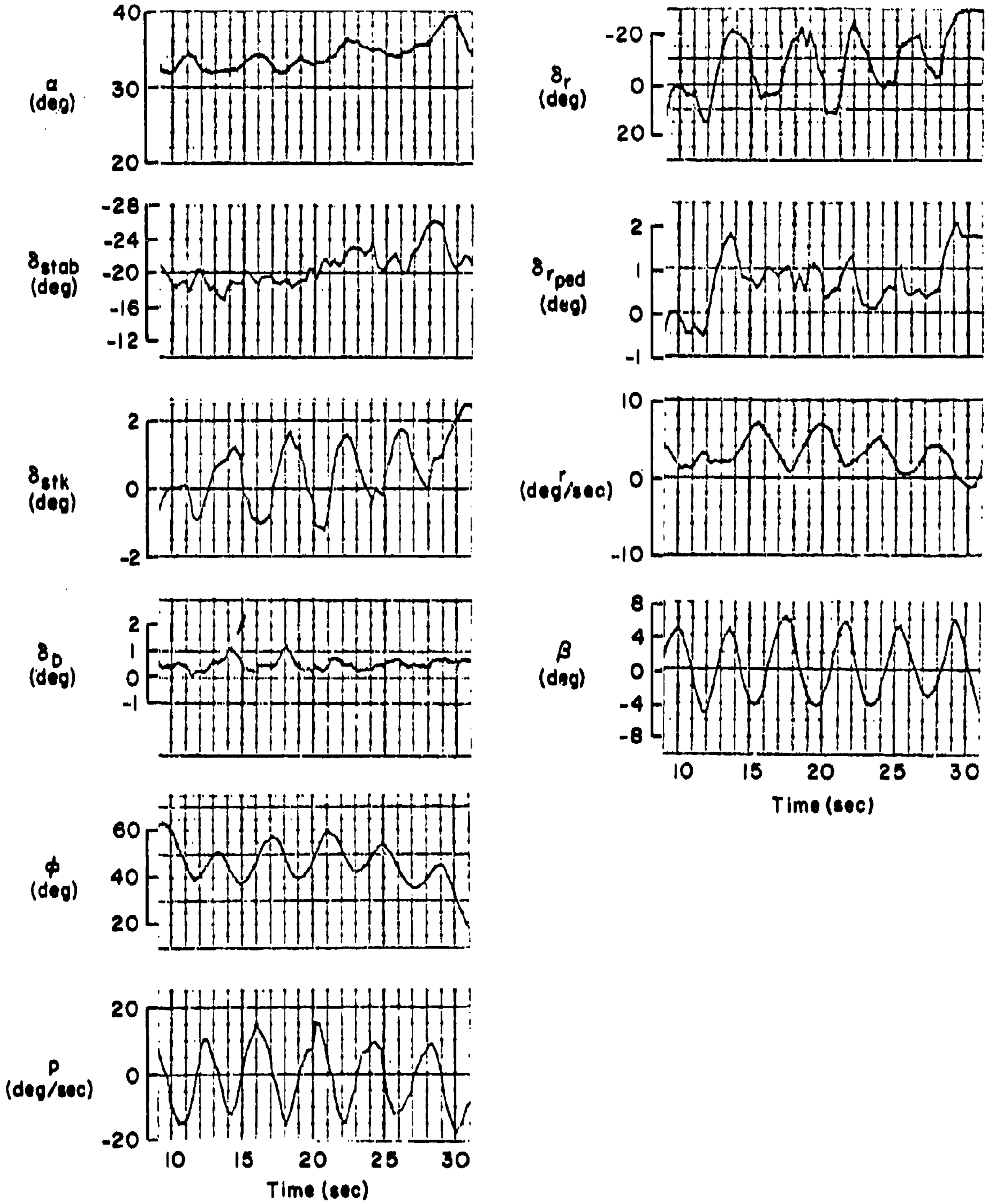

Figure 82. Flight 230-5 Traces

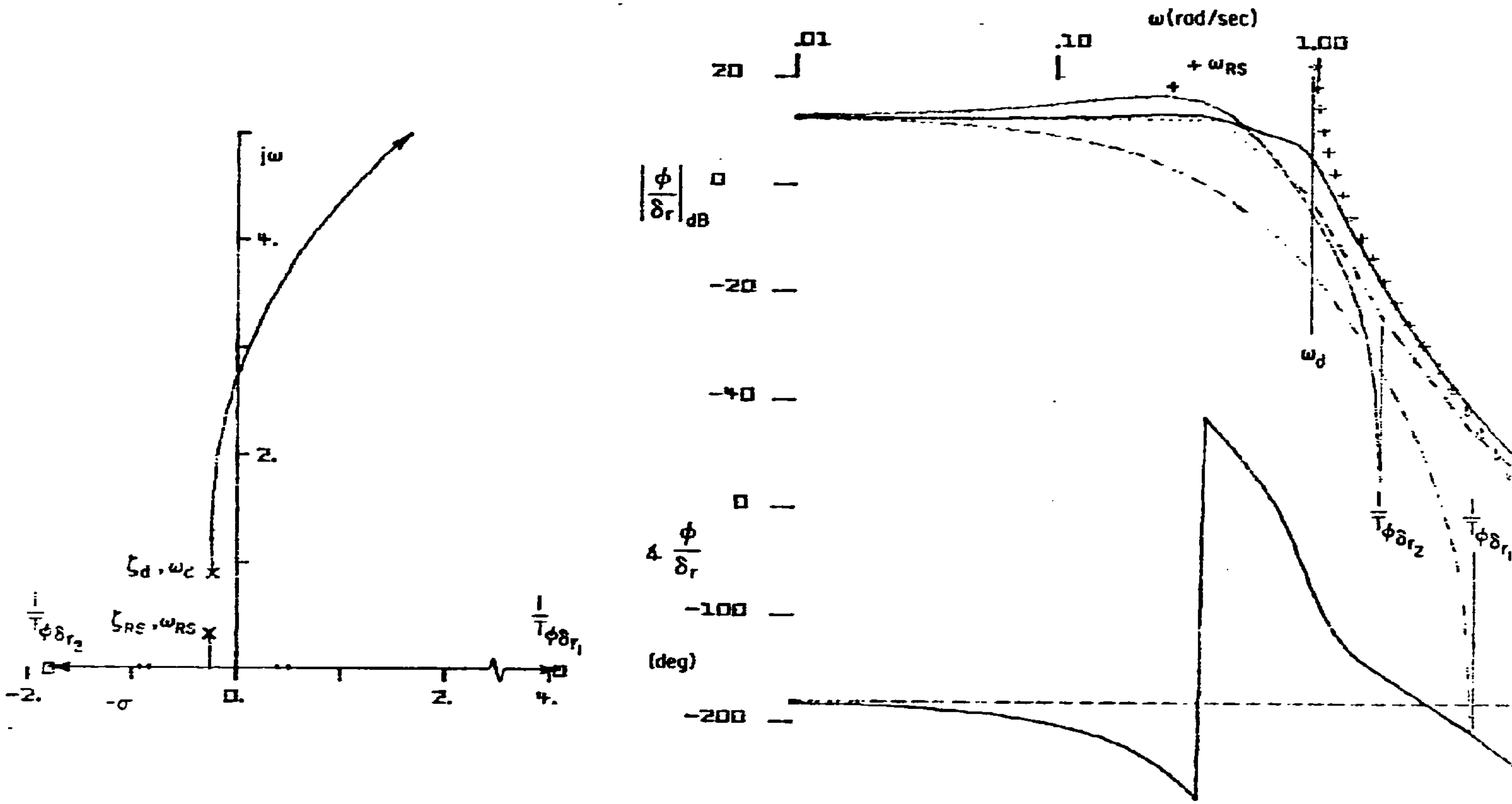

Figure 83. System Survey of a $\varphi \rightarrow \delta_r$ Loop Closure

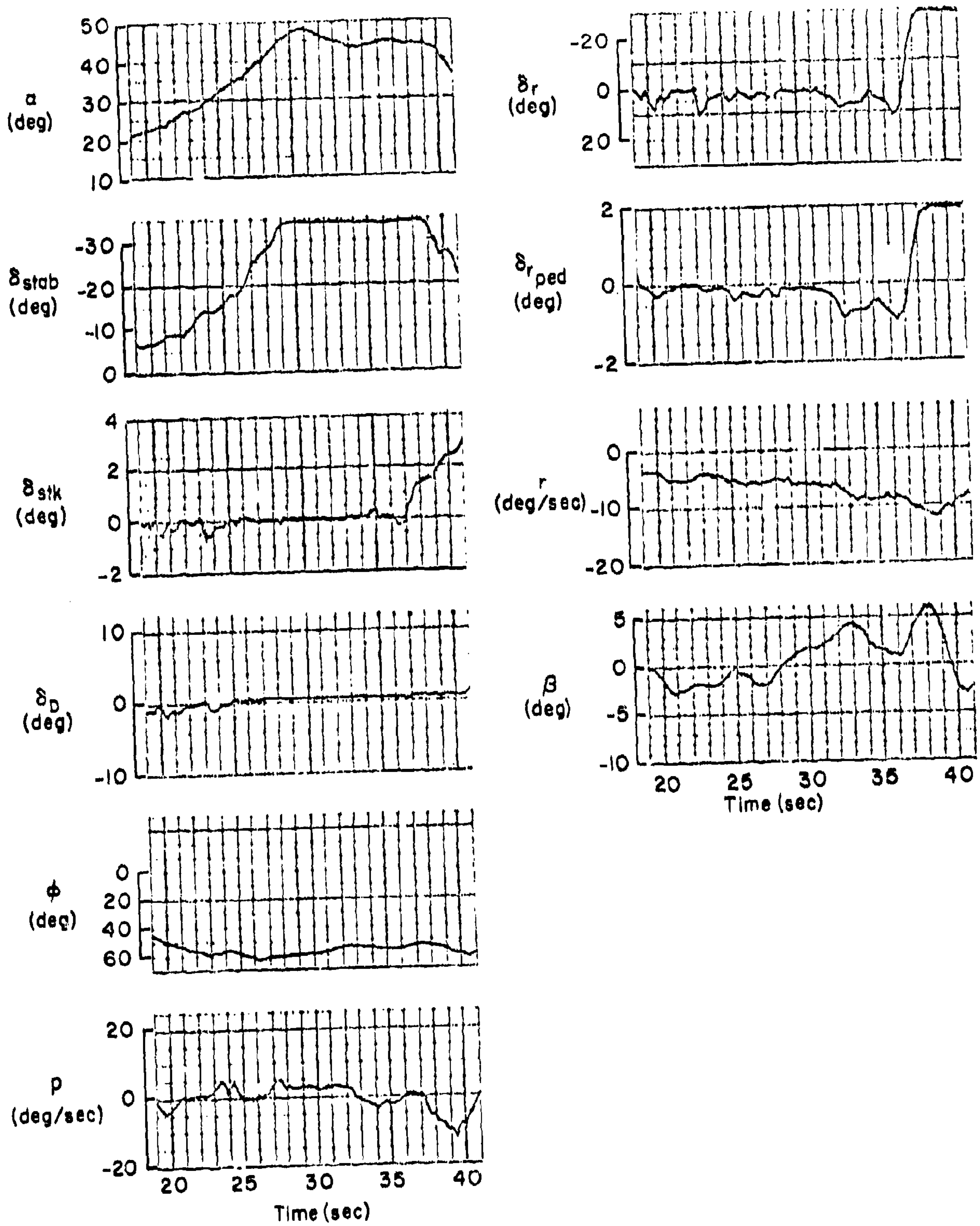

Figure 84. Flight 230-6 Traces

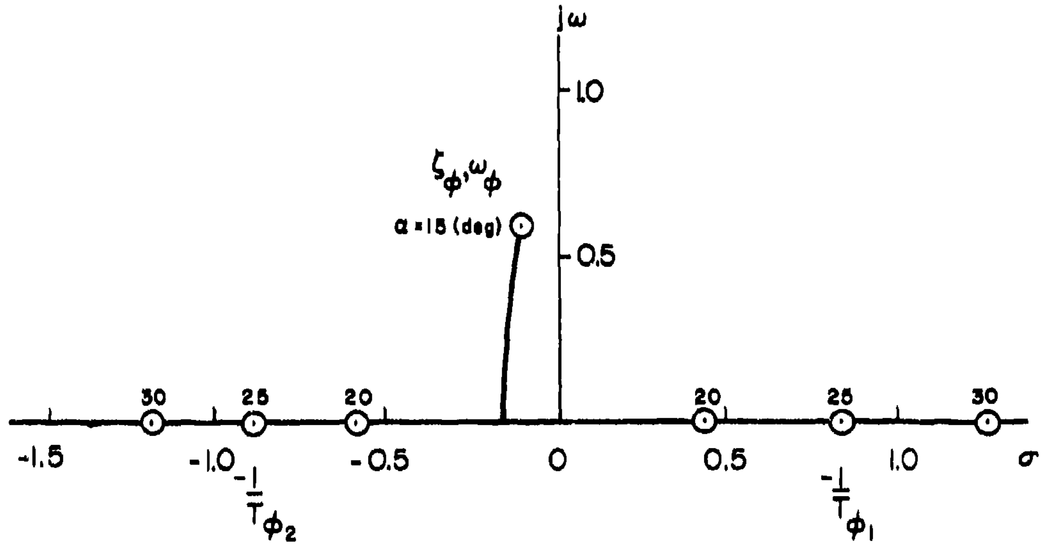

Figure 85. Migration of $N_{\delta_a}^{\varphi}$ Zeroes With Angle of Attack, $\beta_0 = 0$

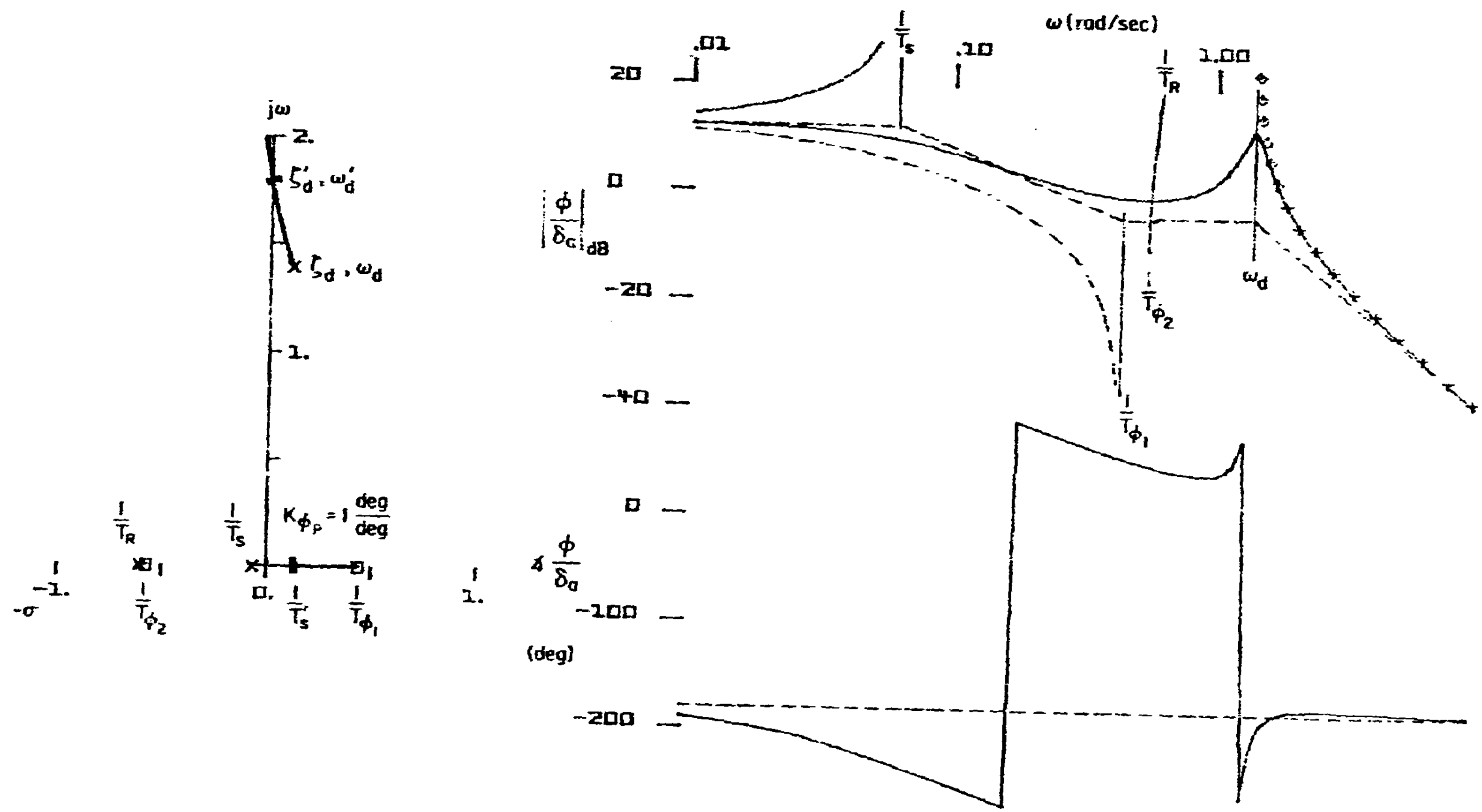

Figure 86. System Survey of Pure Gain $\phi \rightarrow \delta_a$ Closure with Conventional Gain (Left Stick for Right Roll) in the Roll Reversal Region (α = 20 deg)

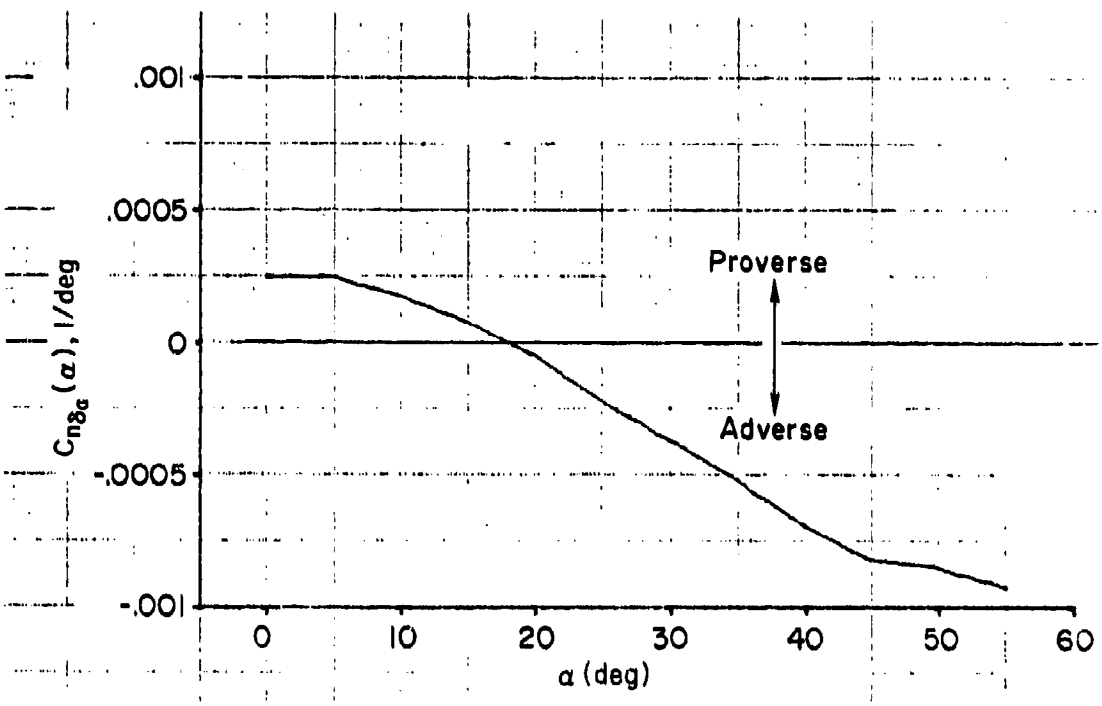

Figure 87. Variation of Yaw-Due-To-Differential Stabilizer with Angle of Attack

REFERENCES

1. McRuer, Duane, Irving Ashkenas, and Dunstan Graham, Aircraft Dynamics and Automatic Control, Princeton Univ. Press, 1973.

2. Anglin, Ernie L., Static Force Tests of a Model of a Twin-Jet Fighter Airplane for Angles of Attack from −10° to 110° and Sideslip Angles from −40° to 40°, NASA TN D-6425, Aug., 1971.

3. Bowser, D. K., F-4 High-AOA Data Package, (digitized data from McDonnell Aircraft Co., Rept. MDC A0005, Vol. II), Aug. 1969.

4. Brady, C. C., W. A. Moran, and M. L. Rosenstein, Model F14, Spin Evaluation Program, McDonnell Aircraft Co., Rept. MDC A0005, Vols. I and II, Aug. 1969.

5. Chambers, Joseph R., and Ernie L. Anglin, Analysis of Lateral-Directional Stability Characteristics of a Twin-Jet Fighter Airplane at High Angles of Attack, NASA TN D-5361, Aug. 1969.

6. Grafton, Sue B., and Charles E. Libbey, Dynamic Stability Derivatives of a Twin-Jet Fighter Model for Angles of Attack from −10° to 110°, NASA TN D-6091, Jan. 1971.

7. Meintel, Alfred J., Jr., Jack E. Pennington, and Walter W. Hankins, III, Differential Maneuvering Simulator Validation, NASA TM X-2827, Oct. 1973.

8. McElroy, C. E., 1st Lt., and P. S. Sharp, Sgt., Stall/Near Stall Investigation of the F-4E Aircraft, USAF FTC-SD-70-20, Oct. 1970.

9. Gilbert, William P., L. T. Nguyen, and R. W. Van Gunst, Simulator Study of Applications of Automatic Departure and Spin-Prevention Concepts to a Variable-Sweep Fighter Airplane, NASA TM X-2928, Nov. 1973.

10. Bihrle, William, Jr., and A. C. Hegman, F-14 Spin Avoidance/Prevention Program, Final Report, Vol. II, Grumman Aerospace Corp., A51-335-R-72-1, Mar. 1972.

11. Grafton, Sue B., and E. L. Anglin, Dynamic Stability Derivatives at Angles of Attack from −5° to 90° for a Variable-Sweep Fighter Configuration with Twin Vertical Tails, NASA TN D-6909, Oct. 1972.

12. Bihrle, William, Jr., and B. Barnhart, Effects of Several Factors on Theoretical Predictions of Airplane Spin Characteristics, NASA CR-137521, Aug. 1974.

REFERENCES (cont'd)

13. Boisseau, Peter C., and Joseph R. Chambers, Lateral-Directional Characteristics of a 1/10-Scale Free-Flight Model of a Variable Sweep Fighter Airplane at High Angles of Attack, NASA TM SX-2649, Dec. 1972.

14. Bihrle, William Jr., and R. C. Meyers, "F-14X High Angle-of-Attack Characteristics," J. of Aircraft, Vol. 13, No. 8, Aug. 1976, pp. 576-583.

15. Kelly, C. P., "F-14 Flight Test Data," Grumman Aerospace Corp., EG-GC-LTR-76-02, Nov. 1976.

16. Teper, Gary L., and Donald E. Johnston, F4J Data Package, Systems Technology, Inc., WP-2141-1, Jun. 1974.

★U.S.Government Printing Office: 1981 — 757-002/606